

Chemical Consequences of Air Quality Standards and of Control Implementation  
Programs: Roles of Hydrocarbons, Oxides of Nitrogen, Oxides of Sulfur and  
Aged Smog in the Production of Photochemical Oxidant and Aerosol

Contract No. A6-172-30  
California Air Resources Board  
Final Report  
June 1979

Principal Investigator

Dr. James N. Pitts, Jr.

Program Manager

Dr. Arthur M. Winer

Program Research Staff

Dr. Roger Atkinson  
Dr. William P. L. Carter  
Dr. Karen R. Darnall  
Dr. George J. Doyle  
Dr. Richard A. Graham  
Dr. Ernesto C. Tuazon

Technical Support Staff

Ms. Sara M. Aschmann  
Mr. Frank R. Burleson  
Mr. Dennis R. Fitz  
Mr. L. Michael Kienitz  
Ms. Minn P. Poe  
Mr. Glen C. Vogelaar  
Ms. Laurie A. Willis

STATEWIDE AIR POLLUTION RESEARCH CENTER  
UNIVERSITY OF CALIFORNIA  
RIVERSIDE, CALIFORNIA 92521



## ABSTRACT

The environmental chamber facility established at the Statewide Air Pollution Research Center, University of California, Riverside, under a joint Air Resources Board--University of California (Project Clean Air) program has been employed in investigations:

To establish correlations between ozone formation and hydroxyl radical rate constants and hydrocarbon reactivity scales;

To determine rate constants for the reactions of hydroxyl radicals with selected organic compounds including alkanes, alkenes and alkene oxides;

To obtain data concerning the rates of conversion of sulfur dioxide to sulfate aerosol under simulated atmospheric conditions;

To extend the previous oxidant-HC-NO<sub>x</sub> data base obtained at SAPRC by generating data for 12 hour irradiation experiments employing both constant light intensity and quasi-diurnal light intensity;

To apply both computer kinetic modeling and an empirical mathematical approach to assessments of oxidant-precursor relationships.

This report was submitted in fulfillment of Contract No. A6-172-30 by the Statewide Air Pollution Research Center, University of California, Riverside, under the partial sponsorship of the California Air Resources Board. Work was completed as of September 30, 1978.



The statements and conclusions in this report are those of the contractor and not necessarily those of the California Air Resources Board. The mention of commercial products, their source or their use in connection with material reported herein is not to be construed as either an actual or implied endorsement of such products.



## TABLE OF CONTENTS

	<u>Page</u>
Abstract	1
List of Figures	4
List of Tables	7
Acknowledgments	10
I. Executive Summary	11
II. Facilities and Methods	35
A. Chamber Facility and Analytical Methods	35
B. Experimental Procedures	39
III. A Smog Chamber Study of the Correlation of Hydroxyl Radical Rate Constants with Ozone Formation	42
IV. Comparison of Reactivity Scales Based on Ozone Formation with the Hydroxyl Reactivity Scale	48
V. Rate Constants for the Reactions of Hydroxyl Radicals with Selected Organics	56
VI. Investigation of Rates of Conversion of Sulfur Dioxide to Sulfate Under Simulated Atmospheric Conditions	71
VII. Monitoring of Nitrate Aerosol Precursors	89
VIII. Assessment of Oxidant-Precursor Relationships Utilizing a Computer Kinetic Model	93
IX. Long-Term and Multiple Day Smog Chamber Irradiations	114
X. Assessment of Oxidant-Precursor Relationships Utilizing an Empirical Mathematical Approach	133
XI. Computer Archiving of SAPRC/ARB Surrogate Hydrocarbon-NO <sub>x</sub> -Air Data Base	147
XII. References	153
XIII. List of Publications from SAPRC-ARB Chamber Program	161



## LIST OF FIGURES

<u>Figure No.</u>	<u>Title</u>	<u>Page</u>
1	Relationship Between Peak Chamber Oxidant Observed at Four Laboratories and Experimentally Determined Rate Constants for Reaction with the Hydroxyl Radical	19
2	Root Mean Square Ozone Concentrations at Various Precursor Ratios as Functions of Initial NMHC Concentrations	32
3	Schematic Drawing of All-Glass Chamber Facility	36
4	Air Purification System	40
5	Relationship Between Peak Chamber Oxidant Observed at Four Laboratories and Experimentally Determined Rate Constants for Reaction with the Hydroxyl Radical	51
6	Ozone Reactivity versus Relative OH Rate Constant at Initial Precursor Ratios of 2:1 and 10:1	53
7	Ozone Data of Joshi and Dimitriades as a Function of Hydroxyl Rate Constant	55
8	Plots of $\ln([A_2]_t/[A_1]_t)$ Against Irradiation Time for $A_2 = 2\text{-Methyl-2-Butene}$ and $2,3\text{-Dimethyl-2-Butene}$ and $A_1 = \text{cis-2-Butene}$	60
9	Experimental Wall Loss Constants as a Function of Particle Diameter and Regression Curve	76
10	Dependence of the Loss Constant on Particle Size for the Larger Particles	77
11	Typical Behavior of Sulfur and Aerosol Volume Data During Photooxidation Experiments	84
12	Experimental Data and Regression Calculation for Final Gas-to-Particle Conversion Rates for Sulfur Dioxide vs. Disappearance Rates of 2,3-Dimethylbutane	87
13	Six-Hour Ozone versus $\text{NO}_x$	101
14	Nine-Hour Ozone versus $\text{NO}_x$	102



## LIST OF FIGURES (continued)

<u>Figure No.</u>	<u>Title</u>	<u>Page</u>
15	Effect of Season and Stratospheric Ozone Level on Ambient Air Simulations: Calculated Daily Maximum Ozone versus $\text{NO}_x$ Level for Highest and Lowest NMHC Level	106
16	Effect of Model on Ambient Air Simulations: Calculated Daily Maximum Ozone versus $\text{NO}_x$ Level for Highest and Lowest NMHC Level	107
17	Calculated Maximum Ozone Attainable for Given NMHC Levels	108
18	Calculated $\text{NO}_x$ at which Maximum Ozone Attained for Given NMHC Levels	109
19	Diurnal Variation of Light Intensity Profiles	115
20	Effect of Relative Humidity on Ozone Production for 100% Constant Light Intensity, 307 K	124
21	Effect of Relative Humidity on Ozone Production for 70% Constant Light Intensity, 303 K	125
22	Ozone Profiles for Replicate Standard 12-Hour Experiments at Constant Light Intensity	126
23	Ozone Profiles for Replicate Standard 12-Hour Experiments at Constant and Diurnal Light Intensities	127
24	Ozone Profiles for Runs with High Initial NMHC/ $\text{NO}_x$ Ratio	128
25	Ozone Profiles for Runs with Low Initial NMHC/ $\text{NO}_x$ Ratio	129
26	Ozone Profiles for Runs with Intermediate Initial NMHC/ $\text{NO}_x$ Ratio	130
27	Effects of Temperature and Light Intensity on Ozone Production	132
28	Root Mean Square Ozone Concentrations at Various Precursor Ratios as Functions of Initial NMHC Concentrations	134



LIST OF FIGURES (continued)

<u>Figure No.</u>	<u>Title</u>	<u>Page</u>
29	Relative Contribution of Second Jacobi Polynomial to Ozone Profiles as a Function of Precursor Ratio for Various Initial NMHC Concentrations	136
30	Relative Contribution of Third Jacobi Polynomial to Ozone Profiles as a Function of Precursor Ratio for Various Initial NMHC Concentrations	137
31	Representative Dimensionless Ozone Profiles	138
32	Profile Shapes at Precursor Ratio of 4 for Various NMHC Concentrations	139
33	Delay Time Contours on the Logarithmic NMHC- $\text{NO}_x$ Plane for Surrogate	141
34	Graphs of First Three Orthonormal Polynomials	144



## LIST OF TABLES

<u>Table No.</u>	<u>Title</u>	<u>Page</u>
1	Research Proposed and Work Completed for ARB A6-172-30	12
2	Summary of the Ozone Profiles from the Mini-Surrogate Irradiations	17
3	Rate Constants for Reaction of OH Radicals with Organic Compounds Obtained Using the Modified Chamber Method	21
4	Gas-to-Particle Conversion Rates for Sulfur Dioxide in Photooxidizing Surrogate Mixture	22
5	Conditions Employed and Results of Smog Chamber Simulation Calculations	25
6	Experimental Conditions and 12-Hour Ozone Levels for Long-Term Irradiations	29
7	Parameter Estimates	31
8	Chemical and Physical Parameters Measured in Glass Chamber Studies	37
9	Mini-Surrogate Hydrocarbons and Their OH Radical Rate Constants	43
10	Initial Conditions for Mini-Surrogate Experiments	45
11	Summary of the Ozone Profiles from the Mini-Surrogate Irradiations	46
12	Parameter Estimates for Equation 2	50
13	Rate Constants $k_2$ for the Reaction of OH Radicals with Selected Alkanes at 300 K	61
14	Comparison of the Literature Room Temperature Rate Constants $k_2$ for $\geq C_3$ Alkanes with the Values Obtained in this Study and with Those Calculated from Equation 5	62
15	Rate Constants $k_2$ for the Reaction of OH Radicals with 2-Methyl-2-Butene and 2,3-Dimethyl-2-Butene at $300 \pm 1$ K, Together with the Available Room Temperature Literature Values	67



## LIST OF TABLES (continued)

<u>Table No.</u>	<u>Title</u>	<u>Page</u>
16	Rate Constants for $k_2$ for the Reaction of OH Radicals with Propene Oxide and 1-Butene Oxide at $300 \pm 1$ K	68
17	O( <sup>3</sup> P) Atom and OH Radical Room Temperature Rate Data for Reaction with Selected Nitrogen- and Oxygen-Containing Organics	70
18	Decay Data for Various Particle Sizes in the All-Glass Chamber During Irradiation and at Operating Temperature	75
19	Properties Assigned to Test Aerosol Particles in Deriving an Expression for Wall Loss as a Function of Particle Size	79
20	Data Used in Estimating Particulate Wall Losses from Electric Mobility Classification	80
21	Summarized Data on Sulfur Dioxide to Particle Conversion Rates Promoted by Photooxidizing Surrogate	85
22	Rate Constants Used in Discussion	86
23	Pollutant Concentration in Riverside Air	91
24	Composition of Surrogate Mixture for Simulation of Hydrocarbon Emissions in Los Angeles	95
25	Experimental and Calculated Ozone for Various Initial Surrogate Hydrocarbons and NO <sub>x</sub> Levels for Photolysis in the SAPRC Glass Chamber	100
26	Conditions Employed in Ambient Air Simulation Calculations	104
27	Calculated 1-Day Ozone Maxima for Various Initial Surrogate Hydrocarbon and NO <sub>x</sub> Levels Assuming Diurnal Solar Irradiation and an Absence of Chamber Effects	105
28	Initial Conditions for Long-Term Irradiations	117
29	Actinometry Data for Long-Term Irradiations	118



LIST OF TABLES (continued)

<u>Table No.</u>	<u>Title</u>	<u>Page</u>
30	Reactivity Data for Long-Term Irradiations	121
31	Experimental Conditions for Long-Term Irradiations Summarized According to Initial NMHC and NO <sub>x</sub> Levels	123
32	Parameter Estimates	145



## ACKNOWLEDGMENT

Stimulating discussion and valuable exchanges of technical information, for which we express our appreciation, took place at various times during this program with the following members of the California Air Resources Board staff:

Mr. Frank Bonamassa

Dr. Alvin O. Gordon

Dr. John R. Holmes

Mr. Tom Quinn

Dr. Jack K. Suder



## I. EXECUTIVE SUMMARY

In order to provide an experimental data base relating to major unresolved issues concerning photochemical smog formation, the SAPRC environmental chamber facility was designed and constructed (1970-73) with support from the California Air Resources Board. The facility was initially (1973-75) utilized in a study of oxidant formation from hydrocarbon-oxides of nitrogen (HC-NO<sub>x</sub>) mixtures irradiated under conditions simulating those found in the California South Coast Air Basin. Using a 12-hydrocarbon mixture as a surrogate for the ambient pollutant mix, HC and NO<sub>x</sub> concentrations ranging from those found in present-day polluted atmospheres down to those to be expected from the implementation of emission control strategies aimed at meeting the State and Federal ambient air quality standards were investigated.

It was found that under these simulated atmospheric conditions, an essentially constant hydroxyl (OH) radical concentration was maintained and it was possible to determine rate constants for the reactions of organics with the OH radical (when no other major loss processes were occurring). Thus, a large number of compounds, including some which were not amenable to study by more fundamental kinetic techniques, could be reliably studied and relative rate constants for reactions with OH determined using the chamber method. Taking advantage of the resulting extensive data base, a reactivity scale based on the reaction of organics with the OH radical was formulated last year.

The work undertaken in the present year and the results reported in this document are outlined in Table 1. A summary of the results for each sub-program is given in the following pages of the Executive Summary while Sections II-XI provide a detailed report of the work carried out.

### A. A Smog Chamber Study of the Correlation of Hydroxyl Radical Rate Constants with Ozone Formation (Section III)

The continued need for more rational and practical assessments of hydrocarbon reactivity for use in formulating control strategies has led to suggestions that OH radical reactivity be used as a criterion for predicting oxidant formation. In order for such a reactivity scale to have maximum utility, correlations between the rates of reaction of hydroxyl

Table 1. Research Proposed (in Renewal to ARB 5-385) and Work Completed for ARB A6-172-30

PROPOSED	RUNS	COMPLETED	RUNS
<p>A. Use of a mini-surrogate (alkane + alkene + aromatic) to study the relationship between rates of reaction with OH and amounts of ozone formed</p> <ol style="list-style-type: none"> <li>1. Substitute an isomeric compound with different OH rate constant at same concentration.</li> <li>2. Substitute isomer at different concentration so that reactivity (i.e. concentration x OH rate constant) is same</li> </ol>	4	<p>A. The mini-surrogate study has been carried out. Most of the effects of O<sub>3</sub> production were observed in the constant concentrations runs. Substitution of isopentane for n-pentane yielded almost identical NO<sub>2</sub> and O<sub>3</sub> time-concentration profiles, indicating that these two alkanes have very similar OH radical rate constants contrary to the literature. This was confirmed by experiments carried out under section C. Substitution of o- or p-xylene or ethylbenzene for m-xylene gave rise to a marked decrease in reactivity, more so than substitution of 1-butene for trans-2-butene or of neopentane + 1-butene for n-pentane + trans-2-butene. For the constant reactivity runs there is much less variation in O<sub>3</sub> profiles, the major exceptions being neopentane, p-xylene and ethylbenzene substitutions. Except for neopentane substitution, the maximum O<sub>3</sub> yields are essentially unaltered, showing that maximum O<sub>3</sub> does not appear to depend on the <u>amount</u> of carbon present.</p>	19
<p>B. Statistical analysis of existing smog chamber data to evaluate relationships between rates of consumption of organics and ozone formation</p> <ol style="list-style-type: none"> <li>1. Comparison of reactivity scales based on ozone formation with our OH reactivity scale</li> <li>2. Develop method(s) for weighting organic emissions on basis of their oxidant-forming potential</li> </ol>	-	<p>B. A general non-mathematical discussion of the relationship between the OH and O<sub>3</sub> reactivity scales was prepared in response to a letter to the editor of ES&amp;T. A mathematical treatment indicates that the relationship between OH reactivity and 6 hour O<sub>3</sub> yields can be expressed equally well for the available data by either (a) O<sub>3</sub> reactivity = 1 - e<sup>-kD</sup> where k is the OH rate constant and D a constant (dimensionally a radical dosage) or (b) O<sub>3</sub> reactivity = k/(k + B) where B is a constant (B = 1.43) for k relative to k for methane. Computer modeling studies of an n-butane system with a variable k for OH + n-butane leads to O<sub>3</sub> reactivity = k/(k + Ak<sup>1/2</sup> + B), but with the available data this is no improvement over the simple expressions given above.</p>	-
<p>C. Determination of OH rate constants using chamber relative rate method</p> <ol style="list-style-type: none"> <li>1. Glycol ethers (cellosolves)</li> <li>2. Olefin oxides</li> <li>3. Organic nitrates</li> </ol>	12	<p>C. Rate constants for the reaction of the OH radical with propane, isobutane, n-pentane, isopentane, neopentane, cyclopentane, 2,3-dimethyl-2-butene, propene oxide and 1-butene oxide have been obtained at 300 ± 1 K using the chamber technique. These rate data have resolved certain of the discrepancies in the literature, showing for instance that n-pentane and isopentane</p>	39

(continued)

Table 1. (Continued) - p.2

PROPOSED	RUNS	COMPLETED	RUNS
		have almost identical OH radical rate constants, as indicated by the mini-surrogate study (section A). Difficulties in the gas chromatographic analyses for the organic nitrates (ethyl, n-propyl, 2-butyl, 2-butyl, 2-pentyl, and 3-pentyl) and for methyl cellosolve precluded the determination of OH radical rate constant data for these organics.	
D. Photochemically-promoted formation of inorganic sulfate aerosol		D. Thermoelectric behavior of the sulfur flash ignition circuit of the sulfate analyzer was mathematically analyzed to aid circuit design. The circuit and cell were then designed, built, and calibrated. The TSI aerosol generator was employed to produce test aerosols for accurate chamber characterization and for use as seed aerosols. Irradiation experiments were then carried out in which SO <sub>2</sub> -to-sulfate conversion rates were determined as a function of initial HC and NO <sub>x</sub> levels.	
1. Development of sulfate analyzer	-		
2. Characterization of particulate lifetime as a function of size using monodisperse submicron aerosols	4		
3. Experimental program to determine effects of various potential control strategies for HC and NO <sub>x</sub> control or changes in ambient SO <sub>2</sub> levels on SO <sub>2</sub> conversion rates	18		
E. Monitoring of nitrate aerosol precursors, NH <sub>3</sub> and HNO <sub>3</sub> , in ambient air using 1-km pathlength multiple reflection cell with an FT-IR spectrometer	-	E. Long path Fourier transform infrared absorption spectroscopy has been used to monitor NH <sub>3</sub> and HNO <sub>3</sub> concentrations for three days during a stagnant air episode in October 1976 and for eight selected days during July, Spetember and October 1977. NH <sub>3</sub> concentrations were often in the range 20-40 ppb with maximum values as high as 130 ppb. HNO <sub>3</sub> concentrations were generally in the range 10-15 ppb with a maximum value of 20 ppb.	-
F. Application of a validated detailed computer kinetic model to assessment of oxidant-precursor relationships	12	F. Predicted six hour and nine hour O <sub>3</sub> yields, as calculated using a propene + n-butane model and a semi-detailed model, could be made consistent with most of the SAPRC glass chamber surrogate data if suitably adjusted values of the uncertain chamber effect parameters are used. Ambient air simulations were then carried out using these models with diurnally varying photolysis rates and the chamber effects removed. The effects on the model	
1. Validation of propene-butane model against surrogate chamber data			
2. Modification of model or approach as necessary			
3. Determination of light source and chamber parameters and modification of model for ambient applications			
4. Application of model to prediction of ozone formed from under a variety of conditions			

(continued)

Table 1. (Continued) - p.3

	PROPOSED	RUNS	COMPLETED	RUNS
			calculations of altering the light intensity and duration due to seasonal changes, of increasing the UV radiation by reducing stratosphere O <sub>3</sub> , of altering the emissions or dilution model, have been examined. In addition calculations were carried out duplicating the conditions employed by Dodge to generate O <sub>3</sub> isopleths, and these predictions were compared with those of Dodge. At the present time it appears that there are still too many uncertainties in the models for this combined smog chamber-modeling technique to be used with great confidence in developing control strategies for O <sub>3</sub> formation.	
1/4	G. Multiple day irradiation experiments for simulation of stagnant air episodes 1. Ambient air sample with and without addition of fresh pollutants on 2nd and 3rd days - in coordination with aerosol study 2. HC-NO <sub>x</sub> -SO <sub>2</sub> surrogate with and without added fresh pollutants on 2nd and 3rd day	4	G. A 3-day irradiation of an ambient air sample was carried out concomitant with the aerosol project experiment	1
	H. Ten-hour HC-NO <sub>x</sub> surrogate irradiation experiments for evaluation of ozone production and of hydrocarbon reactivity under long-term irradiation conditions 1. High HC and 6 NO <sub>x</sub> levels 2. Low HC and 6 NO <sub>x</sub> levels	12	H. Previous surrogate ozone data have been condensed into the form of an empirical relationship relating all ozone levels ≥0.05 ppm for an irradiation period of up to ten hours to irradiation time and initial precursor concentrations. The estimates of the parameters have been verified against the entire file of surrogate data (through 1976) using a non-linear parameter estimation procedures. A total of 24 long term irradiations have been conducted. The experiments were designed to meet both the needs of this section and those specified in F above to provide data for model validation.	24

(continued)

Table 1. (Continued) - p. 4

PROPOSED	RUNS	COMPLETED	RUNS
<p>I. Computer archiving of SAPRC-ARB oxidant-HC-NO<sub>x</sub> data base to facilitate model validation (see F) and dissemination of these data to others</p>	-	<p>I. Organization of the archive disc data set (ADDS) has been established, and the necessary programs for inputting data from previous runs organized in the old formats, correcting and editing the data on the data set, and for printing and plotting the data on the data set have been developed. Because of differences between organization of the data in the old format and the ADDS format, and because of special problems with some of the data, the process of archiving old runs is necessarily time-consuming. The detailed procedures for this process has been worked out, and representative runs have been archived. This overall process is currently underway, and is expected to be completed in several months. Following that, the ADDS data set will be transferred to tape for dissemination.</p>	-

radicals with organics and rates and levels of ozone formation must be established. To this end 9-hr irradiations of  $\text{NO}_x$ -hydrocarbon-air mixtures consisting of an alkane, an alkene and an aromatic were carried out in a 6400-l all-glass smog chamber. The "standard" mixture consisted of n-pentane, m-xylene and trans-2-butene, since the rate constants were known both for their reactions, and that of at least one isomer, with the OH radical. In one case the respective isomers were substituted sequentially at the same initial concentration and the effect of differences in OH rate constants on  $\text{O}_3$  production for constant carbon number was examined. In a second set of runs the initial concentrations of organics were changed so as to maintain constant the OH reactivity (i.e.,  $[\text{HC}] \times k_{\text{OH}}$ ). A summary of the ozone profile data for these experiments is given in Table 2. To a good approximation the rates of formation and yields of ozone in the earlier stages ( $\leq 6-9$  hours) of irradiation depended primarily on the OH radical reactivity and to a much lesser extent on the amount of carbon present.

B. Comparison of Reactivity Scales Based on Ozone Formation with the Hydroxyl Radical Reactivity Scale (Section IV)

In addition to the experimental study described in the previous section, a mathematical analysis of the correlations between the rates of reaction of hydroxyl radicals with organics and rates and levels of ozone formation has been carried out. Using the chamber data obtained by the General Motors, Shell, Battelle and Bureau of Mines Laboratories on formation of ozone from a wide variety of individual organic compounds, regression relationships have been derived.

Two requirements were imposed on the regression relationship: (a) the  $\text{O}_3$  reactivity must approach zero as the OH radical rate constant decreases and (b) the  $\text{O}_3$  reactivity must approach a constant value (taken to be unity in these calculations) for very large OH radical rate constants. Two simple regression relationships, (1) and (2), were found which are equally satisfactory in correlating the relatively imprecise experimental data.

$$R = 1 - e^{-kD} \quad (1)$$

$$R = k/(k + B) \quad (2)$$

Table 2. Summary of the Ozone Profiles from the Mini-Surrogate Irradiations

Run <sup>a</sup> Type Cpd.	O <sub>3</sub> (ppm)			O <sub>3</sub>		Comments <sup>b</sup>
	3 hr	6 hr	9 hr	Max (ppm)	Time (hr)	
Standard	0.376 ±0.014	0.479 ±0.019	0.500 ±0.010	0.493 ±0.020	8-9	
C iC <sub>5</sub>	0.379	0.471	0.479	0.479	8-9	Same reactivity
C p-X	0.185 ±0.029	0.342 ±0.031	0.440 ±0.007	---	---	Lower reactivity
C 1-C <sub>4</sub> <sup>=</sup>	0.344	0.471	0.476	0.479	7-9	Very slightly lower reactivity
C neoP/1-C <sub>4</sub> <sup>=</sup>	0.330	0.432	0.452	0.452	8.25-9	Slightly lower reactivity
C o-X	0.259	0.437	0.471	0.471	8.5-9	Lower reactivity
C eth B	0.117	0.225	0.325	---		Much lower reactivity
R neoP	0.483 ±0.012	0.551 ±0.006	0.549 ±0.009	0.556 ±0.002	5-9	Higher reactivity, more O <sub>3</sub>
R p-X	0.242	0.415	0.425	0.427	7.25-8.75	Lower reactivity
R 1-C <sub>4</sub> <sup>=</sup>	0.403	0.476	0.484	0.484	7.25-9	Very slightly higher reactivity
R o-X	0.388 ±0.005	0.466 ±0.002	0.478 ±0.002	0.478 ±0.002	8-9	Same reactivity
R eth B	0.213	0.381	0.418	0.420	8-9	Lower reactivity

<sup>a</sup>Type: C - constant concentration; R - constant reactivity

Cpd: Isomer(s) substituted in the standard mini-surrogate (n-pentane/trans-2-butene/m-xylene):  
 iC<sub>5</sub> = isopentane; p-X = p-xylene; 1-C<sub>4</sub><sup>=</sup> = 1-butene; neoP = neopentane; o-X = o-xylene;  
 eth B = ethylbenzene.

<sup>b</sup>Based primarily on the data for 3 and 6 hours of irradiation.

R is the six-hour ozone yield on a 0-1 scale and k is the OH radical rate constant. In (1), D is a constant which has the dimensions of a radical dosage. Its estimated value corresponds to a six-hour average concentration of  $\sim 10^6$  molecule  $\text{cm}^{-3}$ , the order of magnitude of observed chamber OH radical concentrations. In (2), B is a constant which is dimensionally a rate constant with an estimated value of  $1.43 \times 10^3$  if k is expressed relative to k for methane, or  $1.14 \times 10^{-11}$   $\text{cm}^3$  molecule $^{-1}$  sec $^{-1}$  on an absolute basis. The scatter of the experimental O<sub>3</sub> data obscures any advantages of one of these relationships over the other.

Most work was carried out using relationship (2) which was mathematically easier to apply. Relationship (2) and the scaled experimental data are shown in Figure 1. The scale factor, A, was estimated for the data from each laboratory as a part of the least squares computations carried out in deriving the parameters in the trial regression relationships. The scale factors  $A = Z/R$  (where Z is the observed O<sub>3</sub> six-hour yield for a given organic in a given laboratory) were: A = 0.44 ppm for Shell; 1.05 for Battelle; 0.98 for the Bureau of Mines; and 0.60 for General Motors. Equation (2) allows estimations of ozone reactivity to  $\pm 0.12$  on a 0-1 scale. Examination of the data reveals systematic deviations from the calculated curve according to the particular class of organic involved with alkanes tending to fall below the curve and alkenes above it.

For comparison, ozone reactivities were simulated using the SAPRC n-butane-NO<sub>x</sub>-air model with a varying OH + n-butane rate constant. The computer-simulated six-hour ozone reactivities precisely fit the equation

$$Z/0.576 = k/(k + 0.6054 k^{1/2} + 0.0138) \quad (3)$$

where Z is ozone concentration. Attempts to use a regression of the form of equation (3) to fit the chamber-derived ozone reactivities failed. There are at least three possible reasons for this. (1) The precision of the data is not sufficient to permit the evaluation of two parameters in addition to the four laboratory scale factors. (2) The least squares procedure used, based on linearization of the problem and approximate compensation for this by weighting, is not adequate. And (3) the form equation (3) is not appropriate when considering a multiplicity of different compounds which differ in details of their photooxidation mechanisms.

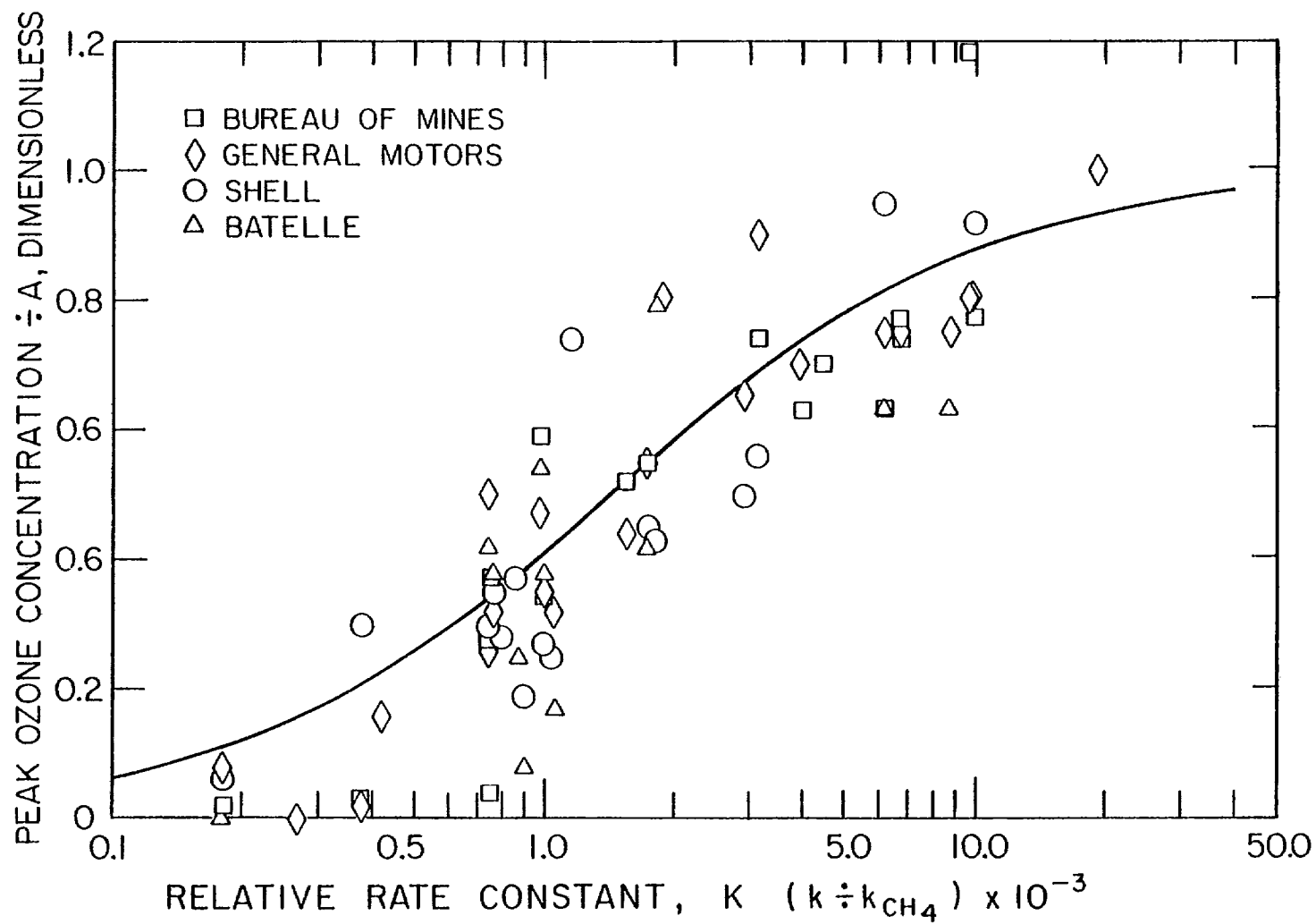


Figure 1. Relationship Between Peak Chamber Oxidant Observed at Four Laboratories and Experimentally Determined Rate Constants for Reactions with the Hydroxyl Radical (Photolyzable Organics Excluded).

In a separate analysis, we have treated a number of issues raised by Farley concerning relationships between hydrocarbon disappearance rates and oxidant maxima or hydroxyl reactivity and oxidant maxima. One result was a demonstration of good agreement between relative rates of hydrocarbon disappearance determined in the SAPRC all-glass environmental chamber with published rate constants for the reaction of hydrocarbons with OH radicals. These results are presented in Environmental Science and Technology (Pitts, et al., 1978) in tandem with Farley's note and will not be repeated here.

C. Rate Constants for the Reactions of Hydroxyl Radicals with Selected Organics (Section V)

For many organics, such as the alkanes, which do not react with ozone at significant rates or do not photolyze in the actinic region, reaction with the OH radical is essentially their sole loss process in the troposphere. With the increasing emphasis towards lowering the reactivity of the organics emitted from stationary sources and our development of a reactivity scale based upon the rates of reaction of organics with the OH radical, OH rate constant data are needed for additional selected organics which have not been adequately studied to date.

Utilizing a modification of the previously employed all-glass chamber technique (involving the use of a non-rigid Teflon bag inside the chamber to avoid loss of the organics via dilution) rate constants at  $300 \pm 1$  K have been determined for the reaction of the OH radical with 11 organics (Table 3).

The relative rates of disappearance of the organics in the chamber were placed on an absolute basis using either n-butane or cis-2-butene as the reference organic with a well established OH radical rate constant.

In addition, attempts were made to obtain rate constant data for five alkyl nitrates and two cellosolves; however, due to gas chromatographic analysis problems, no useful data could be obtained.

In general, the rate constants obtained are in reasonable agreement with the literature, where available, with two notable exceptions: (a) the rate constant obtained for n-pentane is almost a factor of two lower than the one available literature value, and is virtually identical with the rate constant for the reaction of OH radicals with isopentane, as

indicated by the mini-surrogate data (Section III), (b) the rate constant obtained for 2,3-dimethyl-2-butene is approximately a factor of 2 higher than a recent flash photolysis-resonance fluorescence value, suggesting wall losses of the 2,3-dimethyl-2-butene in the static reaction vessel used in that study.

Table 3. Rate Constants for Reaction of OH Radicals with Organic Compounds Obtained Using the Modified Chamber Method

Organic	$10^{12} \times k$ ( $\text{cm}^3 \text{ molecule}^{-1} \text{ sec}^{-1}$ )	Reference
Alkanes		
Propane	$1.59 \pm 0.22$	a
Isobutane	$2.52 \pm 0.05$	a
Neopentane	$1.04 \pm 0.17$	a
n-Pentane	$3.74 \pm 0.13$	a
Isopentane	$3.78 \pm 0.07$	a
Cyclopentane	$4.72 \pm 0.28$	a
2,3-Dimethylbutane	$5.67 \pm 0.29$	a
Alkenes		
2-Methyl-2-butene	$87 \pm 6$	b
2,3-Dimethyl-2-butene	$122 \pm 8$	b
Alkene Oxides		
Propene Oxide	$1.3 \pm 0.5$	b
1-Butene Oxide	$2.4 \pm 0.4$	b

<sup>a</sup>Darnall, Atkinson and Pitts, J. Phys. Chem., 82, 1581 (1978).

<sup>b</sup>Atkinson, Darnall, Lloyd, Winer and Pitts, Advan. Photochem., 11, 375 (1979).

D. Investigation of Rates of Conversion of Sulfur Dioxide to Sulfate Under Simulated Atmospheric Conditions (Section VI)

These experiments were done to determine the effects of various simulated control strategies on the rate of conversion of sulfur dioxide to particulate sulfate by a photooxidizing mixture of hydrocarbons and nitrogen oxides in 50% RH air. Experiments were carried out in the all-glass chamber lined with Teflon film to minimize wall effects and to exclude

exchange with room air. Irradiation was at 70% of maximum which has  $k_1 = 0.43 \text{ min}^{-1}$ . The hydrocarbon mixture used was the standard SAPRC surrogate mixture, and initial nitrogen oxides consisted of a 50-50 mixture of nitric oxide and nitrogen dioxide. The reference experimental mixture consisted of 1.4 ppmC of surrogate, 0.24 ppm  $\text{NO}_x$  and 0.094 ppm  $\text{SO}_2$ .

The experimental data obtained for various HC surrogate- $\text{NO}_x$  mixtures are summarized in Table 4. Sulfur dioxide conversion occurred at varying rates, and was faster during the first one to two hours of an experiment than during the remaining four to five hours. Since the transition was quite abrupt the rates are conveniently expressible as two rates of conversion accompanied by the time of transition and these are given in Table 4. The estimates of initial rates are more uncertain than those for final rates because the former are more greatly influenced by transient effects at the start of the experiment.

Table 4. Gas-to-Particle Conversion Rates for Sulfur Dioxide in Photo-oxidizing Surrogate Mixture

Exp. No. AGC	Surrogate (ppmC)	Nitrogen Oxides (ppm)	Sulfur Dioxide (ppm)	$\text{SO}_2$ Conversion Rates		Transition Time <sup>a</sup> (hrs)
				<u>Initial</u> (percent per hr)	<u>Final</u> (percent per hr)	
341	1.66	0.249	0.094	6.8	2.0	1.5
342	1.45	0.258	0.133	2.9	0.9	1.5
347	0.99	0.377	0.130	0.9	0.3	1.5
348	1.38	0.060	0.030	3.2	1.3	1
349	0.69	0.121	0.039	1.2	0.7	1
350	0.34	0.041	0.014	0.8	0.5	2
338	1.48	0.222	0.080	3.1	1.6	2
340	1.04	0.211	0.082	3.1	1.8	1.5
343	1.50	0.018	0.344	1.7	0.6	1

<sup>a</sup>See text.

The results suggest that for a given HC surrogate level, high or low nitrogen oxides concentrations suppress SO<sub>2</sub> conversion while a general reduction of the primary pollutants at constant ratio reduces the conversion rate approximately in proportion.

These experiments are discussed in greater detail in Section VI. In obtaining the data summarized in Table 4 a considerable effort was expended to characterize the all-glass chamber with respect to aerosol lifetimes and to develop methods of data reduction. The more detailed discussion includes discussion of the chemical kinetic implications of these data.

#### E. Monitoring of Nitrate Aerosol Precursors (Section VII)

Ammonia, emitted from agricultural and industrial sources in the South Coast Air Basin is thought to play an important role in the stabilization of nitric acid as ammonium nitrate aerosol. High levels of particulate nitrates have been measured in the eastern end of the South Coast Air Basin and characterization of ambient concentrations of both NH<sub>3</sub> and HNO<sub>3</sub> are important in understanding mechanisms of gas-to-particle conversion. Only recently has routine monitoring of these nitrogenous compounds in ambient air become possible, using long path Fourier transform infrared absorption spectroscopy. Using this technique, ambient air monitoring of NH<sub>3</sub> and HNO<sub>3</sub> at Riverside has been carried out on a continuing basis.

The NH<sub>3</sub> and HNO<sub>3</sub> concentrations were monitored for three days during a stagnant air episode in October, 1976, and for eight selected days during July, September and October, 1977. It was found that NH<sub>3</sub> levels of ~20-40 ppb are common with much higher levels (i.e. ~100 ppb) possible since Riverside is normally downwind of agricultural sources of ammonia. HNO<sub>3</sub> levels were generally in the range 5-15 ppb with maximum levels of ~20 ppb. On several occasions (October 6, 1976; September 9, 1977; and October 26, 1977) NH<sub>3</sub> and HNO<sub>3</sub> were observed to co-exist at appreciable levels, while at other times there appeared to be an anticorrelation. Further monitoring of ammonia and nitric acid concentrations in the South Coast Air Basin is underway to attempt to further refine our understanding of the relationship between gaseous NH<sub>3</sub> and HNO<sub>3</sub>, and particulate ammonium nitrate.

F. Assessment of Oxidant-Precursor Relationships Utilizing a Computer Kinetic Model (Section VIII)

A quantitative understanding of how ozone formation in photochemical air pollution is affected by changes in emissions of its hydrocarbon and nitrogen oxides precursors is necessary for the formulation of cost-effective oxidant control strategies. One technique, referred to as the empirical kinetic modeling approach (EKMA), involves validating a computer kinetic model against smog chamber data, and then using the suitably modified model to calculate oxidant-precursor relations appropriate for ambient air conditions. Although this technique is currently under active investigation by the EPA, we believe that an independent study of this method, with different assumptions concerning poorly understood chamber effects, and using a different data base for model validation would be a useful test of the overall consistency of the predictions of this method.

In our study, the extensive SAPRC-ARB hydrocarbon surrogate-glass chamber data base was employed for model validation. Results of over 50 irradiations were used, with initial nonmethane hydrocarbon (NMHC) levels ranging from ~0.4 to ~2.4 ppmC and with initial total oxides of nitrogen (NO<sub>x</sub>) ranging from 0.005 to 0.5 ppm. The experimental conditions and detailed tabulations of results are given in our previous reports to the ARB.

The kinetic models employed in this study are based on a detailed propene + n-butane-NO<sub>x</sub>-air photooxidation mechanism which has been developed at SAPRC to be consistent with current basic kinetic and mechanistic chemical data and with the well characterized smog chamber experiments carried out at SAPRC using the evacuable chamber facility. This model was applied to a surrogate hydrocarbon mixture in two ways. In the propene + n-butane model, all the reactive hydrocarbons in the surrogate mixture were represented by propene, n-butane and formaldehyde. Formaldehyde represented all oxygenated hydrocarbons initially present, and the other reactive organics were represented by propene and n-butane, with concentrations chosen so that the propene + n-butane mixture had the same ppmC and the same OH reactivity (i.e. the sum of the initial hydrocarbon concentrations x the OH + hydrocarbon rate constants) as the hydrocarbon mixture they represented. The semi-detailed model was less

approximate in that the initial consumption reactions of all the reactive organics were treated separately; but it was assumed that the subsequent reactions following the initial attack of the organic by OH, O<sub>3</sub> or O(<sup>3</sup>P) for all hydrocarbons of the same type (alkane, alkene or aromatic) were the same. Both models had exactly the same inorganic and chamber-dependent mechanisms. The major chamber-dependent portions of our model concern:

- (a) The photolysis rate constants
- (b) Radical input from unknown chamber sources
- (c) The N<sub>2</sub>O<sub>5</sub> + H<sub>2</sub>O → 2HNO<sub>3</sub> reaction
- (d) Ozone destruction on the walls

Four sets of chamber simulation calculations were done, three employing the propene + n-butane model with varying chamber-dependent parameters and one employing the semi-detailed model. The conditions and qualitative descriptions of the fit to the experimental O<sub>3</sub> yields as a function of initial hydrocarbon/NO<sub>x</sub> ratios are given in Table 5.

Table 5. Conditions Employed and Results of Smog Chamber Simulation Calculations

Label	Hydrocarbon Model <sup>a</sup>	Radical Input <sup>b</sup>	k(N <sub>2</sub> O <sub>5</sub> +H <sub>2</sub> O)	Fits to O <sub>3</sub> <sup>d</sup>	
				High HC/NO <sub>x</sub>	Low HC/NO <sub>x</sub>
A <sub>1</sub>	P + B	0.15	0	very low	OK
B <sub>1</sub>	P + B	0.30	0	OK	OK-low
B <sub>2</sub>	P + B	0.30	max <sup>c</sup>	low	OK-low
C <sub>1</sub>	SD	0.30	0	OK	OK-low

<sup>a</sup>P + B = propene + n-butane model used; SD = semi-detailed model used.

<sup>b</sup>The values given are constant hydroxyl input rates in ppb min<sup>-1</sup>.

<sup>c</sup>The maximum rate constant for N<sub>2</sub>O<sub>5</sub> + H<sub>2</sub>O is taken to be 2 x 10<sup>-5</sup> ppm<sup>-1</sup> min<sup>-1</sup>, based on results of Morris and Niki (1973).

<sup>d</sup>"OK" = calculated O<sub>3</sub> fit the data to within experimental variability.

"Low" = calculated O<sub>3</sub> significantly lower than experimental. See Section VIII for quantitative results.

It can be seen from Table 5 that the ozone predictions of both the propene + n-butane model and the semi-detailed model are similar, and that the ozone predictions of both models can be made consistent with most of the surrogate-glass chamber data, if suitably adjusted values of the uncertain chamber-effect parameters are used. Specifically, better fits are obtained if it is assumed that hydroxyl radical input rates are significant and increase with increasing initial  $\text{NO}_x$  and that the  $\text{N}_2\text{O}_5 + \text{H}_2\text{O}$  reaction is negligible. This is consistent with our results in modeling evacuable chamber experiments.

Ambient Air Simulations. Calculations were performed using diurnally varying photolysis rates with the chamber effects removed. The effects of season, stratospheric  $\text{O}_3$  level, dilution rate and emissions model were examined. In addition, in order to obtain a more clear-cut comparison of our EKMA model predictions with those of the EPA, calculations (designated "DS") were done duplicating the conditions employed by Dodge to generate the EPA's published calculated ozone isopleths for the ambient air.

The results of these calculations are presented in Section VIII, and are summarized briefly below.

- The nature of  $\text{O}_3$ -NMHC- $\text{NO}_x$  relationships calculated for the ambient air case are significantly different from those calculated for smog chamber conditions. In general, the  $\text{O}_3$  yields are somewhat less sensitive to initial hydrocarbon levels and much less sensitive to initial  $\text{NO}_x$  levels in the smog chamber simulations, and the  $\text{NO}_x$  levels for which maximum  $\text{O}_3$  is obtained (for a given NMHC level) is significantly higher. Therefore, raw smog chamber results should not be directly applied to predicting oxidant-precursor relations for the ambient air.

- The propene + n-butane and the semi-detailed models gave similar results, although the semi-detailed model predicts ~20% lower  $\text{O}_3$  levels than the propene + n-butane model. This suggests that the formulation of  $\text{O}_3$  control strategies may not be as sensitive to details of the hydrocarbon oxidation mechanisms as may initially be expected.

- It appears to be invalid to assume a single set of  $\text{O}_3$ -NMHC- $\text{NO}_x$  relationships can be applied independently of solar lighting conditions. Not only do the ozone yields calculated using light intensities and durations appropriate for the summer increase relative to those calculated for the spring/fall equinox, but the dependence of these yields on initial  $\text{NO}_x$

also changes. A similar effect is observed in calculations which assume enriched UV intensity due to significant reductions in stratospheric O<sub>3</sub>.

- The nature of the O<sub>3</sub>-NMHC-NO<sub>x</sub> relationships does not appear to be strongly influenced by dilution rates or details of the emissions models. Except at the highest NO<sub>x</sub>/NMHC ratios, models assuming continuous pollutant emission give predictions similar to those which assume full initial loading, provided both models would give the same primary pollutant dose if they did not react.

- There appears to be a significant discrepancy between the predictions of our model and those of the Dodge model concerning the dependence of O<sub>3</sub> on initial NO<sub>x</sub> concentrations. The Dodge model predicts that the NO<sub>x</sub> values which result in maximum O<sub>3</sub> formation for given hydrocarbon levels are significantly greater than those predicted by our model, and also that the dependence of these values on the hydrocarbon levels is much greater. The exact reasons for this discrepancy are unknown, but it is probably due in large part to the fact that the models treat important chamber effects differently.

With the current state of our knowledge, it appears that the model predictions of the maximum O<sub>3</sub> formation potential for a given NMHC level are much more reliable than predictions of the dependence of O<sub>3</sub> on initial NO<sub>x</sub>. In order to improve this situation, additional modeling studies are required to more clearly identify which of the many uncertain aspects of chamber-consistent models most strongly affect ambient air simulations, and more experimental studies are required to elucidate these critical areas. At the present time, the most important uncertainties probably concern chamber effects. The discrepancies between the existing models and their attendant uncertainties indicate that the combined smog chamber-modeling technique must presently be used with great caution in developing oxidant control strategies.

#### G. Long-Term and Multiple Day Smog Chamber Irradiations (Section IX)

Long-Term Irradiations. In previous years a large number (~130) of surrogate hydrocarbon-NO<sub>x</sub>-air irradiations have been carried out under controlled conditions and at constant light intensities. These irradiations constitute a portion of the data base which is a necessary prerequisite to

the development of a validated chemical computer model and which is useful in the formulation of  $\text{NO}_x$ -NMHC precursor relationships for  $\text{O}_3$  formation. This previous SAPRC surrogate data base consists of six-hour irradiations of  $\text{NO}_x$ -hydrocarbon-air mixtures using several discrete NMHC levels (0.4, 0.7, 1.4, and 2.2 ppmC) and various  $\text{NO}_x$  levels. In order to extend the data base from six-hour irradiations at constant light intensity to twelve-hour irradiation with diurnal variation of light intensity, a series of long-term experiments was conducted. Twelve-hour irradiations at four selected NMHC- $\text{NO}_x$  ratios (using two of the NMHC levels employed in the previous studies) were carried out, both with constant light intensity and with a quasi-diurnal light intensity. Duplicate irradiations were carried out for several of these to check reproducibility, and the effects of varying constant light intensity, chamber temperature, and relative humidity were investigated. A summary of the experimental conditions, including initial  $\text{NO}_x$  and NMHC levels, light intensity, temperature, and relative humidity is given in Table 6.

Briefly, the results may be summarized as follows.

- A standard run (2.2 ppm NMHC, 0.19 ppm  $\text{NO}_x$ , 85°F, 50% RH) carried out with constant light intensity (70% of maximum) four times during the course of this study gave 12 hour ozone yields which were in agreement to within  $\pm 5\%$  ( $0.37 \pm 0.02$  ppm) (see Table 6). A replicate pair of the standard runs carried out with diurnal variation of light intensity also agreed to within  $\pm 5\%$ . Repeats of two other runs at constant light intensity gave excellent agreement (better than  $\pm 3\%$ ). Repeats of a run with lower (0.8 ppm) initial NMHC with diurnal variation of light intensity gave more scattered results ( $\pm 20\%$ ).

- Time-concentration profiles for ozone production from diurnal variation versus constant (70%) light intensity gave, as expected, curves of significantly different shapes. However, at any given time after 6 hours of irradiation the ozone concentrations differ by no more than  $\sim 0.05$  ppm at the higher NMHC level and  $\sim 0.025$  ppm at the lower NMHC level. Thus, in the latter half of a 12-hour smog chamber day, the ozone produced by a pseudo-diurnal variation of intensity is within 20% (30% if variation observed from duplicate experiments is included) of that produced for constant light intensity at 70% of maximum. This gives an indication of the uncertainty associated with using the previously obtained, constant

Table 6. Experimental Conditions and 12 Hour Ozone Levels for Long-Term Irradiations

Initial Concentration (ppm)			Light Intensity <sup>b</sup> (% max)	Temp. <sup>c</sup> (°F)	RH <sup>c</sup> (%)	Run No.	O <sub>3</sub> at 12 hr (ppm)
Surrogate NMHC <sup>a</sup>	NO <sub>x</sub>	NMHC/NO <sub>x</sub>					
2.4 <sup>d</sup>	0.22	11	100	93	50	228, 230	0.564, 0.561
			100	93	22	232	0.572
			100	93	2	231	0.562
			di	93	50	229	0.459
2.2	0.19	12	70	85	50	310, 312, 316, 323	0.351, 0.386 0.361, 0.352
			70	85	15	324	0.403
			70	95	50	318	0.42
			di	85	50	311, 322	0.347, 0.386
			85	85	50	315	0.400
			100	85	50	317	0.465
2.2	0.11	20	70	85	50	320, 328	0.322, 0.312
			di	85	50	321	0.325
0.8	0.19	4	70	85	50	313	0.182
			di	85	50	314, 327	0.154, 0.102
0.8	0.11	7	70	85	50	325	0.215
			di	85	50	326	0.188

<sup>a</sup>Surrogate NMHC are the hydrocarbons in the surrogate mixture as monitored in the chamber at the beginning of the run and do not include trace aldehydes, ketones, and nonsurrogate HC.

<sup>b</sup>di = pseudo-diurnal variation over 12 hrs; timer controlled.

<sup>c</sup>Approximate values; precise data are given on data sheets in the archives.

<sup>d</sup>Preliminary runs (228-232); diurnal variation was done manually and is not the same intensity profile as that of remaining runs.

light intensity data base for application to ambient conditions. In addition, these experiments provide a data base for model validation using diurnal variation of light intensity.

- Effects of varying relative humidity were slight, a slower initial rate of ozone formation occurring at lower RH. Substantial effects were seen for increasing temperature or constant light intensity. Approximately a 20% increase in final ozone concentration occurs for a  $10^{\circ}\text{F}$  increase in temperature and a ~30% increase occurs for an increase in light intensity from 70% to 100% of maximum.

Multiple-Day Irradiation. In conjunction with the aerosol study conducted in the SAPRC outdoor bag a three-day irradiation of an ambient air mixture has been carried out in the all-glass chamber. Data are included in the archives (Run No. AGC-270).

H. Assessment of Oxidant-Precursor Relationships Utilizing an Empirical Mathematical Approach (Section X)

Our previously obtained HC surrogate-ozone data have been condensed into the form of an empirical relationship relating all ozone levels  $\geq 0.05$  ppm for an irradiation period of up to 10 hours to various initial precursor concentrations. The estimates of parameters have been verified against the file of surrogate data (through Run No. 156) using a non-linear parameter estimation procedure.

The surrogate ozone profiles have been mathematically analyzed with respect to the precursor  $\text{NO}_x$  and non-methane hydrocarbon (NMHC) concentrations in two time segments: (a) the delay time  $t_D$  before the start of ozone production and (b) the time after the onset of ozone production. The delay time  $t_D$  can be suitably represented by

$$t_D = \frac{N}{(p_1 + p_3 N^2) + r(p_2 + p_4 N^2)}$$

Here  $t_D$  = delay time in hours;  $N$  = initial  $\text{NO}_x$  concentration in ppm;  $C$  = initial NMHC concentration in ppm;  $r$  = precursor ratio  $C/N$ , and the  $p$ 's are adjustable parameters. The values of  $p_1$  and  $p_4$  as estimated by least squares analysis of the data are given in Table 7.

Table 7. Parameter Estimates

Parameter	Estimate	Parameter	Estimate
1	+0.19973 ppm hr <sup>-1</sup>	10	-0.18800
2	-0.00084 ppm <sup>2</sup> ppmC <sup>-1</sup> hr <sup>-1</sup>	11	+0.56240 ppmC <sup>-1</sup> ppm <sup>-1</sup>
3	-1.06170 ppm <sup>-1</sup> hr <sup>-1</sup>	12	+0.06460 ppmC <sup>2</sup> ppm <sup>-1</sup>
4	+0.29840 ppmC <sup>-1</sup> hr <sup>-1</sup>	13	+3.69020 ppmC <sup>2</sup> ppm <sup>-2</sup>
5	-0.07330 ppm	14	-1.76140 ppmC <sup>3</sup> ppm <sup>-2</sup>
6	+0.39970 ppm <sup>1/2</sup> ppmC <sup>1/2</sup>	15	+0.07330
7	+1.10180 ppm <sup>1/2</sup> ppmC <sup>-1/2</sup>	16	-1.27478 ppmC ppm <sup>-1</sup>
8	-0.68760	17	+0.18066 ppmC <sup>2</sup> ppm <sup>-1</sup>
9	-1.22600 ppmC <sup>-1/2</sup>	18	+3.71376 ppmC <sup>2</sup> ppm <sup>-2</sup>
		19	-1.07172 ppmC <sup>3</sup> ppm <sup>-2</sup>

After the NO to NO<sub>2</sub> conversion period, each ozone profile can be accurately represented by three numbers A<sub>0</sub>, A<sub>1</sub> and A<sub>2</sub>. The trends of these numbers with precursor concentrations have been investigated and empirical representations found which allow estimation of the ozone concentrations from the precursor concentrations with a standard error of ±0.06 ppm:

$$\begin{aligned}
 A_0 &= p_5 + 1/\sqrt{r}[p_6 + p_7C] + 1/r[p_8C + p_9C^{3/2}] \\
 A_1/A_0 &= p_{10} + 1/r[p_{11} + p_{12}/C] + 1/r^2[p_{13} + p_{14}/C] \\
 A_2/A_0 &= p_{15} + 1/r[p_{16} + p_{17}/C] + 1/r^2[p_{18} + p_{19}/C]
 \end{aligned}$$

Table 7 shows estimates of the parameters p<sub>5</sub> to p<sub>19</sub> along with "units" required to rationalize the dimensions of A<sub>0</sub>, A<sub>1</sub> and A<sub>2</sub>. The quantity [A<sub>0</sub><sup>2</sup> + A<sub>1</sub><sup>2</sup> + A<sub>2</sub><sup>2</sup>]<sup>1/2</sup> measures overall trends in ozone concentration over a period of around ten hours, and is best regarded as a root mean square (rms) estimate of the average ozone concentrations for a 10-hour period. Its dependence on precursor concentration is shown in Figure 2. The salient features are: (1) at high precursor ratios (>16 ppmC ppm<sup>-1</sup> NO<sub>x</sub>) the rms ozone increases monotonically with increasing primary pollutant concentrations, implying decreasing ozone on dilution; (2) at lower ratios, ozone first increases, then decreases, with increasing

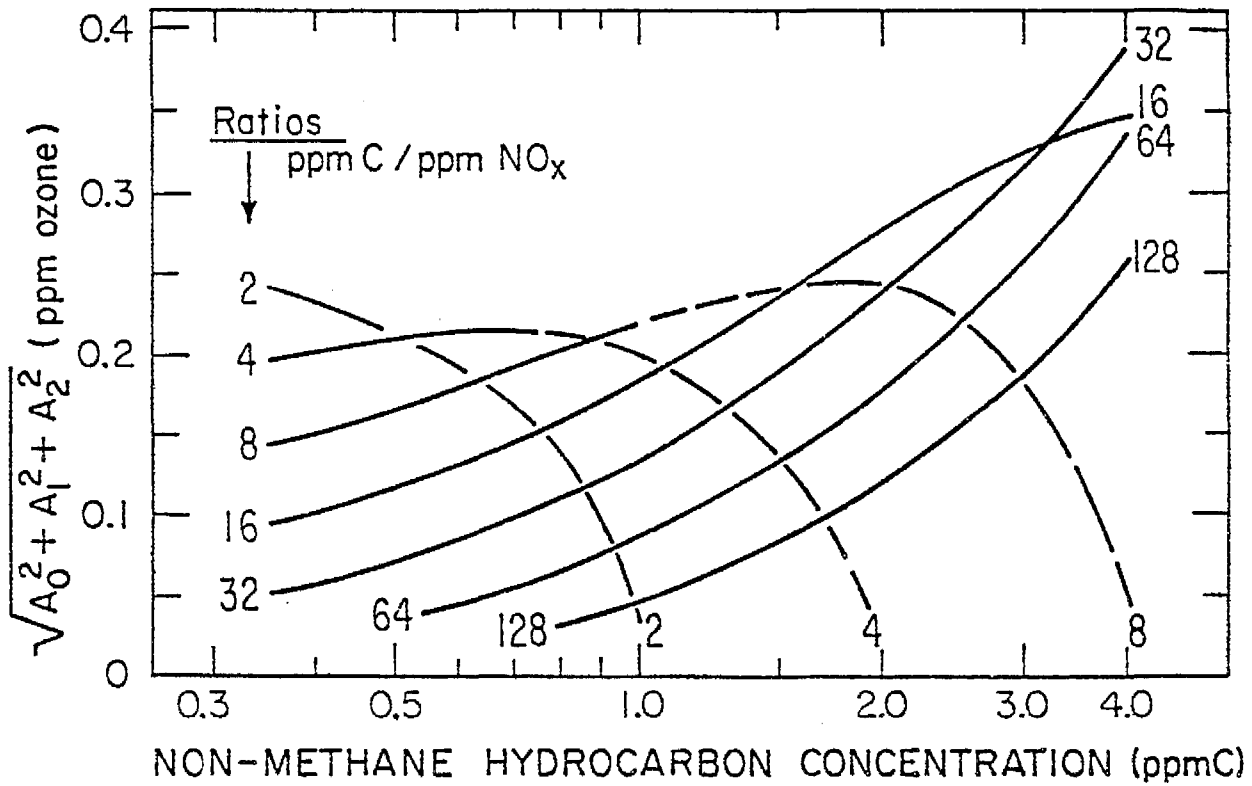


Figure 2. Root Mean Square Ozone Concentrations at Various Precursor Ratios as Functions of Initial NMHC Concentrations.

primary pollutant concentrations and each ratio has a corresponding NMHC concentration producing the maximum rms ozone for the ratio. For example, from Figure 2 we have the optimum ratio, NMHC concentration pairs (16, >4 ppmC) (8, 1.9 ppmC), (4, 0.75 ppmC), (2, <0.4 ppmC) with rms ozone maxima increasing with the ratio.

The behavior at lower ratios and higher precursor concentrations has important implications for downwind oxidant control and the effects of NO<sub>x</sub> reductions for this situation. Dilution of these pollutant mixtures can lead to increased rms ozone levels with the major contributions to the mean being at long irradiation times (see discussion of profile shapes, Section X). Reduction of nitrogen oxides to increase the ratio is always helpful for these cases, although it can concurrently increase ozone levels at moderate dilutions.

I. Computer Archiving of SAPRC/ARB Surrogate Hydrocarbon-NO<sub>x</sub>-Air Data Base (Section XI)

Under previous contracts with the ARB we have provided detailed chemical and physical data for more than 150 surrogate hydrocarbon-NO<sub>x</sub>-air smog chamber irradiations, amounting to a data base of over 50,000 individual values. Although these data are available in the previous progress reports in printed form, such a large data base can only be efficiently and effectively utilized with the aid of a computer. For this reason, these data are being archived in computer-readable formats so that they can be disseminated on computer tapes and can be employed to maximum potential by any workers with access to appropriate computing facilities.

This project has been divided into four major tasks. (1) Definition of the organization of the data as it will be used on the computer; (2) processing and storing of all the data under that organization; (3) writing and debugging of the programs for retrieving the data from the direct access data set; and (4) definition of the organization of the data as it is to be stored on tape for dissemination, and writing and debugging of the programs required to move the data to the tape from the direct access data set, and vice-versa.

At the present time, tasks (1) and (3) are largely complete, and task (2), converting the data into the archive disc data set format is

currently in progress. This has become the most time-consuming task in this project because of the large number of runs which must be archived. Moreover, the variety of ways in which the past data have been treated produces a variety of problems which require case-by-case examination before archiving. The procedures for treating these problems have been worked out, and progress is being made in converting the data for the individual smog chamber runs. However, this extremely time-consuming task will take several additional months. The final task of this project, (4), converting the data to computer tape format for dissemination, is still in the planning stage; but its completion is not expected to be particularly difficult, once all the data is available on the direct access disc data set.

## II. FACILITIES AND METHODS

### A. Chamber Facility and Analytical Methods

The experiments in this study were carried out in a 6400-liter (226 ft<sup>3</sup>), all-glass (Pyrex) chamber (Pitts et al., 1975c; 1976d) which has a surface-to-volume ratio of 3.4 m<sup>-1</sup> (1.04 ft<sup>-1</sup>). The dimensions of the glass chamber are 8' x 8' x 4' (i.e., a flat box). Photolyzing radiation is provided by two externally mounted, diametrically opposed banks of forty Sylvania 40-W BL (black light) lamps, which are backed by arrays of Alzak-coated reflectors. The supporting analytical facilities employed in the glass chamber studies are shown schematically in Figure 3 and are described in detail below.

The current physical and chemical measurement methods and the range, precision, and accuracy of measurement of each of these parameters are given in Table 10. The details of the analytical and data processing procedures are described below for each species or variable monitored. The data obtained are computer-processed and have not been corrected for losses due to sampling from the chamber.

OZONE (O<sub>3</sub>) was monitored by ultraviolet absorption analyzers (Dasibi-1003 or AH-1003). Until January 1976, these instruments were calibrated against 2% neutral buffered potassium iodide (AIHL, 1969). Since it has been demonstrated (Pitts et al., 1976c; ARB, 1975) that at ~50% RH this calibration procedure yields ozone values which are too high by a factor of ~1.25, all ozone data obtained prior to January 1976 have been corrected by a factor of 0.8. In January 1976 the instruments were respanned using the UV absorption method adopted by the ARB in June, 1973.

NITROGEN OXIDES (NO, NO<sub>2</sub>, and NO<sub>x</sub>) were monitored by chemiluminescent detection (TECO 14B). The NO<sub>2</sub> and NO<sub>x</sub> modes of this and similar chemiluminescent NO-NO<sub>x</sub> analyzers have been shown to respond quantitatively to other nitrogen-containing compounds, such as peroxyacetyl nitrate (PAN) and organic nitrates and nitrites (Winer et al., 1974, Spicer and Miller, 1974). All NO<sub>2</sub> and NO<sub>x</sub> data reported here have been corrected by subtraction of measured or interpolated PAN concentrations.

SULFUR DIOXIDE (SO<sub>2</sub>) was monitored by the pulsed fluorescence method (TECO 43). Approximate calibrations were obtained using chamber samples. A more precise calibration was carried out using a Monitor Labs model

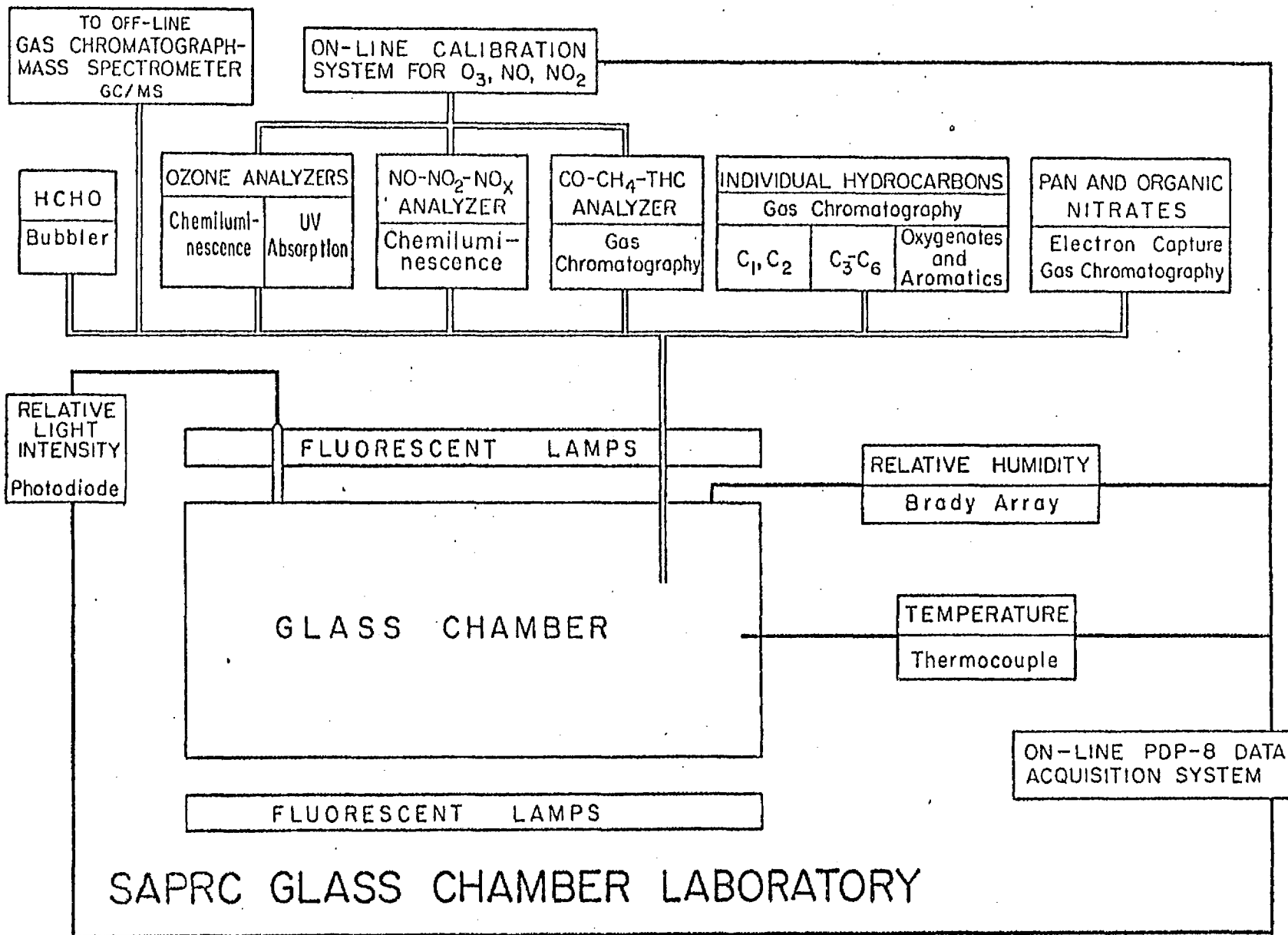


Figure 3. Schematic Drawing of All-Glass Chamber Facility.

Table 8. Chemical and Physical Parameters Measured in Glass Chamber Studies

Parameter	Range	Method	Sampling Rate	Precision	Accuracy
Ozone	0-20 ppm	UV Absorption Analyzer	570 ml/min	± 0.005 ppm	± 5%
NO	0-10 ppm	Chemiluminescent Analyzer	895 ml/min	± 2% F.S.	± 5%
NO <sub>2</sub>	0-10 ppm			By difference	By difference
NO <sub>x</sub>	0-10 ppm			± 2% F.S.	± 5%
SO <sub>2</sub>	0-5 ppm	Pulsed Fluorescence	1000 ml/min	± 0.005 ppm	± 5%
PAN	>1 ppb	GC		± 0.5 ppb	± 10%
Formaldehyde	>10 ppb <sup>a</sup>	Chromotropic Acid	1 l/min (30 min samples)	± 5%	± 10%
Individual HCs	0.5-1 ppb	GC		± 15%	Limited by calibration standard (typically ± 5%) and/or by sampling techniques
	1-2 ppb	GC		± 10%	
	>2 ppb	GC		± 2%	
CO	0-10 ppm	GC	100 ml/min	± 2% F.S.	± 10%
Temperature	15° to 40°C	Thermometer		± 0.02°C	± 0.5°C
		Thermocouple		± 0.1°F	± 2°F
Light Intensity	0-1 Solar Constant Relative	NO <sub>2</sub> Actinometry		± 5%	b
		Photodiode			
Relative Humidity	0-100%	Brady Array		± 1% RH	± 5%

<sup>a</sup> Determined by practical values of sampling time and flow rate

<sup>b</sup> See discussion on page 9.

8500 permeation-type calibrator.

CARBON MONOXIDE (CO) was monitored by gas chromatography (Beckman-6800). The instrument was calibrated daily with a standard gas sample.

PEROXYACETYL NITRATE (PAN) was monitored by gas chromatography with electron capture detection (GC-ECD) (Darley et al., 1963; Stephens and Price, 1973). Samples were taken in a 100-ml precision bore syringe and transferred to the GC sampling system as quickly as possible. Peak heights were read from the strip chart and converted to concentration units using a calibration function which was determined periodically.

FORMALDEHYDE (HCHO) was monitored using the chromotropic acid method (Smith et al., 1970). Air from the chamber was drawn through a bubbler at the rate of 1 l min<sup>-1</sup> and the total volume per sample was determined using a timer-controlled shutoff system. Generally, a 30-min. sample was taken. The concentration was recorded at the midpoint of this time interval, except for the initial value, which was taken in the 30 minutes prior to lights on, and the final sample, which was taken in the 30 minutes prior to lights off. Absorbances were read on a Bausch and Lomb Spectronic 20, and calculations of the HCHO concentration from the absorbance and volume of air samples (HCHO vol) were made from the following equation:

$$\text{HCHO (ppm)} = \frac{\text{HCHO } (\mu\text{g}) \times 2.037}{\text{HCHO (vol)}}$$

where HCHO ( $\mu\text{g}$ ) is taken from the least squares fit of the experimentally determined calibration function of HCHO ( $\mu\text{g}$ ) vs. absorbance.

The SAMPLE TEMPERATURE was read from either a Doric Thermocouple indicator ( $^{\circ}\text{F}$ ), using a thermocouple suspended in the chamber (TS2), or from a 19-35 $^{\circ}\text{C}$  (0.01 degree/division) thermometer hung free inside the chamber close to the end window, but not in the direct light path (TS1).

RELATIVE HUMIDITY (RH) was measured using a Brady array (Thunder Scientific). The response in volts (V) was converted to percent RH, using the calibration function supplied by the manufacturer.

HYDROCARBONS (HC) were monitored by gas chromatography with flame ionization detection (GC-FID), using the columns and methods developed by Stephens and Burlison (1969; Stephens, 1973). Methane and C<sub>2</sub> HC's were analyzed using a 5' Poropak N Column, C<sub>3</sub>-C<sub>6</sub> HC's using a 36' 2,4-dimethyl sulfolane column, and aromatics and oxygenates using a special

three-part column. Oxygenates were also monitored using a 10' Carbowax 600 column. Each GC was calibrated frequently using specially prepared sample (Stephens and Burleson, 1969). Computer processing of the data includes calculation of the concentration in ppbC for each data point.

#### B. Experimental Procedures

Following each experiment in this program, the glass chamber was flushed with dry air provided by an air purification system (Doyle et al., 1977) (see Figure 4) for about 2 hours at a flow of ~12 cfm. The chamber was then flushed with humidified pure air for about one hour just prior to the start of a run to achieve the desired initial RH. The temperature of the chamber prior to turning on the lamps was adjusted to the operating temperature anticipated during the irradiation by means of infrared lamps. During all flushing procedures, the two sonic pumps were in operation to provide maximum release of materials from the chamber walls.

The matrix air used during the flushing procedure and for the final fill for the experiment generally contained less than a total 60 ppbC of all hydrocarbons except methane, which was typically at a concentration between 550-850 ppb (Doyle et al., 1977). After completion of filling, analysis of the matrix air prior to injections showed somewhat higher hydrocarbon values due to off-gassing from the chamber walls, but generally these values were less than 200 ppbC nonmethane hydrocarbon.

Following flushing, starting materials were injected by using 100-ml precision bore syringes or micropipettes, and rapid mixing was obtained by brief (~5 minutes) use of the sonic pumps. During the run, the sample temperature was controlled at  $32 \pm 2^{\circ}\text{C}$  by means of a variable air flow past the chamber walls.

Light intensity ( $k_1$ ) was periodically determined, using the method of Holmes et al. (1973) which employs the initial rate of  $\text{NO}_2$  photolysis in  $\text{N}_2$  as a measure of absolute photon flux in the glass chamber in the actinic region (300-450 nm). However, some  $\text{O}_2$  (of order tens of ppm or higher) will be present in the chamber which cannot be evacuated, but instead must be flushed repeatedly with  $\text{N}_2$ . Oxygen present in concentrations greater than approximately 10 ppm will lead to somewhat low values

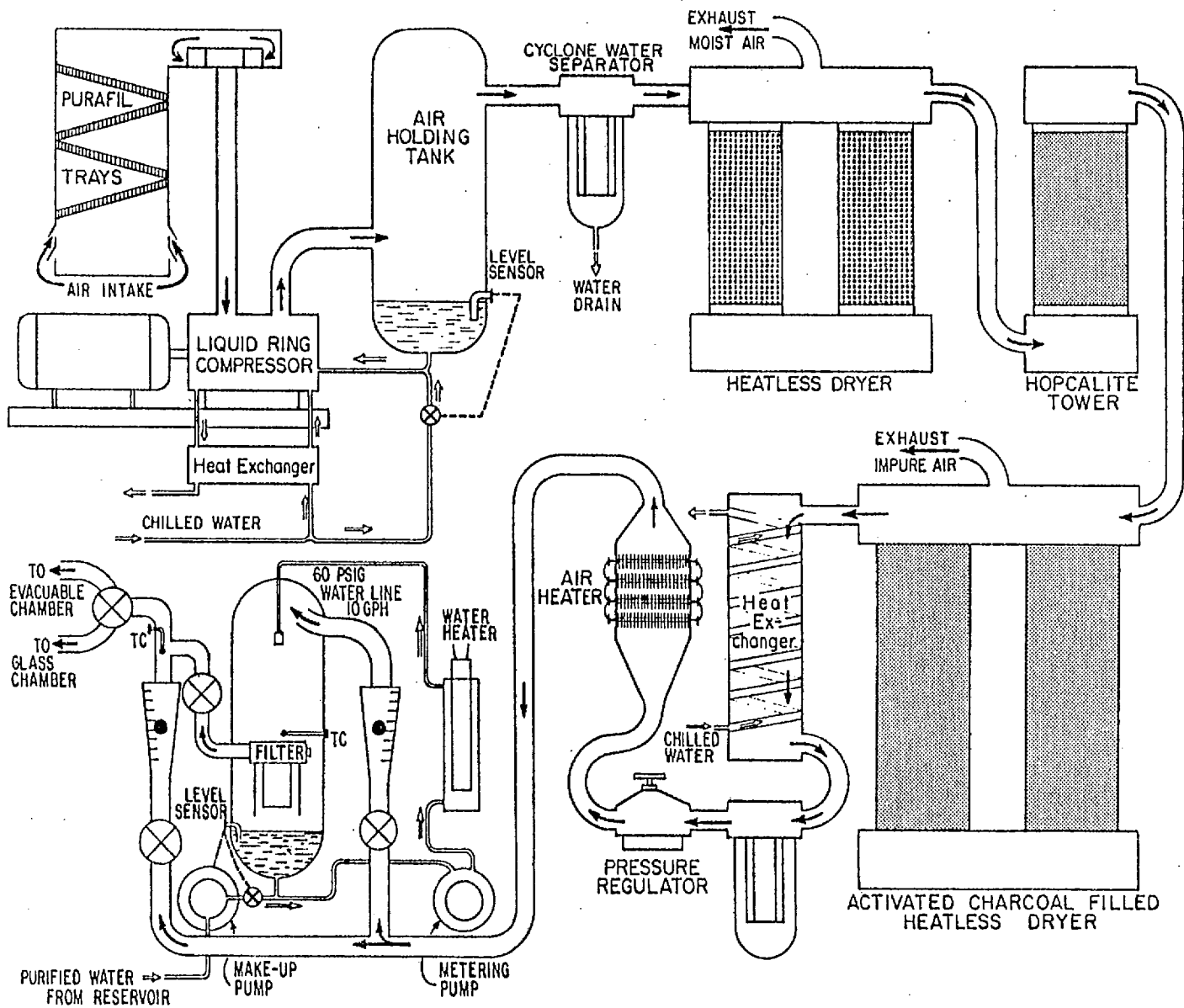


Figure 4. Air Purification System.

for  $k_1$  which would be observed for the complete absence of  $O_2$ . Based on the purity of the nitrogen used (with respect to oxygen content) and a calculated efficiency for repetitive flushing of the chamber, it is estimated that the observed  $k_1$  could be as much as 25% low with respect to the true  $k_1$ .

At full light intensity  $k_1$ 's of  $0.41 \text{ min}^{-1}$  (Oct. 25, 1976) and  $0.43 \text{ min}^{-1}$  (Sept. 9, 1977) were obtained. The oxygen concentration within the chamber was measured during the latter experiment and found to be of the order of 200-250 ppm. Based on the Holmes et al. (1973) analysis, this suggests that the actual  $k_1$  should be approximately  $0.5 \text{ min}^{-1}$ .

Half-lives for ozone decay, measured at various times in this program under standard conditions of temperature, relative humidity, and light intensity, were  $\geq 25$  hours in the dark and 12 to 15 hours with irradiation. These half-lives are significantly longer than those reported for other chambers with comparable dimensions, surface to volume ratios, and light intensities and result in correspondingly smaller perturbations on ozone rates of formation and maximum ozone concentrations in the glass chamber experiments.



### III. A SMOG CHAMBER STUDY OF THE CORRELATION OF HYDROXYL RADICAL RATE CONSTANTS WITH OZONE FORMATION

Recently a reactivity classification for organics has been formulated based on the rates of reaction of the OH radical with these organics (Darnall et al., 1976b; Pitts et al., 1976a; 1977b). This is derived from the knowledge that in most cases (i.e., for alkanes and aromatics) the major loss process in polluted urban atmospheres is via reaction with the OH radical. However, the degree to which such a reactivity classification reflects changes in reactivity as measured by ozone production, the major phenomenon of photochemical air pollution, has not been quantitatively investigated to date.

In order to investigate the relationship between rates of reaction with OH and rates and amounts of ozone formed, a matrix of nine-hour, NO<sub>x</sub>-hydrocarbon-air irradiations has been carried out using a mini-surrogate consisting of one alkene, one alkane and one aromatic. The compounds were chosen such that rate constants for both their reactions, and that of at least one isomer, with the hydroxyl radical are known. Two types of experiments were conducted with the mini-surrogate, one in which the the respective isomers were substituted sequentially at the same initial concentration, and the effect of differences in OH rate on ozone production for constant carbon number were examined, and the second in which the concentrations were changed so as to keep constant the reactivity (i.e., the product of concentration times the OH rate constants).

Experimental. Experiments were carried out in the all-glass chamber, using the general procedures and analytical methods described in Section II. During the runs the sample temperature was controlled at  $303 \pm 1$  K by means of a variable air flow past the chamber walls. The light intensity, based on the method of Holmes et al. (1973) for the determination of  $k_1$ , was estimated to be  $\sim 0.4 \text{ min}^{-1}$  for these experiments.

Results. Table 9 shows the alkenes, alkanes and aromatics used in the mini-surrogate-NO<sub>x</sub>-air irradiations and their rate constants for reaction with the OH radical as obtained from an evaluation of the literature. The mini-surrogate was originally designed to have equal amounts of reactivity contributions from each class, i.e.,  $k_{\text{alkane}}^{\text{OH}} [\text{alkane}] = k_{\text{alkene}}^{\text{OH}} [\text{alkene}] = k_{\text{aromatic}}^{\text{OH}} [\text{aromatic}]$ , with a total concentration of  $\sim 5000$  ppbC. However,

with the newer rate constant data obtained subsequent to this study (see Section V), the reactivity contribution of the standard mini-surrogate alkane dropped from ~33% to ~23%, with the alkene and aromatic then contributing ~39% of the total hydrocarbon reactivity each.

Two sets of experiments were carried out: a) type C runs, where the respective isomers were substituted sequentially in the mini-surrogate at the same initial concentration, thus maintaining a constant HC/NO<sub>x</sub> ratio and b) type R runs, where the isomers were substituted sequentially but with their concentrations changed so as to maintain the  $k_{\text{HC}}^{\text{OH}}[\text{HC}]$  constant.

Table 9. Mini-Surrogate Hydrocarbons and Their OH Radical Rate Constants

Hydrocarbon in Standard Mini- Surrogate	$10^{12} \times k$ (cm <sup>3</sup> molecule <sup>-1</sup> sec <sup>-1</sup> )		Isomer	$10^{12} \times k$ (cm <sup>3</sup> molecule <sup>-1</sup> sec <sup>-1</sup> )	
	a	b		c	b
n-Pentane	6.2	(3.7)	Isopentane	3.1	(3.8)
			Neopentane	0.8 <sup>d</sup>	(1.0) <sup>b</sup>
trans-2-Butene	70 <sup>e</sup>		1-Butene	35 <sup>e</sup>	
m-Xylene	24 <sup>f</sup>		p-Xylene	15 <sup>f</sup>	
			o-Xylene	14 <sup>f</sup>	
			Ethylbenzene	7.5 <sup>c</sup>	

<sup>a</sup>Wu, Japar and Niki, Environ. Sci. Health, A11, 191 (1976).

<sup>b</sup>Values in parentheses were obtained from a determination of the rate constants k for a series of alkanes subsequent to the design of this study [Darnall, Atkinson and Pitts, J. Phys. Chem., 82, 1581 (1978)].

<sup>c</sup>Lloyd, Darnall, Winer and Pitts, J. Phys. Chem., 80, 789 (1976).

<sup>d</sup>Greiner, J. Chem. Phys., 53, 1070 (1970).

<sup>e</sup>Atkinson and Pitts, J. Chem. Phys., 63, 3591 (1975).

<sup>f</sup>Perry, Atkinson and Pitts, J. Phys. Chem., 81, 296 (1977).

Table 10 gives the initial conditions for these experiments, while Table 11 summarizes the NO<sub>2</sub> and O<sub>3</sub> profile data--including averaging the standard run (five of which were carried out) and other duplicate runs. As can be seen from the low standard deviations obtained on the data from experiments for which replicate runs were carried out (Table 11), the reproduceability of the the experiments was very good.

Discussion. Table 11 contains brief comments as to the reactivity of the differing mini-surrogate systems relative to that for the standard mixture. The following points may be noted:

1) Substitution of isopentane for n-pentane results in an almost identical time for NO<sub>2</sub> maximum and an almost identical O<sub>3</sub> time concentration profile. This is totally consistent with the subsequent observation (Darnall et al., 1978) that n-pentane and isopentane have essentially identical rate constants for reaction with the OH radical at  $300 \pm 1$  K (Table 9).

2) Most of the major effects on the reactivity are observed in the constant concentration (type C) runs, as may be expected. Furthermore, the reactivity trends in the type C runs are totally in line with the trend of the OH radical rate constants (Table 9).

3) As n-pentane and isopentane have the same reactivity towards OH, neopentane was substituted for isopentane. The only type C run carried out for neopentane was, in fact, a double substitution as it was a neopentane/1-butene/m-xylene surrogate mixture. However, by reference to Table 11 it can be seen that this mixture was somewhat less reactive than the n-pentane/1-butene/m-xylene mixture which may be regarded as the "standard" for this particular run. This may well imply some additivity to the reactivity versus OH rate constant relationship.

4) Substitution of o-xylene, p-xylene or ethylbenzene for m-xylene gives rise to a marked decrease in reactivity--more so than substitution of 1-butene for trans-2-butene (which has approximately the same relative decrease in  $k_{\text{hydrocarbon}}^{\text{OH}}$ ). In addition, it may be noteworthy that the o-xylene run is more reactive than the p-xylene run even though these two xylenes have very similar OH radical rate constants. Obviously there are other factors involved beyond merely the OH rate constants.

5) For the constant reactivity runs, there is much less variation

Table 10. Initial Conditions for Mini-Surrogate Experiments

No.	Run <sup>a</sup>		NO (ppm)	NO <sub>x</sub> (ppm)	NO <sub>2</sub> /NO <sub>x</sub>	Butene (ppm)	Pentane (ppm)	Xylene (ppm)	Neopentane (ppm)	HCHO (ppm)
	Type	Cpd.								
246		Stand.	0.203	0.243	0.160	0.050	0.576	0.144	0.018	0.0
247	C	iC <sub>5</sub>	0.206	0.249	0.169	0.046	0.754	0.142	0.018	0.010
248	C	p-X	0.192	0.230	0.170	0.049	0.560	0.151	0.016	0.036
254	C	1-C <sub>4</sub> <sup>=</sup>	0.205	0.243	0.160	0.044	0.482	0.153	0.016	0.046
255	C	neoP/1-C <sub>4</sub> <sup>=</sup>	0.206	0.249	0.189	0.045	0.486	0.144	see C <sub>5</sub>	0.058
256		Stand.	0.209	0.249	0.165	0.046	0.494	0.145	0.017	0.020
257	R	p-X	0.210	0.254	0.177	0.050	0.519	0.300	0.018	0.024
258	R	1-C <sub>4</sub> <sup>=</sup>	0.207	0.249	0.165	0.093	0.522	0.148	0.017	0.038
259	R	neoP	0.208	0.245	0.151	0.047	4.018	0.155	see C <sub>5</sub>	0.0
260		Stand.	0.211	0.248	0.145	0.048	0.516	0.145	0.018	0.010
261	C	p-X	0.211	0.249	0.157	0.050	0.518	0.159	0.017	0.0
262	C	o-X	0.200	0.243	0.181	0.046	0.518	0.157	0.017	0.020
263	R	neoP	0.209	0.248	0.157	0.050	2.771	0.150	see C <sub>5</sub>	0.001
264	R	o-X	0.200	0.243	0.173	0.052	0.524	0.262	0.017	0.003
265		Stand.	0.194	0.244	0.205	0.052	0.547	0.141	0.017	0
266	C	eth B	0.205	0.239	0.146	0.049	0.539	0.154	0.016	0.017
267	R	eth B	0.205	0.243	0.152	0.052	0.561	0.437	0.018	0.006
268		Stand.	0.206	0.241	0.145	0.050	0.566	0.160	0.018	0.003
269	R	o-X	0.206	0.247	0.166	0.053	0.565	0.277	0.018	0.0

<sup>a</sup>Type: C - constant concentration; R - constant reactivity

Cpd: Isomer(s) substituted in the standard mini-surrogate (n-pentane/trans-2-butene/m-xylene): iC<sub>5</sub> = isopentane; p-X = p-xylene; 1-C<sub>4</sub><sup>=</sup> = 1-butene; neoP = neopentane; o-X = o-xylene; eth B = ethylbenzene.

Table 11. Summary of the Ozone Profiles from the Mini-Surrogate Irradiations

Run <sup>a</sup> Type Cpd.	O <sub>3</sub> (ppm)			O <sub>3</sub>		Comments <sup>b</sup>
	3 hr	6 hr	9 hr	Max (ppm)	Time (hr)	
Standard	0.376 ±0.014	0.479 ±0.019	0.500 ±0.010	0.493 ±0.020	8-9	
C iC <sub>5</sub>	0.379	0.471	0.479	0.479	8-9	Same reactivity
C p-X	0.185 ±0.029	0.342 ±0.031	0.440 ±0.007	---	---	Lower reactivity
C 1-C <sub>4</sub> <sup>=</sup>	0.344	0.471	0.476	0.479	7-9	Very slightly lower reactivity
C neoP/1-C <sub>4</sub> <sup>=</sup>	0.330	0.432	0.452	0.452	8.25-9	Slightly lower reactivity
C o-X	0.259	0.437	0.471	0.471	8.5-9	Lower reactivity
C eth B	0.117	0.225	0.325	---		Much lower reactivity
R neoP	0.483 ±0.012	0.551 ±0.006	0.549 ±0.009	0.556 ±0.002	5-9	Higher reactivity, more O <sub>3</sub>
R p-X	0.242	0.415	0.425	0.427	7.25-8.75	Lower reactivity
R 1-C <sub>4</sub> <sup>=</sup>	0.403	0.476	0.484	0.484	7.25-9	Very slightly higher reactivity
R o-X	0.388 ±0.005	0.466 ±0.002	0.478 ±0.002	0.478 ±0.002	8-9	Same reactivity
R eth B	0.213	0.381	0.418	0.420	8-9	Lower reactivity

<sup>a</sup>Type: C - constant concentration; R - constant reactivity

Cpd: Isomer(s) substituted in the standard mini-surrogate (n-pentane/trans-2-butene/m-xylene):  
 iC<sub>5</sub> = isopentane; p-X = p-xylene; 1-C<sub>4</sub><sup>=</sup> = 1-butene; neoP = neopentane; o-X = o-xylene;  
 eth B = ethylbenzene.

<sup>b</sup>Based primarily on the data for 3 and 6 hours of irradiation.

in O<sub>3</sub> profiles--the only exceptions being for neopentane, p-xylene and ethylbenzene (for neopentane, use of the lower OH radical rate constant may have overestimated the reactivity). Except for neopentane, the maximum O<sub>3</sub> yields are essentially unaltered, showing that maximum O<sub>3</sub> does not appear to depend on the amount of carbon present.

6) PAN yields and rates of formation are in very good agreement with the O<sub>3</sub> yields and rates of formation and show that PAN may also be used as a reactivity indicator.

In conclusion, the above data show that the major effect on O<sub>3</sub> yields and formation rates arises from OH radical reactivity and not from the amount of carbon present.

Computer kinetic modeling of these irradiations was carried out using the SAPRC propene/n-butane model (Carter et al., 1979). By adjusting the propene/n-butane ratio and their concentrations, both the overall OH radical reactivity and the total carbon concentrations were made equal to the mini-surrogate reactivity and carbon concentration. The calculated three-hour O<sub>3</sub> yields and the maximum O<sub>3</sub> concentrations generally showed the same trends with substitution (for both constant concentration and constant reactivity) as the experimental data. However, the calculated O<sub>3</sub> profiles yielded ~30% higher final O<sub>3</sub> concentrations than the experimental data. This can be readily explained by neglect of the reaction of RO<sub>2</sub> + NO yielding alkyl nitrates for the pentanes (Darnall et al., 1976a) in the computer model. Inclusion of such termination reactions would lead to a substantial reduction in O<sub>3</sub> yield, especially at longer irradiation times. In addition, the use of such a simplified model to simulate experiments involving aromatics may well lead to larger errors.

However, in view of the same trends in both the computer model calculations and the experimental data, further work will be carried out, including the development of a model realistically involving the pentanes.

#### IV. COMPARISON OF REACTIVITY SCALES BASED ON OZONE FORMATION WITH THE HYDROXYL REACTIVITY SCALE

It has been proposed that the rate constant for reaction of a compound with the hydroxyl radical (OH) is a useful index of organic reactivity in polluted urban atmospheres (Darnall et al., 1976b; Pitts et al., 1976a; 1977b). This proposed reactivity classification requires careful validation to make it useful for pollution control decisions. One approach to such a validation is to quantify the relationship of the OH reactivity scale to the empirical reactivity scales currently used for control purposes. The ozone (or oxidant) reactivity scale is the most important empirical scale because it is directly related to the manifestation to be controlled and because it is the major justification for those selective control rules now in effect.

The Empirical Ozone Reactivity Scale. The current ozone reactivity scale is based on relative values of maximum ozone concentrations observed within a fixed period of chamber irradiation. Most laboratories contributing data to establishing the scale have fixed the period at around six hours, although there have been some studies involving longer irradiations. The rationale of an empirical test of this sort requires rigidly fixed conditions resulting in an emphasis on the popular six-hour irradiation. In most cases precursor concentrations used are a few ppm (molar) of the compound under test and a precursor molar ratio around 2, based on an early estimate of the morning DOLA ratio during severe smog episodes. The test is tailored for the Los Angeles area and is intended to simulate a worst case air parcel along a short trajectory such as DOLA to Pasadena and environs.

It is necessary to combine data from several laboratories to build up a comprehensive scale, since each laboratory had differing objectives in their tests, e.g., Battelle concentrated on solvents while the Bureau of Mines looked at exhaust hydrocarbons. However, there is general agreement between laboratories on the relative ranks of overlapping compounds with some exceptions. Absolute values of observed ozone concentrations for the same compound differ widely between laboratories, an effect attributable to wide differences in smog chambers and experimental procedure. To reconcile data from different laboratories, the technique of

ratioing ozone concentrations to the ozone concentration observed in testing toluene has been used, thus assigning toluene an ozone index of one for all laboratories. However, this placed undue emphasis on the precision of data for toluene and a better method of reconciling ozone data from different laboratories seems a necessary preliminary to relating the scales. In this work the toluene standard was abandoned in favor of assigning scale factors to the laboratories. Values for the factors are estimated as part of the least squares computations associated with estimating parameters of various trial regression relationships. This requires rejection of data from laboratories contributing sparse or narrowly grouped data, since a meaningful estimate of the scale factor cannot be made in these cases. This requirement rules against accepting the SRI data on solvents, which is also unacceptable on the grounds of non-standard precursor concentrations and ratio. Data from the laboratories of General Motors, Shell, Bureau of Mines, and Battelle are used to establish an oxidant scale in these calculations.

Two reasonable requirements were imposed on trial regression relationships, it must approach zero ozone reactivity as the rate constant decreases and it must approach a constant value for very large rate constants. In calculations this upper limit is taken as one, an inconsequential choice for the validity of the calculations.

The first relationship tried was

$$\frac{Z_{ij}}{A_i} = 1 - e^{-\lambda K_j} \quad (1)$$

where  $Z_{ij}$  is the ozone concentration observed at laboratory  $i$  for compound  $j$ ,  $A_i$  is the laboratory scale factor,  $K_j$  the hydroxyl rate constant for compound  $j$  and  $\lambda$  a parameter to be determined. Equation 1 was fairly successful in describing the mean trend of ozone reactivity with rate constant. An interesting aspect of equation 1 is that the estimate of  $\lambda$  (dimensionally a radical dosage) corresponds to a time averaged OH concentration near  $10^6 \text{ cm}^{-3}$  for six hours which is of the order of magnitude of estimated OH radical concentrations in smog chambers.

To date, most correlative work has been done using the simpler relationship

$$\frac{Z_{ij}}{A_i} = \frac{K_j}{K_j + B} \quad (2)$$

where the  $A_i$  and  $B$  (dimensionally a rate constant) are the parameters to be determined. Computationally, equation 2 requires less effort than equation 1, which requires successive approximations to estimate the parameters. The scatter of ozone data about the regression is sufficient to obscure any advantages one relationship may have over the other. Figure 5 shows the regression curve (minimum rms percent error) and the data. The parameter estimates are given in Table 12.

Table 12. Parameter Estimates for Equation 2

Laboratory	$A_i$		B	
	ppm	Toluene Equiv.	Relative to Methane $\times 10^{-3}$	$\text{cm}^3 \text{sec}^{-1}$ $\times 10^{+11}$
Shell	0.44	3.36		
Battelle	1.05	2.39	1.43	1.14
B of M	0.98	2.71		
GM	0.60	1.99		

These values allow estimation of ozone reactivity to a  $\pm 0.12$  standard error of estimate when reactivity is scaled from 0 to 1. Correlation between estimates and the ozone data divided by the  $A_i$ 's is +90%. The values of the scale factors are noteworthy. They suggest that toluene normalization is only mildly successful in reconciling data and are nearly equal for the very similar chambers at Battelle and the Bureau of Mines.

Detailed analysis of the oxidant data revealed no significant difference between data from the four laboratories in conforming to the regression. However, some barely resolvable differences due to compound type were found. The t-test indicated that reactivity data for alkanes and alkenes are somewhat better represented by correcting the regression values. For alkanes the indicated correction is to take 75% of the regression reactivity and reduce it by 0.07. For alkenes 67% of the regression value incremented by 0.24 is a better representation of the data. Arenes conform closely to the regression reactivities. However, statistical

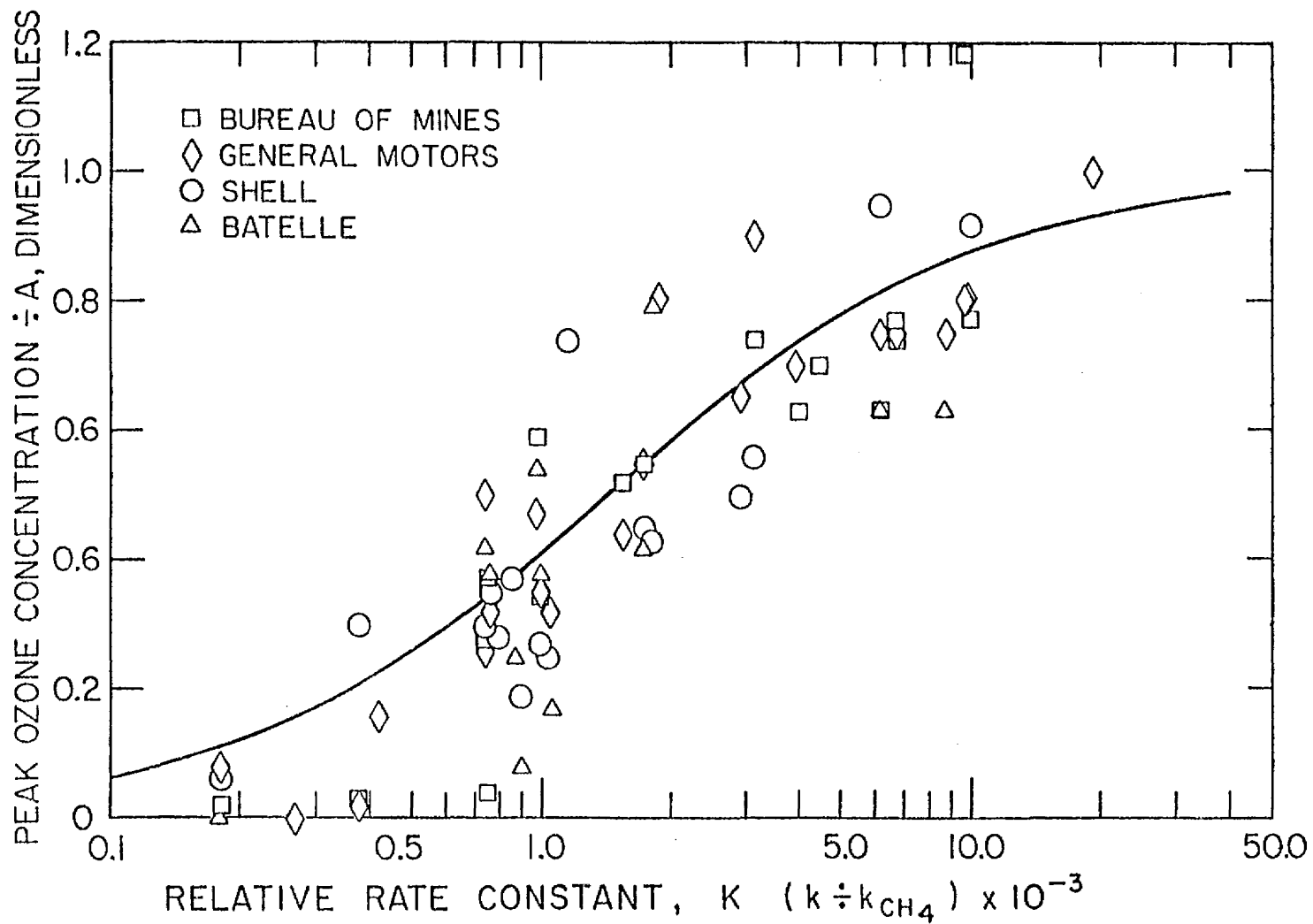


Figure 5. Relationship Between Peak Chamber Oxidant Observed at Four Laboratories and Experimentally Determined Rate Constants for Reactions with the Hydroxyl Radical (Photolyzable Organics Excluded).

confidence in the values of these corrective constants and indeed, in the existence of these deviations from the regression is not high. They would not be quoted if there were not independent evidence that behavior of this sort is reasonable.

The oxidant reactivity data includes many ketones, some alcohols, some acetate esters, and a few miscellaneous compounds. For these compounds reaction rate measurements are sparse. Reactivities were predicted from estimated rate constants (Atkinson, 1977) and compared with the scaled oxidant data. Since estimated rate constants have an estimated geometric deviation of two from the correct value, these estimated reactivities are fairly uncertain. Only the ketone data indicated a fairly significant deviation from the regression values. As a group they seem less reactive than predicted; only methyl t-butyl ketone (3,3-dimethyl-2-butanone or pinacolone) seems much more reactive than predicted from its low estimated rate constant. However, since only three of the 13 ketones considered have measured rate constants, this behavior could be partly due to systematic over-estimation of the rates.

Model Simulations of Ozone Reactivity Data. The SAPRC model for butane in a chamber environment (Carter et al., 1979) was used to calculate 12-hour ozone profiles using various assigned rate constants for the reaction of n-butane with the hydroxyl radical. One ppm of hydrocarbon was assumed as the initial concentration and results were obtained at two precursor ratios, 2 and 10. This results in precise ozone reactivity data and elucidates the probable effect of irradiation time and ratio on ozone reactivity. Figure 6 shows ozone reactivity plotted against logarithmic rate constant for these simulations at the 2:1 ratio (solid curves) and the 10:1 ratio (dashed curve). The ten to one results are not dependent on irradiation times in excess of four hours, since the profiles peaked out at or before that time.

As irradiation period increases, the relationship between simulated ozone reactivity and rate constant becomes less abrupt and apparently approaches a quasilinear relationship to the logarithms of the rate constant. The limiting curve for 2:1 will resemble the 10:1 curve. These results suggest a very gradual variation of oxidant reactivity with rate constant for the longer irradiation times required by realistic atmospheric

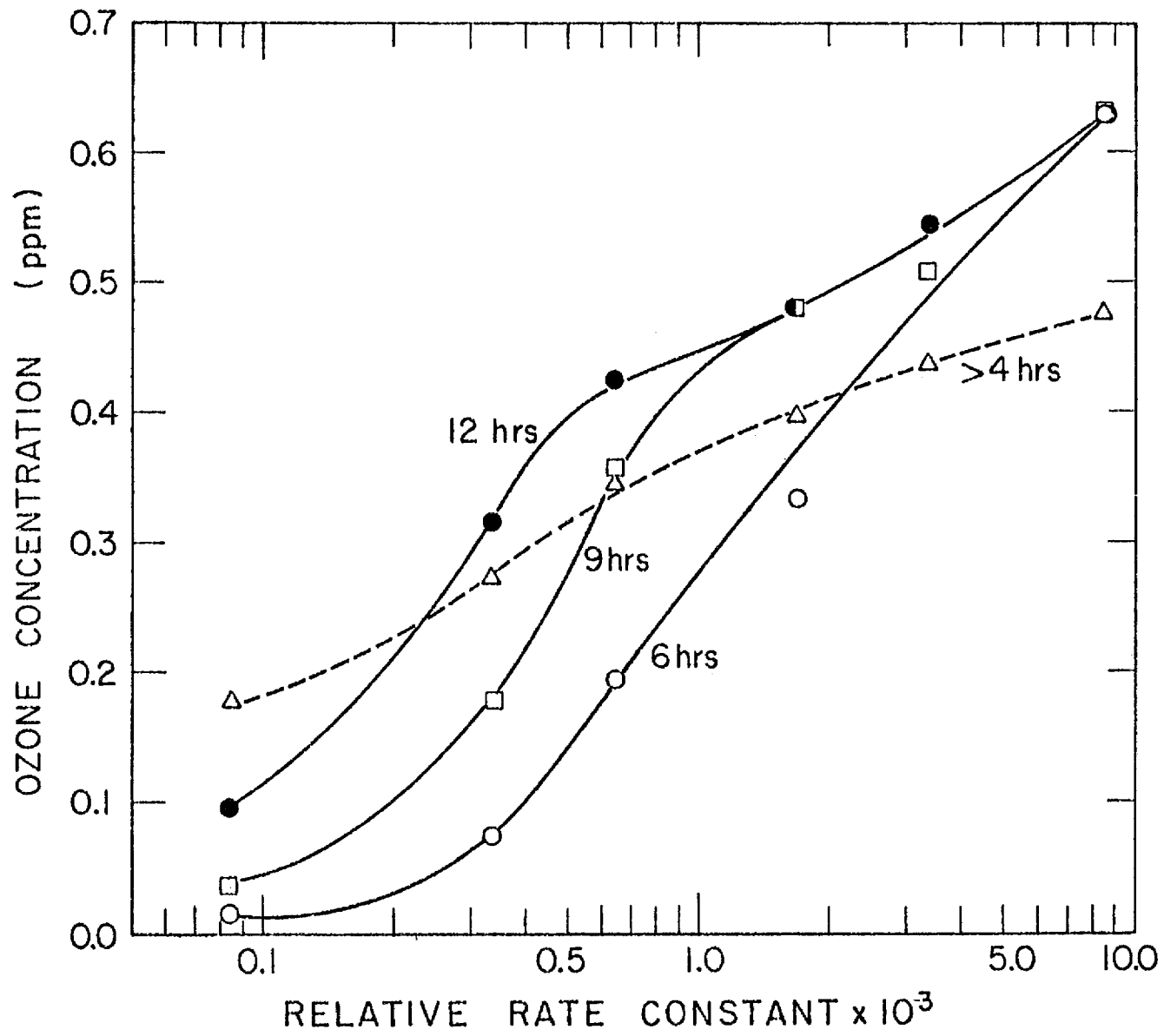


Figure 6. Ozone Reactivity vs Relative Oil Rate Constant at Initial Precursor (NMHC:NO<sub>x</sub>) Ratios of 2:1 (●, ◻, ◯) and 10:1 (Δ).

transport periods. The long period experimental reactivities at a ratio of 20 shown in Figure 7 (Dimitriades and Joshi, 1977) lend some support to these suggestions. This implies that fitting the experimental six-hour oxidant reactivity curve is a somewhat academic but useful exercise. Based on these computer simulations the tentatively proposed reactivity classes based on rate constant decades (Darnall et al., 1976b, Pitts et al., 1976a; 1977b) is not unrealistic. However, Figure 6 suggests a finer subdivision in terms of logarithmic rates, with a relative rate near 20 (ethane has a relative rate of 35) for the lower boundary. Since relative rate constants have an upper limit of around 20,000 imposed by collision rates, this will give a dynamic range of three decades to be subdivided into classes. As experimental rate constants have a standard percent error around  $\pm 20\%$ , up to 10 reactivity classes can be justified for such a dynamic range. Of course, consideration of other factors, such as incomplete characterization of reactivity by rate constant, can reduce the number of classes below this maximum value. It remains to be seen if further work substantiates these suggestions derived from computer simulations.

The simulated six-hour reactivities precisely fit the equation

$$\frac{Z}{0.576} = \frac{K}{K + 0.6054 K^{1/2} + 0.0138}$$

Trial of this form with six-hour ozone reactivity data was unsuccessful; apparently the precision of these data cannot support more than five parameters.

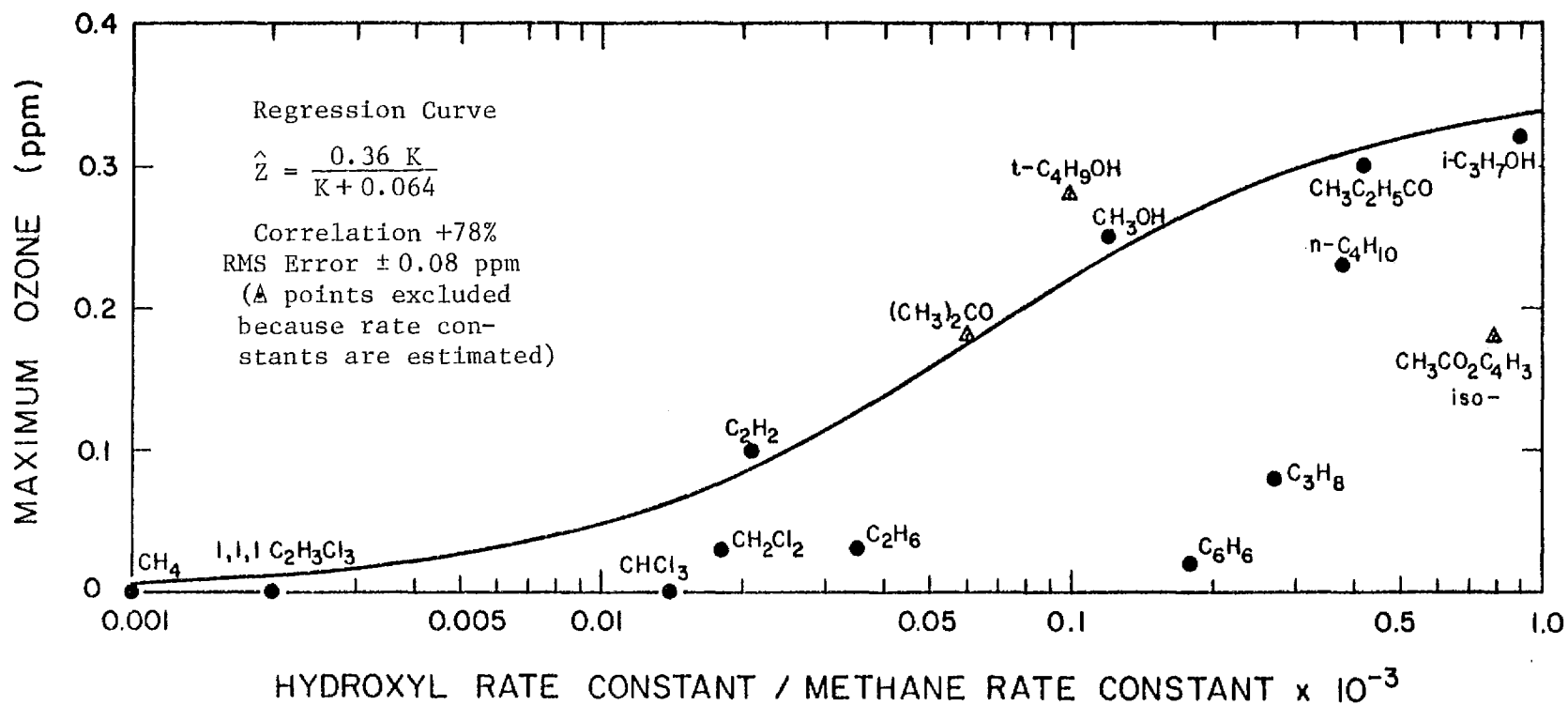


Figure 7. Ozone Data of Joshi and Dimitriadis (●) as a Function of Hydroxyl Rate Constant (4 ppm HC, ratio 20).

## V. RATE CONSTANTS FOR THE REACTIONS OF HYDROXYL RADICALS WITH SELECTED ORGANICS

The hydroxyl radical is known to play a dominant role in the chemistry of the atmosphere and in combustion processes. For many organics, such as the alkanes, which do not react with ozone at significant rates or do not photolyze in the actinic region, reaction with the OH radical is essentially their sole loss process in the troposphere. With the increasing emphasis towards lowering the reactivity of the organics emitted into the troposphere and the development of a reactivity scale based upon the rates of reaction of these organics with the OH radical (Darnall et al., 1976b; Pitts et al., 1976a; 1977c) rate constant data for the reaction of the OH radical with a large variety of organics have become necessary. Measurements for the rate constants for the reaction of OH radicals with the following organics have been made or were attempted.

- (a) A series of alkanes (neopentane, propane, isobutane, n-pentane, isopentane, 2,3-dimethylbutane and cyclopentane), as there are significant discrepancies in the literature data (Atkinson et al., 1979).
- (b) 2,3-dimethyl-2-butene, as there is a discrepancy of a factor of ~3 between the available literature values (Atkinson et al., 1979).
- (c) The epoxides propene oxide and 1-butene oxide since these organics are formed from  $O(^3P)$  atom reactions with the corresponding alkenes and no literature data exists on their OH radical rate constants.
- (d) A series of nitrates (ethyl, n-propyl, 3-pentyl, and 2-pentyl), as nitrates are formed in smog chamber  $NO_x$ -hydrocarbon-air irradiations (Pitts et al., 1977a; Darnall et al., 1976a) and no OH radical rate data exists.
- (e) Cellosolves, as these organics are used in the solvent industry.

Experimental. The experimental techniques used to determine OH radical rate constants have been described in detail previously (Lloyd et al., 1976a; Doyle et al., 1975); hence only a brief summary will be given here with emphasis on the modifications to the techniques pertinent to this study. Irradiations of the  $NO_x$ -hydrocarbon-air mixtures were carried out

in a non-rigid Teflon bag of ~5500-liter volume which was placed inside the all-glass environmental chamber (see Section II). The chamber temperature was maintained at  $300 \pm 1$  K during the irradiations. The organic concentrations were monitored as a function of irradiation time by gas chromatography (FID) using the following columns: (a) for the alkanes, a 36 ft. x 1/8 in. stainless steel column of 10% 2,4-dimethylsulfolane on C-22 Firebrick (60-80 mesh) followed by a 18 in. x 1/8 in. stainless steel column of 10% Carbowax 600 on C-22 Firebrick (60-80 mesh) operated at 273 K; (b) for 2,3-dimethyl-2-butene and the epoxides, a 20 ft. x 1/8 in. stainless steel column of 5% total DC 703 silicone oil/Carbowax 20M on Chromosorb G AW-DMCS, (100-120 mesh) operated at 333 K; (c) for the nitrates, a combination column consisting of a 10 ft. 5% TCEP plus 5 ft. 5% bentone 34/5% dinonyl phthalate plus 3 ft. 10% Carbowax E600, all 1/8 in. stainless steel, on 100-120 mesh Chromosorb W, HMDS treated, operated at 338 K, and a 10 ft x 1/8 in. stainless steel column of 10% Carbowax E600 on 100-120 mesh A.W. Firebrick (C-22) operated at 348 K; (d) Cellosolves (glycol ethers): a 5 ft. x 1/8 in. stainless steel column of Poropak A operated at 403 K. Two other columns were also used with no success.

Initial conditions for the irradiations for which reliable rate data were obtained were: (a) for the alkanes: propane, ~0.048 ppm; n-butane ~0.074 ppm; isobutane ~0.057 ppm; neopentane ~0.056 ppm; n-pentane ~0.132 ppm; isopentane ~0.110 ppm; cyclopentane ~0.165 ppm; and 2,3-dimethylbutane ~0.110 ppm. In addition, propene, isobutene and HCHO were also initially present in order to obtain a reactive hydrocarbon- $\text{NO}_x$  mixture; (b) for the alkenes: isobutene and cis-2-butene ~0.024 ppm; 2-methyl-2-butene ~0.043 ppm; 2,3-dimethyl-2-butene ~0.059 ppm. Initial  $\text{NO}_x$  levels were:  $\text{NO}$  ~0.32 ppm and  $\text{NO}_2$  ~0.08 ppm; (c) for the alkene oxides, n-butane and neopentane ~0.35 ppm; propene oxide ~0.5 ppm; 1-butene oxide ~0.5 ppm. HCHO, isobutene and cis-2-butene were also added to the initial  $\text{NO}_x$ -hydrocarbon mixture to ensure adequate reactivity; (d) for the final two nitrate runs: n-butane ~0.36 ppm; neopentane ~0.37 ppm; ethyl nitrate ~0.25 ppm; n-propyl nitrate ~0.24 ppm; 3-pentyl nitrate ~0.18 ppm; 2-pentyl nitrate ~0.43 ppm. Isobutene, cis-2-butene and HCHO were added to the initial  $\text{NO}_x$ -hydrocarbon mixture to ensure an adequate reactivity.

Rates of disappearance of the organics were determined from irradiations of NO<sub>x</sub>-hydrocarbon-air mixtures at atmospheric pressure and 300 ± 1 K. With the present experimental system, dilution losses of the reactants due to sampling were eliminated, as confirmed by non-irradiated control experiments. For the rate constant determination for 2,3-dimethyl-2-butene, the NO<sub>x</sub>-alkene ratio and the light intensity were adjusted to delay the formation of ozone during the irradiations ([O<sub>3</sub>] < 1 ppb) so that the alkene disappearance could be ascribed only to reaction with the OH radical. At the OH radical concentrations observed in the irradiations (see below), reaction with O<sub>3</sub> could thus be calculated to account for <10% of the 2,3-dimethyl-2-butene disappearance rate under all conditions used. Hence the disappearance of the organics during these irradiations is solely due to reaction with the OH radical:

$$-d\ln[\text{organic}]/dt = k[\text{OH}] \quad (1)$$

where k is the rate constant for the reaction



In all the irradiations it was generally observed that, within the analytical errors, plots of ln[organic] against irradiation time were linear, indicating that in each case the OH radical concentration was essentially constant over the duration of the irradiation. This has been noted in previous OH radical rate studies from this laboratory using this technique (Doyle et al., 1975; Lloyd et al., 1976a). Using the literature rate constant for the reaction of OH radicals with n-butane (Perry, Atkinson and Pitts 1976) or with isobutene (Atkinson and Pitts, 1975) the OH radical concentrations during the irradiations were in the range (2-6) × 10<sup>6</sup> molecules cm<sup>-3</sup>, similar to the concentrations observed in the previous rate studies (Doyle et al., 1975; Lloyd et al., 1976a,b; Darnall et al., 1976c; Winer et al., 1976; 1977).

Equation (1) could hence be used in the integrated form

$$\ln([\text{organic}]_t / [\text{organic}]_{t_0}) = k[\text{OH}](t - t_0) \quad (2)$$

where [organic]<sub>t</sub> and [organic]<sub>t<sub>0</sub></sub> are the organic concentrations at time t and t<sub>0</sub>, respectively. Furthermore, errors due to small differences in sampling volumes were eliminated by ratioing the gas chromatographic

responses to those for a reference organic, generally n-butane or cis-2-butene. Thus

$$k_2 = \frac{-1}{[\text{OH}](t-t_0)} \ln \frac{[\text{A}_2]_t [\text{A}_1]_{t_0}}{[\text{A}_1]_t [\text{A}_2]_{t_0}} + k_1 \quad (3)$$

where  $[\text{A}_1]_{t_0}$ ,  $[\text{A}_2]_{t_0}$  are the concentrations of organics  $\text{A}_1$  and  $\text{A}_2$  at time  $t_0$ ,  $[\text{A}_1]_t$  and  $[\text{A}_2]_t$  are the corresponding concentrations at time  $t$ , and  $k_1$  and  $k_2$  are the rate constants for the reactions of organics  $\text{A}_1$  and  $\text{A}_2$  with the OH radical.

n-Butane or cis-2-butene was used as the reference organic  $\text{A}_1$ , with rate constants at 300 K of  $k_1 = 2.73 \times 10^{-12} \text{ cm}^3 \text{ molecule}^{-1} \text{ sec}^{-1}$  and  $5.29 \times 10^{-12} \text{ cm}^3 \text{ molecule}^{-1} \text{ sec}^{-1}$ , respectively, as calculated from the Arrhenius expressions of Perry, Atkinson and Pitts (1976) and Atkinson and Pitts (1975).

From least squares analyses of plots of  $\ln([\text{A}_2]_t/[\text{A}_1]_t)$  against time (an example being shown in Figure 8), and the OH radical concentrations as obtained from least squares analyses of the n-butane or cis-2-butene disappearance rates, rate constants  $k_2$  were obtained.

Neopentane, Propane, Isobutane, n-Pentane, Isopentane, 2,3-Dimethylbutane and Cyclopentane. After an initial four irradiations involved in obtaining the optimum conditions for the determination of rate data, four 4-hour irradiations were carried out, each with two completely independent analyses of the alkanes every 0.5 hr. In a non-irradiated experiment the alkane concentrations as measured by gas chromatography were invariant over the 4-hr sampling period to better than  $\pm 1.5\%$  (corresponding to  $\leq 4\%$  of the typical reactive losses during an irradiation for the case of n-butane), thus verifying that the alkanes showed no dilution losses due to sampling.

n-Butane was used as the reference alkane, and a total of 8 sets of data were obtained. These rate data were then weighted (Parratt, 1961) using their least squares standard deviation, and the weighted mean values, together with the standard deviations, are given in Table 13. (The unit weighted mean values were within 4% of the weighted mean values, though with somewhat larger standard deviations.)

The rate constants  $k_2$  obtained in this work are compared with literature values in Table 14, which also includes all the available data for

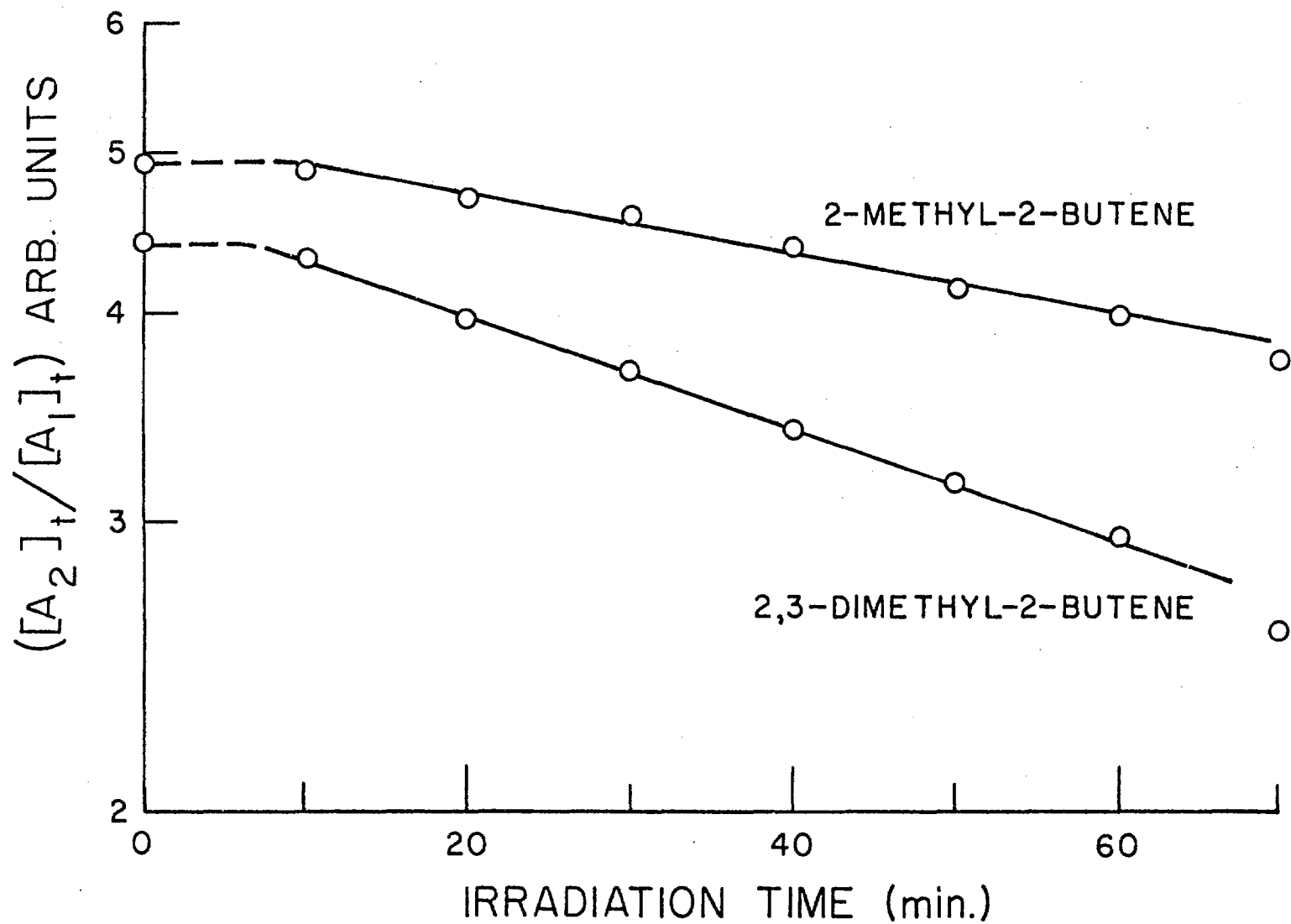


Figure 8. Plots of  $\ln([A_2]_t/[A_1]_t)$  Against Irradiation Time for  $A_2 = 2\text{-Methyl-2-butene}$  and  $2,3\text{-Dimethyl-2-butene}$  and  $A_1 = \text{cis-2-Butene}$ .

Table 13. Rate Constants  $k_2$  for the Reaction of OH Radicals with Selected Alkanes at 300 K

Alkane	$10^{12} \times k_2 \text{ cm}^3 \text{ molecule}^{-1} \text{ sec}^{-1}$ <sup>a,b</sup>
Propane	$1.59 \pm 0.22$
Isobutane	$2.52 \pm 0.05$
Neopentane	$1.04 \pm 0.17$
n-Pentane	$3.74 \pm 0.13$
Isopentane	$3.78 \pm 0.07$
Cyclopentane	$4.72 \pm 0.28$
2,3-Dimethylbutane	$5.67 \pm 0.29$

<sup>a</sup>The indicated error limits are one standard deviation.

<sup>b</sup>Values of  $k_2$  calculated using  $k_1 = 2.73 \times 10^{-12} \text{ cm}^3 \text{ molecule}^{-1} \text{ sec}^{-1}$  for n-butane at 300 K (Perry, Atkinson and Pitts, J. Phys. Chem., 64, 5314 (1976)).

Table 14. Comparison of the Literature Room Temperature Rate Constants  $k_2$  for  $\geq C_3$  Alkanes with the Values Obtained in this Study and with Those Calculated from Equation 5.

Alkane	$10^{12} \times k_2$ $\text{cm}^3 \text{ molecule}^{-1} \text{ sec}^{-1}$	at T K	Reference	$10^{12} \times k_2 \text{ cm}^3 \text{ molecule}^{-1} \text{ sec}^{-1}$ (300 K) Calculated
Propane	1.20	296-299	Greiner (1970)	1.55
	$0.83 \pm 0.17$	300	Bradley et al. (1973)	
	$2.15 \pm 0.54^a$	298	Gorse & Volman (1974)	
	$2.02 \pm 0.10$	$295 \pm 2$	Overend et al. (1975)	
	$1.98 \pm 0.08$ ( $1.62^b$ )	$329 \pm 5$ 300	Harker & Burton (1975)	
	$1.59 \pm 0.22$	300		
n-Butane	2.57	298-301	Greiner (1970)	2.71
	4.1	298	Morris & Niki (1971)	
	$2.35 \pm 0.35$	298	Stuhl (1973)	
	$2.9 \pm 0.7^a$	298	Gorse & Volman (1974)	
	4.22	298	Gordon & Mulac (1975)	
	$2.59 \pm 0.16^c$	292	Campbell et al. (1975)	
	$2.72 \pm 0.27$	298	Perry et al. (1976)	
Isobutane	2.46	297-305	Greiner (1970)	2.69
	$3.5 \pm 0.9^a$	298	Gorse & Volman (1974)	
	$2.1^d$	303	Wu et al. (1976)	
	$1.86 \pm 0.21^c$	305	Butler et al. (1978)	
	$2.52 \pm 0.05$	300	This work	
Cyclobutane	$1.2 \pm 0.3^a$	298	Gorse & Volman (1974)	4.64

(continued)

Table 14 (cont.)

Alkane	$10^{12} \times k_2$	at T K	Reference	$10^{12} \times k_2$
	$\text{cm}^3 \text{ molecule}^{-1} \text{ sec}^{-1}$			$\text{cm}^3 \text{ molecule}^{-1} \text{ sec}^{-1}$ (300 K) Calculated
Neopentane	0.825	292-298	Greiner (1970)	0.78
	$1.04 \pm 0.17$	300	This work	
n-Pentane	$6.2^d$	303	Wu et al. (1976)	3.87
	$3.74 \pm 0.13$	300	This work	
Isopentane	$3.1 \pm 0.6^e$	305	Lloyd et al. (1976a)	3.84
	$3.78 \pm 0.07$	300	This work	
Cyclopentane	$6.1^a$	298	Volman (1975)	5.80
	$4.72 \pm 0.29$	300	This work	
2-Methylpentane	$5.0 \pm 1.0^e$	305	Lloyd et al. (1976a)	5.01
3-Methylpentane	$6.8 \pm 1.4^e$	305	Lloyd et al. (1976a)	5.01
n-Hexane	$5.9 \pm 1.2^e$	305	Lloyd et al. (1976a)	5.03
	$5.7^d$	303	Wu et al. (1976)	
	$6.1 \pm 0.4^e$	292	Campbell et al. (1976)	
Cyclohexane	7.95	295	Greiner (1970)	6.96
	$6.7 \pm 1.5^a$	298	Gorse & Volman (1976)	
	$6.2^d$	303	Wu et al. (1976)	

(continued)

Table 14 (cont.)

Alkane	$10^{12} \times k_2$ $\text{cm}^3 \text{ molecule}^{-1} \text{ sec}^{-1}$	at T K	Reference	$10^{12} \times k_2$ $\text{cm}^3 \text{ molecule}^{-1} \text{ sec}^{-1}$ (300 K) Calculated
2,3-Dimethylbutane	7.45	300	Greiner (1970)	4.98
	$4.8 \pm 1.0^d$	305	Darnall et al. (1976c)	
	$4.3 \pm 1.4^f$	303	Atkinson et al. (1976a)	
	$5.67 \pm 0.31$	300	This work	
2,2,3-Trimethylbutane	5.05	296-303	Greiner (1970)	3.08
	$3.6 \pm 0.7^d$	305	Darnall et al. (1976c)	
2,2,3,3-Tetramethylbutane	1.12	294-301	Greiner (1970)	1.17
2,2,4-Trimethylpentane	3.73	298-305	Greiner (1970)	4.24
n-Octane	8.42	295	Greiner (1970)	7.35

a) Relative to OH + CO, placed on an absolute basis using  $k(\text{OH} + \text{CO}) = 1.5 \times 10^{-13} \text{ cm}^3 \text{ molecule}^{-1} \text{ sec}^{-1}$  (Perry, Atkinson and Pitts 1977a).

b) Converted to 300 K using the activation energy obtained by Greiner (1970).

c) Relative to OH + CO; carried out at 100 torr total pressure of CO or  $\text{N}_2 + \text{O}_2$ . It is assumed that CO is analogous to  $\text{N}_2 + \text{O}_2$  as a third body in the OH + CO pressure dependence, and a value of  $k(\text{OH} + \text{CO}) = 1.75 \times 10^{-13} \text{ cm}^3 \text{ molecule}^{-1} \text{ sec}^{-1}$  has been used (Atkinson et al., 1979a).

d) Relative to OH + isobutene or OH + cis-2-butene, placed on an absolute basis using  $k(\text{OH} + \text{isobutene})$  or  $k(\text{OH} + \text{cis-2-butene})$  calculated from the Arrhenius expression of Atkinson and Pitts (1975).

e) Relative to OH + n-butane, placed on an absolute basis using  $k(\text{OH} + \text{n-butane})$  calculated from the Arrhenius expression of Perry, Atkinson and Pitts (1976).

f) Relative to OH + ethane, placed on an absolute basis using  $k(\text{OH} + \text{ethane})$  calculated from the Arrhenius expression of Greiner (1970).

C<sub>3</sub> alkanes (for many of the relative rate studies the reference reaction rate constant has been reevaluated to take into account more recent rate constant data). In many cases it can be seen that the present rate constants are in agreement with the literature data within the cumulative error limits, but there are obviously significant discrepancies, especially for n-pentane and 2,3-dimethylbutane. For 2,3-dimethylbutane, the present value of  $k_2$  is substantially lower than the absolute rate constant determined by Greiner (1970), while it is somewhat higher than, though in agreement within the cumulative error limits with, the two previous rate constant determinations (Atkinson et al., 1976a; Darnall et al., 1976c) from this laboratory. The present rate constant for propane ( $k_2 = (1.59 \pm 0.22) \times 10^{-12} \text{ cm}^3 \text{ molecule}^{-1} \text{ sec}^{-1}$ ) is seen to be approximately in the middle of the room temperature literature values (Greiner, 1970; Bradley et al., 1973; Overend, Paraskevopoulos and Cvetanovic, 1975; Gorse and Volman, 1974) though it is in excellent agreement with  $k_2 = 1.62 \times 10^{-12} \text{ cm}^3 \text{ molecule}^{-1} \text{ sec}^{-1}$ , calculated using the Arrhenius activation energy of Greiner (1970) to convert the rate constant of Harker and Burton (1975), obtained at 329 K, to 300 K.

Using a formula completely analogous to that of Greiner (1970)

$$k_2 = N_{\text{prim}}k_{\text{prim}} + N_{\text{sec}}k_{\text{sec}} + N_{\text{tert}}k_{\text{tert}} \quad (4)$$

where  $N_{\text{prim}}$ ,  $N_{\text{sec}}$ , and  $N_{\text{tert}}$  are the number of primary, secondary and tertiary C-H bonds in the alkane, and  $k_{\text{prim}}$ ,  $k_{\text{sec}}$ , and  $k_{\text{tert}}$  are the corresponding rate constants for H atom abstraction per C-H bond, then the rate constant data in Table 14 are judged to be best fit [based mainly on the present study and those of Greiner (1970), Perry, Atkinson and Pitts (1976) and Darnall et al. (1976c)] at 300 K by

$$k_2 = N_{\text{prim}} \times 6.5 \times 10^{-14} + N_{\text{sec}} \times 5.8 \times 10^{-13} + N_{\text{tert}} \times 2.1 \times 10^{-12} \text{ cm}^3 \text{ molecule}^{-1} \text{ sec}^{-1} \quad (5)$$

(Greiner's original formula yielded  $k_{\text{prim}} = 6.6 \times 10^{-14} \text{ cm}^3 \text{ molecule}^{-1} \text{ sec}^{-1}$ ;  $k_{\text{sec}} = 5.6 \times 10^{-13} \text{ cm}^3 \text{ molecule}^{-1} \text{ sec}^{-1}$  and  $k_{\text{tert}} = 2.9 \times 10^{-12} \text{ cm}^3 \text{ molecule}^{-1} \text{ sec}^{-1}$ , the major difference obviously being in  $k_{\text{tert}}$ .) Using the new values of  $k_{\text{prim}}$ ,  $k_{\text{sec}}$  and  $k_{\text{tert}}$ , equation (5) fits the available rate constant data to better than approximately  $\pm 20\%$ , the

exception being cyclobutane, probably due to the effects of ring strain. Because of the closeness of the present values of  $k_{\text{prim}}$  and  $k_{\text{sec}}$  with those derived by Greiner (1970) and because the only temperature dependence rate constant studies for  $\geq C_3$  alkanes are those of Greiner (1970) and Perry, Atkinson and Pitts (1976) [which agree very well for n-butane, the only alkane studied by Perry, Atkinson and Pitts, (1976)], the Arrhenius activation energies of Greiner (1970) for  $k_{\text{prim}}$  and  $k_{\text{sec}}$  can be used to derive  $k_2$  as a function of temperature. For the alkanes containing tertiary C-H bonds, an activation energy of  $E_{\text{tert}} \sim 0$  kcal mole<sup>-1</sup> gives a good fit to the high temperature ( $\sim 493$ - $498$  K) rate data of Greiner (1970). Hence the equation

$$k_2 = 1.01 \times 10^{-12} e^{-1635/RT} \times N_{\text{prim}} + 2.41 \times 10^{-12} e^{-850/RT} \times N_{\text{sec}} + 2.10 \times 10^{-12} \times N_{\text{tert}} \text{ cm}^3 \text{ molecule}^{-1} \text{ sec}^{-1} \quad (6)$$

fits the available literature data over the temperature range 300-500 K within acceptable limits ( $\sim \pm 20\%$  or better) and can hopefully be used to calculate rate constants for the reaction of OH radicals with  $\geq C_3$  alkanes, apart from cyclobutane (and by analogy, cyclopropane) for which no data presently exist.

2,3-Dimethyl-2-Butene. After an initial six irradiations to determine the optimum conditions, four 70-120 minutes irradiations were carried out with analysis of the alkenes every 10 minutes. No loss of the alkenes was observed in non-irradiated mixtures. 2-Methyl-2-butene was included in the alkenes studied since it is the alkene whose reactivity towards both  $O_3$  (Japar, Wu and Niki, 1974; Huie and Herron, 1975) and the OH radical (Atkinson et al., 1979a) is closest to 2,3-dimethyl-2-butene, and its OH radical rate constant is also known to a good degree of accuracy (Atkinson, Perry and Pitts, 1976b; Atkinson and Pitts, 1978a; Atkinson et al., 1979a).

For the irradiations carried out, plots of  $\ln[\text{alkene}]$  against time were, within the analytical errors, linear after an initial induction period of  $\sim 10$  minutes (see Figure 8), indicating that the OH radical concentrations were essentially constant over the duration of the irradiations. For 2,3-dimethyl-2-butene, the disappearance rate increased somewhat after  $\sim 60$ - $90$  minutes, presumably due to a small contribution from reaction with  $O_3$ ; these data points were neglected in the analyses. Four

Table 15. Rate Constants  $k_2$  for the Reaction of OH Radicals with 2-Methyl-2-butene and 2,3-Dimethyl-2-butene at  $300 \pm 1$  K, Together with the Available Room Temperature Literature Values

Alkene	$10^{11} \times k_2 \text{ cm}^3 \text{ molecule}^{-1} \text{ sec}^{-1}$		
	This Work <sup>a</sup>	Literature	Reference
2-Methyl-2-butene	8.9±0.5	11.9 <sup>c</sup>	d
	9.3±0.8	8.7±0.6 <sup>b</sup>	e
	8.4±0.6		f
	8.6±0.5		
2,3-Dimethyl-2-butene	12.1±0.5	15.3 <sup>c</sup>	d
	13.8±1.8	12.2±0.8 <sup>b</sup>	g
	11.9±1.0		h
	12.2±1.1		

<sup>a</sup>Values of  $k_2$  calculated using  $k_1 = 5.29 \times 10^{-11} \text{ cm}^3 \text{ molecule}^{-1} \text{ sec}^{-1}$  for cis-2-butene at 300 K [Atkinson and Pitts, J. Chem. Phys., 63, 3591 (1975)]. The indicated error limits are two least squares standard deviations.

<sup>b</sup>Weighted mean values, the indicated error limits being two standard deviations.

<sup>c</sup>The errors on these rate constants are a combination of the errors on these rate constants relative to propene [ $\pm 10\%$  (see reference d) and the error limit on the absolute rate constant for propene [ $\pm 25\%$  (Morris, Stedman and Niki, J. Amer. Chem. Soc., 93, (1971)], and are hence  $\sim 25\%$ .

<sup>d</sup>Morris and Niki, J. Phys. Chem., 75, 3640 (1971).

<sup>e</sup>Atkinson, Perry and Pitts, Chem. Phys. Lett., 38, 607 (1976).

<sup>f</sup>Atkinson and Pitts, J. Chem. Phys., 68, 2992 (1978).

<sup>g</sup>Ravishankara, Wagner, Fischer, Smith, Schiff, Watson, Tesi and Davis, Int. J. Chem. Kinet., 10, 783 (1978).

<sup>h</sup>Perry, Ph.D. Thesis, University of California, Riverside, August, 1977.

sets of rate constants,  $k_2$ , for 2-methyl-2-butene and 2,3-dimethyl-2-butene were obtained. These rate data, and the weighted mean values of  $k_2$ , are given in Table 15 along with the literature room temperature values.

It can be seen that the present rate constant  $k_2$  for 2-methyl-2-butene is in excellent agreement with the two literature values obtained using a flash photolysis-resonance fluorescence technique (Atkinson, Perry and Pitts, 1976b; Atkinson and Pitts, 1978), and, within the cumulative errors, with that obtained by Morris and Niki (1971), thus lending confidence to the present experimental technique. The present value of  $k_2$  for 2,3-dimethyl-2-butene is also in good agreement, within the cumulative errors, with the rate constants determined by Perry (1977) and by Morris and Niki (1971). However, the rate constant  $k_2$  obtained by Ravishankara et al. (1978) is lower by a factor of  $\sim 2$  than the present value, possibly due to adsorption of the 2,3-dimethyl-2-butene on the walls of the static reaction system used in that study.

Propene Oxide and 1-Butene Oxide (1,2-Epoxybutane). Two initial irradiations were carried out to optimize conditions, i.e., to obtain a sufficiently reactive  $\text{NO}_x$ -hydrocarbon mixture to achieve a significant disappearance of the oxides. Two 120-minute irradiations were then carried out with analysis of the alkanes n-butane and neopentane and the oxides every 15 minutes. The rate constants  $k_2$  given in Table 16 were obtained.

Table 16. Rate Constants for  $k_2$  for the Reaction of OH Radicals with Propene Oxide and 1-Butene Oxide at  $300 \pm 1$  K

Oxide	$10^{12} \times k_2 \text{ cm}^3 \text{ molecule}^{-1} \text{ sec}^{-1}{}^a$		
	#297	#298	Average <sup>b</sup>
Propene oxide	$1.68 \pm 0.55$	$0.86 \pm 0.61$	$1.3 \pm 0.5$
1-Butene oxide	$2.20 \pm 0.41$	$3.05 \pm 0.85$	$2.4 \pm 0.4$

<sup>a</sup> The indicated errors are a single standard deviation. A value of  $k_2 = 2.73 \times 10^{-12} \text{ cm}^3 \text{ molecule}^{-1} \text{ sec}^{-1}$  for n-butane at 300 K (Perry, Atkinson and Pitts, J. Phys. Chem., 64, 5314 [1976]) was used.

<sup>b</sup> Weighted average; indicated error is a single weighted standard deviation.

Despite the rather large error limits, the values of  $k_2$  for the oxides can be seen to be similar to, but somewhat smaller than, the rate constants for the reaction of OH radicals with the corresponding alkanes [ $k_2(\text{propane}) = 1.6 \times 10^{-12} \text{ cm}^3 \text{ molecule}^{-1} \text{ sec}^{-1}$  (Darnall et al., 1978);  $k_2(\text{n-butane}) = 2.7 \times 10^{-12} \text{ cm}^3 \text{ molecule}^{-1} \text{ sec}^{-1}$  (Perry et al., 1976)]. This is then completely analogous to the case for  $\text{O}(^3\text{P})$  atom reactions, where ethene oxide is slightly less reactive than ethane towards  $\text{O}(^3\text{P})$  atoms (Herron and Huie, 1973). This indicates that H-atom abstraction is the operative reaction pathway for OH radical reaction with the two oxides studied here.

Ethyl Nitrate, n-Propyl Nitrate, 2-Butyl Nitrate, 2-Pentyl Nitrate and 3-Pentyl Nitrate. A total of nine irradiations were carried out, the first seven having somewhat low OH radical concentrations ( $[\text{OH}] \sim 1 \times 10^6 \text{ molecule cm}^{-3}$ ) so that the amounts of organics reacted were small and hence the errors were large. HCHO ( $\sim 1 \text{ ppm}$ ) was added in the final two irradiations and OH radical concentrations were then  $\sim 6 \times 10^6 \text{ molecule cm}^{-3}$ . In most of the irradiations distinctly different nitrate disappearance rates were observed on the two columns used. The results are summarized as follows: on the Carbowax E600 column the values of  $k_2$  obtained agreed reasonably well from run to run (to within  $\pm 30\%$ ) with rate constants  $k_2$  of ( $\times 10^{12} \text{ cm}^3 \text{ molecule}^{-1} \text{ sec}^{-1}$ ): ethyl nitrate  $< 1$ ; n-propyl nitrate  $< 1$ ; 2-butyl nitrate  $\sim 2.0$ ; 2-pentyl nitrate  $\sim 1.5-2.9$ ; 3-pentyl nitrate  $\sim 1.1-2.1$ . However, on the other column the rate constants derived from the observed disappearance rates varied widely ranging from reasonable agreement with those quoted above to being a factor of  $\sim 6$  higher (i.e., in the  $(1-2) \times 10^{-11} \text{ cm}^3 \text{ molecule}^{-1} \text{ sec}^{-1}$  range for the butyl and pentyl nitrates studied). Unfortunately there is, a priori, no basis for choosing the "best" rate constants.

However, as noted for the alkene oxides, OH radical rate constants generally show the same trend with organic structure as those for  $\text{O}(^3\text{P})$  atoms (Atkinson et al., 1979). Table 17 shows the  $\text{O}(^3\text{P})$  atom and OH radical rate constants at room temperature for selected nitrogen and oxygen containing organics. From this table it would appear that the rate constants for the reaction of OH radicals with methyl nitrate and ethyl nitrate should be  $\sim 1 \times 10^{-12} \text{ cm}^3 \text{ molecule}^{-1} \text{ sec}^{-1}$  and  $\sim (1.0-1.5) \times 10^{-12}$

Table 17. O(<sup>3</sup>P) Atom and OH Radical Room Temperature Rate Data for Reaction with Selected Nitrogen- and Oxygen-Containing Organics

Reactant	$10^{15} \times k^{O(^3P)}$ cm <sup>3</sup> molecule <sup>-1</sup> sec <sup>-1</sup>	$10^{12} \times k^{OH^a}$ cm <sup>3</sup> molecule <sup>-1</sup> sec <sup>-1</sup>
CH <sub>3</sub> NO <sub>2</sub>	3.2 <sup>b</sup>	1.07
CH <sub>3</sub> ONO	3.5 <sup>c</sup>	1.56
CH <sub>3</sub> ONO <sub>2</sub>	3.5 <sup>d</sup>	--
C <sub>2</sub> H <sub>5</sub> ONO <sub>2</sub>	7.1 <sup>d</sup>	--
CH <sub>3</sub> OH	14 <sup>e</sup>	1.1
C <sub>2</sub> H <sub>5</sub> OH	54 <sup>e</sup>	3.5
n-Butane	22 <sup>f</sup>	2.7

<sup>a</sup>Atkinson, Darnall, Lloyd, Winer and Pitts, Adv. Photochem., 11, 375 (1979).

<sup>b</sup>Campbell and Goodman, Chem. Phys. Lett., 34, 105 (1975).

<sup>c</sup>Davidson and Thrush, J. Chem. Soc., Faraday Trans. I, 71, 2413 (1975).

<sup>d</sup>Salter and Thrush, J. Chem. Soc., Faraday Trans. I, 73, 1098 (1977).

<sup>e</sup>Owens and Roscoe, Can. J. Chem., 54, 984 (1976).

<sup>f</sup>Atkinson, Perry and Pitts, Chem. Phys. Lett., 47, 197 (1977).

cm<sup>3</sup> molecule<sup>-1</sup> sec<sup>-1</sup>, respectively, which tends to cast doubts on the values obtained in the Carbowax E600 column. However, at best, this study is inconclusive and the data obtained must be viewed with skepticism.

Cellosolves. Two multihour irradiations were carried out for methyl-cellosolve using the Porapak column. However, difficulties in the gas chromatographic analyses led to a large degree of scatter in the methyl-cellosolve data, hence no meaningful data could be obtained. Attempts to analyze for the cellosolves using two other columns were unsuccessful and this part of the project was terminated.



## VI. INVESTIGATION OF RATES OF CONVERSION OF SULFUR DIOXIDE TO SULFATE UNDER SIMULATED ATMOSPHERIC CONDITIONS

The objective of this study is to obtain gas-to-particle conversion rates of sulfur dioxide promoted by photooxidizing hydrocarbon-NO<sub>x</sub> mixtures under conditions simulating outcomes of various control implementation scenarios. An incidental objective is to obtain further insight into the mechanism of this process. This facet of air pollution is becoming increasingly important as use of high-sulfur fuels increases.

The rate of conversion of sulfur dioxide to sulfate in the presence of photooxidizing surrogate was to be obtained from three types of data:

- 1) Determining sulfur dioxide chamber profiles and calculating sulfate yield from the decrease in concentration. This involves measurement of small differences in concentration complicated by the necessity of correcting for a SO<sub>2</sub> chamber dark decay rate comparable with anticipated conversion rates.

- 2) Determining size distribution of the chamber aerosol and calculating sulfate from the increase in aerosol volume, corrected for wall losses of particulate. This involves data from the electric mobility method of determining size distribution which will be imprecise when applied over the anticipated narrow size range of 0.4 to 0.2 μm induced by initial seeding of the chamber with 0.1 μm nuclei.

- 3) Directly determining particulate sulfur mass concentrations by analysis of samples collected by filtration and correcting for wall losses. The flash ignition method for sulfur (Husar et al., 1975; Roberts and Friedlander, 1976) is sufficiently sensitive for this purpose and the necessary apparatus was designed and constructed.

In planning these experiments, considerable reliance was placed on two expedients, monitoring the chamber particulate sulfur concentration using the flash ignition method, and restraining particle size in a region of long chamber lifetime by use of added condensation centers. Both expedients turned out to be impractical. Thus, this work was accomplished in the face of considerable difficulties in experimental technique and data interpretation. Consequently, an understanding of the technique and interpretation is a necessary preliminary to judging the implications of the final results. These subjects are discussed below.

Experimental. The study was carried out in the SAPRC glass chamber lined with Teflon film to reduce wall effects and prevent any exchange with ambient air. Prevention of exchange is of paramount importance when small aerosol yields are being monitored. The humidified purified air was filtered through an "absolute" filter to remove any trace of interfering aerosol and then mixed in the chamber with the surrogate hydrocarbon mixture, nitrogen oxides and sulfur dioxide. A few early experiments were done with added monodispersed potassium nitrate aerosols, but this expedient, intended to increase chamber lifetime of aerosol by control of particle size, was not successful. Trial experiments with added potassium nitrate (doped with acid sulfate aerosol with aerosol surface of up to  $8 \text{ cm}^2 \text{ m}^{-3}$  of  $0.10 \text{ }\mu\text{m}$  particles) showed that the sulfur-containing aerosol self-nucleated and grew independently of the added aerosol except, of course, through the coagulation mechanism. The latter is not sufficient to keep particle size within the required range ( $0.02$  to  $0.2 \text{ }\mu\text{m}$ ). The flash ignition method was adequately sensitive, as expected, but the sensitivity was frustrated by a highly erratic blank when using Fluoropore filters followed by extraction for sampling. The blank is small enough (around  $1 \text{ }\mu\text{g}$  of sulfur) to be neglected when sampling cubic meters, but this sample size is impossible for a chamber volume of  $7 \text{ m}^3$ . (The development and testing of the flash ignition sulfur monitor is described at the end of the experimental section.)

It was decided to utilize data from the electric mobility analyzer and the Meloy photometric sulfur analyzer to obtain conversion rates. The rationale of this approach will be discussed later using data from a typical experiment for illustration.

The mobility analyzer allows one to monitor aerosol concentration as a function of particle size from  $0.004 \text{ }\mu\text{m}$  to  $1.0 \text{ }\mu\text{m}$  in nine size classes. These data can be converted into aerosol volume in units of  $\text{cm}^3 \text{ m}^{-3} \times 10^6$ . Aerosol volume vs time profiles can be derived from the data. This would be all that is necessary to obtain a relative measure of aerosol yield if it were not for loss to the walls of aerosol and the possibility of variable sulfur content of the particulate. The latter

could occur if, for example, a few ppb of ammonia were to escape the action of the air purification system or if the surrogate produced some organic aerosol material.

Wall loss for a monodisperse fraction of an aerosol in the chamber can be represented by a differential equation

$$\frac{dn_i}{dt} = -k_i n_i + \phi_i(t) \quad (1)$$

where  $n_i$  is number concentration,  $t$  is time,  $k_i$  is a "pseudomolecular" wall loss constant, and  $\phi_i(t)$  represents the influence on  $n_i$  of all other factors such as particle growth by condensation, appearance, and disappearance in size fraction  $i$  by coagulation and so forth. The detailed nature of  $\phi_i(t)$  does not concern us for this application since we have an experimental measure of its influence through monitoring the particle size distribution. It is a consequence of equation (1) that the quantity

$$n_i = n_i + k_i \int_0^t n_i(s) ds \quad (2)$$

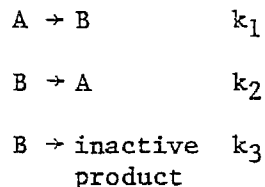
is a measure of the total amount of aerosol that has passed through size fraction  $i$  at time  $t$ , including that lost to the chamber walls. This can be converted to particulate volume in size fraction  $i$  to yield a similar equation. The sum of the volumetric equations over all size classes of the electric mobility analyzer will yield a volume profile corrected for wall loss. Of course, this is subject to the usual errors due to discrete classification of a continuous distribution and to missing data (the extreme ends of the distribution). Fortunately, the latter is not serious for this work except at long times (~5 to 6 hours) when high yield experiments produce some particles larger than  $0.75 \mu\text{m}$ .

Correcting aerosol volume in this manner requires relatively accurate values of the wall loss constants,  $k_i$ , especially for the larger sizes where volume per particles become large. These constants were measured by following the decay of various initially monodisperse aerosols in the irradiated chamber. Aerosols of  $0.05$  to  $0.20 \mu\text{m}$  diameter were generated by atomization of a solution followed by size fractionation using the TSI

electric mobility fractionator. Time profiles for these aerosols were obtained using the electric mobility analyzer. Larger particles were generated using the Berglund Liu vibrating orifice generator and profiles for these were followed by a Climet optical particle counter (OPC).

The electric mobility analyzer is insufficiently sensitive to allow concentrations much below  $10^4 \text{ cm}^{-3}$  in these decay experiments while yielding sufficiently accurate data for estimating the wall loss constant. This circumstance requires that the decay data be treated as a combination first and second order process because the coagulation rate is large enough to influence the estimate of the rate of the first order process, attributed to wall loss. The influence of the second order process is negligible for those experiments using the OPC because of the very low number concentration used ( $\sim 0.5 \text{ cm}^{-3}$ ).

Table 18 gives data obtained from these chamber characterization experiments and the data for the first order constants are plotted as a function of particle size in Figure 9. The classic interpretation of wall losses in stirred chambers uses a model where particles are presumed to diffuse and sediment to surfaces through a quiescent boundary layer at the walls. In accord with this model the steep increase in loss as size increases from 0.1 to 0.5  $\mu\text{m}$  could be attributed to an increasing sedimentation velocity as particulate mass increases. However, if the reciprocals of the experimental constant are plotted as a function of the inverse square of size (Figure 10) it appears that a significant intercept is approached as size increases. The sedimentation model for a well-stirred chamber requires a zero intercept for this sort of plot. This behavior is reminiscent of the behavior of two cascaded first-order processes in chemical kinetics



when species B is present at steady-state concentrations. This mechanism gives an apparent first-order constant  $k_a$

$$\frac{1}{k_a} = \frac{1}{k_1} + \frac{k_2}{k_1 k_3}$$

and, if  $k_1 = k_2$

$$\frac{1}{k_a} = \frac{1}{k_1} + \frac{1}{k_3}$$

The analog of this behavior can be rationalized for particulate wall losses in the glass chamber on realizing that it is not a well-stirred chamber and there is a rate-limiting process corresponding to  $k_1$ , convective transport to the boundary layer. In normal operation the glass chamber is stirred by thermal convection due to small temperature differences between surfaces, a mode of operation chosen to reduce wall losses of chemically active species. For convective transport it is reasonable to assume that the analogs of  $k_1$  and  $k_2$  are equal. This assumption was made to separate presumed boundary layer processes from convective transport and give the results shown in Column 4 of Table 18. It should be remarked that the limiting action of convective

Table 18. Decay Data for Various Particle Sizes in the All-Glass Chamber During Irradiation (70% Lights) and at Operating Temperature (302 K)

Particle Diameter ( $\mu\text{m}$ )	First Order Constant, $\text{hr}^{-1}$	Second Order Constant, $\text{cm}^3 \text{sec}^{-1}$	Boundary Layer Constant, $\text{hr}^{-1}$
0.05	0.215	$2.09 \times 10^{-9}$	0.323
0.10	0.171	$4.28 \times 10^{-9}$	0.233
0.15	0.274	$8.75 \times 10^{-10}$	0.477
0.20	0.459	$8.28 \times 10^{-10}$	1.601
0.50*	0.594*	NI#	7.722
1.05*	0.537*	NI#	3.245

\*These experiments were done at low number concentrations using the OPC to follow profiles. The particle sizes are according to the OPC's polystyrene latex-calibrated scale.

#NI - No information.

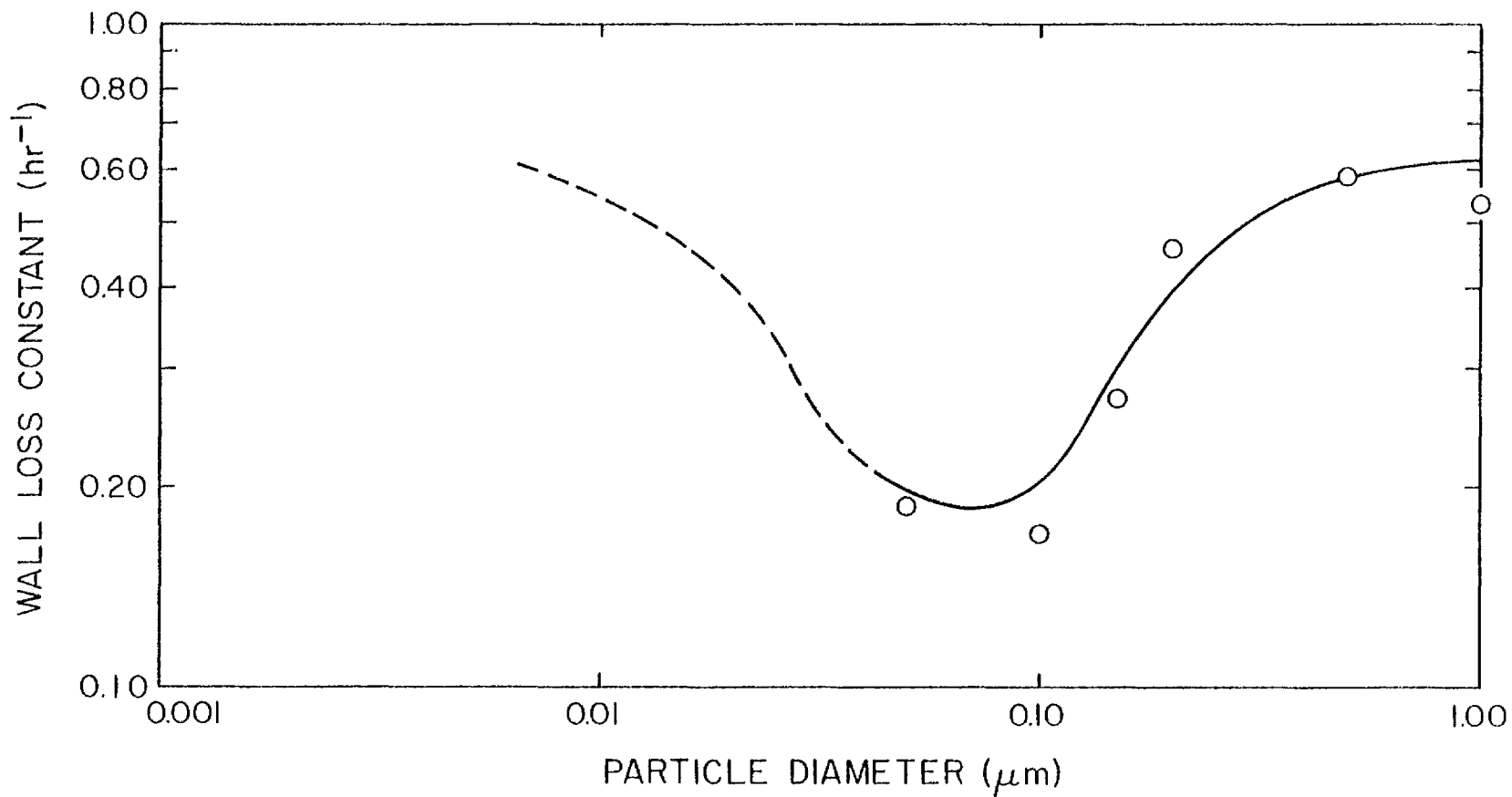


Figure 9. Experimental Wall Loss Constants (O) as a Function of Particle Diameter and Regression Curve (Dashed Portion Indicates Extrapolation).

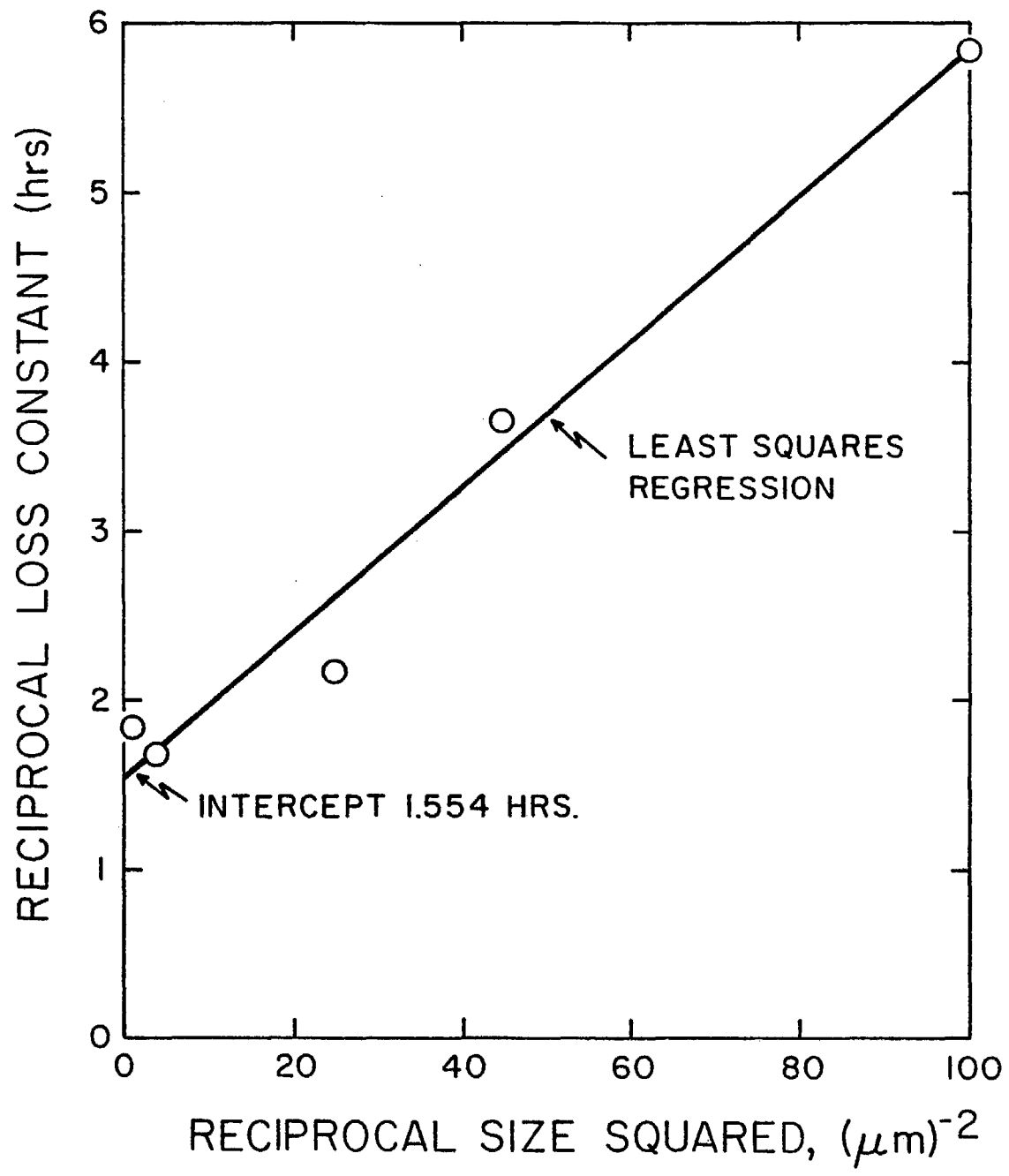


Figure 10. Dependence of the Loss Constant on Particle Size for the Larger Particles.

transport cannot persist as particle sizes increase into the micron range. Eventually sedimentation velocities will become comparable to convection velocities and rate of loss will begin to increase.

The boundary layer constants were fitted to an expression obtained by solving the partial differential equations for diffusion through a layer under the influence of an external force proportional to particulate volume. The steady state approximation was used. The result of this calculation can be written

$$k = \frac{D\mu}{\delta} [A h(x) + B]$$

Here  $D$  = particulate diffusion coefficient,  $\mu$  = chamber surface to volume ratio,  $\delta$  = layer thickness,  $x = CD_p^3/kT$ , and  $h(x) = x + e^{-x} - 1/1 - e^{-x}$ .  $A\mu/\delta$ ,  $B\mu/\delta$ , and  $C/kT$  were taken as parameters to be estimated from the data.

The first three columns of Table 19 shows the particulate properties used for the least squares estimation of the parameters. Least squares estimation of  $A\mu/\delta$  and  $C/kT$  were made difficult by the fact that the function  $h(x)$  is almost first order homogeneous, that is, a function  $f(x)$  which obeys the relationship

$$f(\lambda x) = \lambda f(x)$$

The parameter values found were on the basis of minimum runs percent error. However, the minimum of the objective function is quite shallow indicating many other values of these two parameters would yield nearly as good a fit to the data. Best fit to the data is obtained by the values  $(A\mu/\delta) = 48.4 \text{ cm}^{-2}$ ,  $(B\mu/\delta) = 1.83 \text{ cm}^{-2}$ , and  $(C/kT) = 415 \text{ }\mu\text{m}^{-3}$ . Estimates of wall loss based on these parameter values and a convection rate constant of  $0.644 \text{ hr}^{-1}$  indicate an error of estimate of 15.3% when compared to the experimentally obtained values. The overall fit to the data and the extrapolation to smaller particle sizes is illustrated by the curve drawn in Figure 9.

The fitted relationship is applied to estimate generated particulate volume during experiments on sulfur dioxide gas-to-particle conversion

Table 19. Properties Assigned to Test Aerosol Particles in Deriving an Expression for Wall Loss as a Function of Particle Size

Particle Diameter ( $\mu\text{m}$ )	Mobility <sup>a</sup> ( $\text{sec gm}^{-1} \times 10^7$ )	Diffusion Constant <sup>b</sup> ( $\text{cm}^2 \text{sec}^{-1} \times 10^6$ )	Boundary Layer Loss Rate ( $\text{sec}^{-1} \times 10^4$ )	
			Experimental	Estimated
0.05	57.4	23.9	0.894	0.741
0.10	17.1	7.13	0.644	0.896
0.15	8.54	3.56	1.32	1.54
0.20	5.47	2.28	4.42	2.74
0.50	1.56	0.650	21	16.0
1.05	0.682	0.284	88	65.9 <sup>c</sup>

<sup>a</sup>Mobilities for the smaller particles were estimated from Cercignani and Pagani's results for momentum transport at intermediate Knudsen numbers (Fuchs and Sutugin, 1971; Cercignani and Pagani, 1966).

<sup>b</sup>Diffusion constants were calculated from mobilities, B, by Einstein's equation  $D = kTB$ ,  $T = 302 \text{ K}$ .

<sup>c</sup>Large errors are to be expected for this particle size because the net rate is approximately equal to the estimate of the convection limited rate.

experiments, as discussed above. Table 20 shows the particulate properties and loss rates assigned to class intervals as defined by the electric mobility analyzer (TSI 3030).

At this point a brief discussion of some of the theoretical aspects of the fitted expression for the boundary layer rate constant seems in order. This expression can be rearranged to the form

$$k = \frac{D\mu B}{\delta} \left[ \frac{A}{B} h(x) + 1 \right]$$

According to the model used in obtaining this relationship, A/B should be less than one because it represents the effective fraction of the interior chamber surface perpendicular to the volume proportional force, usually assumed to be gravity (sedimentation). The least squares parameter values yield a value of 26.4 for this ratio. Some of this deviation from theory

Table 20. Data Used in Estimating Particulate Wall Losses from Electric Mobility Classification

Channel No.	Representative Particle Size ( $\mu\text{m}$ ) dia.	Mobility ( $\text{gm sec}^{-1} \times 10^8$ )	Diffusion Constant ( $\text{cm}^2 \text{sec}^{-1} \times 10^6$ )	Loss Constants ( $\text{hr}^{-1}$ )	
				Boundary Layer	Overall
2	0.0075	228	950	6.264	0.585
3	0.0133	73.92	308	2.052	0.491
4	0.0237	23.98	99.9	0.796	0.356
5	0.0422	7.995	33.33	0.311	0.210
6	0.0750	2.864	11.9	0.266	0.188
7	0.133	1.062	4.42	0.464	0.270
8	0.237	0.4333	1.80	1.444	0.446
9	0.422	0.1975	0.823	4.32	0.561
10	0.750	0.09737	0.406	12.31	0.613
Upper Limit	1.335	0.04832	0.201	34.60	0.633

is undoubtedly due to the influence of the quasi-homogeneous nature of  $h(x)$  combined with the mechanics of the least squares fitting process. For example, conformity to the geometrical fraction of horizontal surface of the glass chamber, 0.125, can be approximately obtained by increasing  $C/kT$  from 415 to ~88000. However, a change of this magnitude implies a boundary layer thickness of several centimeters which is inconsistent with the estimated values of the other parameters when interpreted according to the model. It is best to regard the expression as a semi-empirical fit to the data which does not conform to the model's behavior because of model deficiencies including different effective layer thicknesses for diffusion and forced diffusion. In addition there are complications due to the Teflon lining of the chamber. This has a considerably larger projected horizontal surface due to folds and wrinkles than the glass chamber proper. Volume-proportional forces of electrical origin may play a role in attracting particles to the surface when the surface is a thin film of electro-

phobic polymeric insulator. These forces can be attributed to small regions of the film where the discontinuous surface electrostatic charge (Harper, 1967; Henry, 1953) produced by handling the film during fabrication has become neutralized, in part, by accumulation of counter charges from the ambient atmosphere on opposing faces of the film to produce a patchy double layer. Patches of double layer might have a long half-life relative to neutralization by atmospheric ions because of the restricted range of their electric fields.

Flash Ignition Sulfur Monitor. The design was based on analysis of the electrothermal behavior of a series circuit of a resistor and a charged capacitor when the resistor has a temperature coefficient of resistance. This indicated that the recommended capacitance and voltage (Husar et al., 1975; Roberts and Friedlander, 1976) suit a tungsten ignition boat but that different values would be required for other dimensions and/or materials. A circuit was built using a high current capacity silicon control rectifier (SCR) to give a wide choice of flashing voltages and capacitances. A digital panel meter to precisely measure flashing voltage and to enable precise triggering of the SCR were included. A DC circuit to heat the boat and evaporate solvent was included.

The boat was clamped between heavy beryllium copper electrodes inside a glass and Teflon cell flushed by the sample flow ( $100 \text{ ml min}^{-1}$ ) to a photometric sulfur analyzer. An access port allowed liquid sample introduction. The cell volume was  $50 \text{ cm}^3$  to allow for sudden expansion. The cell was in the form of a cylinder capped by a cone. Purging inflow was uniformly distributed by a fine mesh screen. The outflow converged to the  $1/8$ " ID inlet to the analyzer.

In preliminary tests the high temperatures appeared to propagate outward as a thermoelectric "explosion" from a portion of the boat accidentally having a somewhat higher resistance than the rest. The boat was replaced by a section of tungsten ribbon having a swaged dimple to contain the sample. Swaging ensures that resistance is highest at the sample thus centering the "explosion" in the sample area.

Further work using solutions of known sulfur concentration brought out difficulties due to "memory" of previous samples which could not be completely removed by repeated flashing. It was found that this effect

could be reduced by washing the ribbon in situ, drying and igniting, resulting in an uncertainty of  $\pm 2$  ng sulfur due to memory effects.

During the preliminary debugging and calibration, a Hewlett-Packard printing GC integrator was found to be a useful addition to the instrumentation system. Its major contribution is reduction of data processing time and it can be interfaced with a computerized data handling system, if required.

Analysis of extracts from clean filters showed blanks having in the range of hundreds of  $\text{ng cm}^{-2}$  of sulfur for several types of filters, including glass, quartz and polycarbonate membrane (Nucleopore). The results obtained by Coutant (1977) indicate that appreciable sorbtion of  $\text{SO}_2$  can be expected for most of the conventional filter materials except polymeric materials or polymer-coated materials where he found sulfur pickups to be less than  $25 \text{ ng cm}^{-2}$  (his limit of detection).

The usefulness of Fluoropore filters ( $0.2 \mu\text{m}$  pore diameter) for this application was investigated with an objective of  $10 \text{ ng cm}^{-2}$  or less filter blanks, due to the combination of trace sulfate and  $\text{SO}_2$  sorbtion. However when low blank Fluoropore filters were used in tests of the complete procedure against chamber atmospheres, highly variable blanks of the order of  $1 \mu\text{g S}$  (referred to the complete filter extract) were obtained. Prewashing the filters did not affect the observed blanks. Since chamber aerosol concentrations in these experiments peak out at around  $10 \mu\text{g S m}^{-3}$ , adequate accuracy requires aerosol samples of greater than  $1 \text{ m}^3$  (from a  $7 \text{ m}^3$  chamber) in the presence of noise in the  $1 \mu\text{g S}$  region. A greater development effort focused on simplifying sampling and reducing sample manipulation is obviously required before the sensitive flash volatilization technique can be profitably applied to this experimental problem. Since an alternative method for assessing aerosol yield was available (see above) and the required resources for further development were not available, it was decided to postpone solution of this problem for future research.

Results. Experimental data on particulate volumes show that losses to the walls are not serious during the initial period of irradiation lasting one to two hours. This is a consequence of initial low mass per particle and the rapid growth of the aerosol into the region of longer chamber lifetimes (see Figure 9). Following this period losses increase

sufficiently to produce a steady-state situation for suspended particulate volume where generation rate is balanced by wall losses. This fortunate outcome was utilized to estimate conversion rates. Data from one experiment in Figure 11 illustrate this behavior. Figure 11 also shows the photometric response to this mixture of sulfur-containing particulate and gaseous sulfur compounds, assumed to be mostly sulfur dioxide. The more rapid decay during the steady-state period is attributed to loss of sulfur by particulate wall losses and by removal of gaseous sulfur dioxide to the walls because the response to particulate is constant during this period. The response to suspended particulate was estimated during this particular experiment by inserting a lead dioxide diffusive separator into the sample line yielding a response factor of  $260 \text{ ppm m}^3 \text{ cm}^{-3}$ , or about 5 ppb as sulfur dioxide. Wall loss of gaseous dioxide was estimated by assuming a decay rate of 0.62% per hour obtained in a separate dark decay experiment.

The lesser rate of decrease of photometric response during the initial period is assumed to be due to near equivalence in photometric response for particulate sulfur as gaseous dioxide combined with dioxide wall loss, the only major loss mechanism for sulfur during this period. However, these assumptions are not used to estimate conversion rates during the initial period. Conversion rates are directly estimated from photometric data only for the steady-state period. Initial period rates are estimated by multiplying the steady-state conversion rates by the ratio of particulate volume appearance rates for the two periods.

Table 21 shows the data summary for this experimental block as well as three exploratory experiments. Detailed data are available upon request. Table 21 also includes auxiliary data judged pertinent to interpretation of the conversion rates. This includes average ozone concentration, rate of disappearance of an alkane, 2,3-dimethylbutane, as indicator of hydroxyl free radical concentration, and a rate weighted average of ozone-olefin concentration products as a measure of the relative importance of this influence on sulfur dioxide conversion. Table 22 lists the pertinent rate constants assumed.

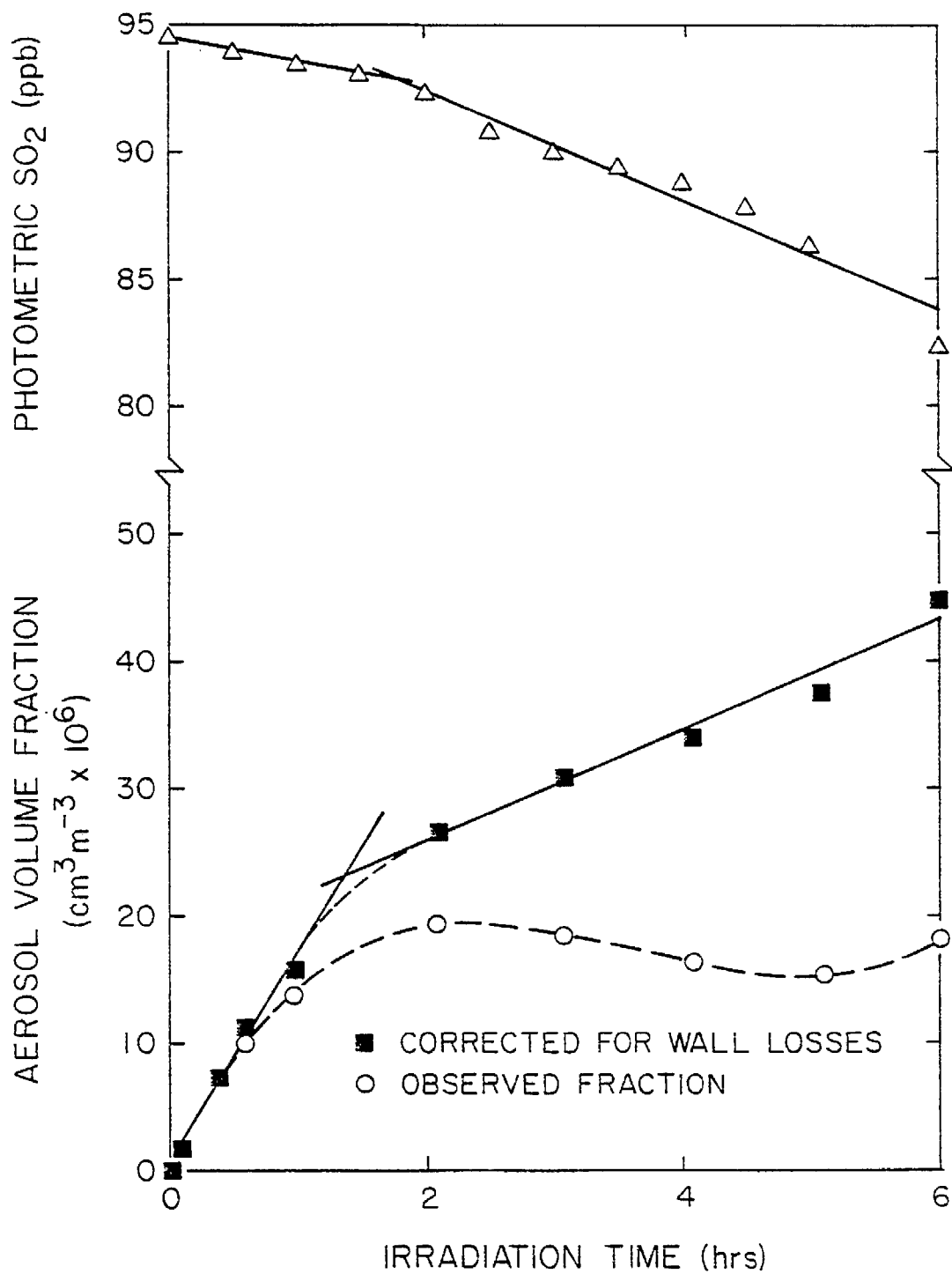


Figure 11. Typical Behavior of Sulfur and Aerosol Volume Data During Photooxidation Experiments (AGC-341).

Table 21. Summarized Data on Sulfur Dioxide to Particle Conversion Rates Promoted by Photooxidizing Surrogate

Exp No. AGC	INITIAL CONCENTRATIONS			OBSERVED RATES <sup>a</sup>					DERIVED DATA			AUXILIARY DATA, FINAL PERIOD		
	NMHC (ppmC)	NO <sub>x</sub> (ppm)	SO <sub>2</sub> (ppm)	DURATION (hrs)	INITIAL		FINAL		PARTIC. EQUIV. FACTOR, <sup>b</sup> $\frac{K}{\text{cm}^3}$ (ppm x m <sup>3</sup> )	CONVERSION RATES		AVERAGE RATE 2,3DMBu (%/hr)	AVERAGE OZONE CONCENT. (ppb)	RATE WEIGHTED OZONE-OLEFIN PRODUCT (ppb <sup>2</sup> )
					PHOTOMETRIC SO <sub>2</sub> (ppb/hr)	AEROSOL $\left(\frac{\text{cm}^3 \text{m}^{-3}}{\text{hr}}\right)$ (x 10 <sup>6</sup> )	PHOTOMETRIC SO <sub>2</sub> (ppb/hr)	AEROSOL $\left(\frac{\text{cm}^3 \text{m}^{-3}}{\text{hr}}\right)$ (x 10 <sup>6</sup> )		INITIAL <sup>c</sup> (%/hr)	FINAL (%/hr)			
341	1.66	0.249	0.094	1.5	-0.92	16.6	-2.17	4.3	370	6.8	2.0	3.1	74	31
342	1.45	0.258	0.133	1.5	-1.10	14.4	-1.91	4.1	260	2.9	0.9	2.9	61	
347	0.99	0.377	0.130	1.5	-2.50	14.1	-1.15	4.2	82	0.9	0.3	1.3	11	10
348	1.38	0.060	0.030	1.0	-0.60	3.6	-0.55	1.4	260	3.2	1.3	4.4	159	46
349	0.69	0.121	0.039	1.0	-0.60	3.8	-0.51	2.2	120	1.2	0.7	3.2	46	11
350	0.34	0.041	0.014	2.0	-0.20	2.9	-0.16	2.0	37	0.8	0.5	4.3	89	6
<u>EXPLORATORY EXPERIMENTS</u>														
338 <sup>d</sup>	1.48	0.222	0.080	2.0	-0.94	7.6	-1.68	3.8	310	3.1	1.6	NI	75	NI
340 <sup>d</sup>	1.04	0.211	0.082	1.5	-1.20	8.5	-1.84	4.6	290	3.1	1.8	NI	59	NI
343 <sup>e</sup>	1.50	0.018	0.344	1.0	-0.00	54.5	-3.97	17.1	110	1.7	0.6	3.8	188	54

<sup>a</sup>The photometric rate includes response to particulate. Particulate responses were experimentally estimated during experiments 341 and 342, giving photometric equivalence factors of 260 and 310 ppm cm<sup>3</sup>/m<sup>3</sup>, respectively.

<sup>b</sup>The equivalence factor is the ratio between SO<sub>2</sub> consumed and aerosol volume generated during the particulate steady-state period. A decay rate of 0.62% per hour is used to correct for chamber lifetime of sulfur dioxide. A constant factor cannot be expected because of probable systematic errors in estimating aerosol volume and variable sulfur content of the aerosol. Typical theoretical factors are 134 for 41% H<sub>2</sub>SO<sub>4</sub>, 336 for (NH<sub>4</sub>)<sub>2</sub>SO<sub>4</sub>, 417 for KHSO<sub>4</sub>.

<sup>c</sup>Estimates of initial rates are quite uncertain because of the paucity of data contributing to the estimate and the possibility that the equivalence factor is variable during aerosol growth.

<sup>d</sup>Experiments 338 and 340 were seeded with KNO<sub>3</sub> aerosol containing 10% (w/w) of KHSO<sub>4</sub>. 338: 4 μg/m<sup>3</sup>, 0.05 μm dia, 2.5 cm<sup>2</sup>/m<sup>3</sup>; 340: 24 μg/m<sup>3</sup>, 0.10 μm dia, 8 cm<sup>2</sup>/m<sup>3</sup>.

<sup>e</sup>Experiment 343 was the result of an accidental overdose of SO<sub>2</sub>.

<sup>f</sup>The experimental rate constants for reaction with hydroxyl free radical are 1.1 and 5.1 for sulfur dioxide and 2,3-dimethylbutane (units, cm<sup>3</sup> molecule<sup>-1</sup> sec<sup>-1</sup> x 10<sup>12</sup>).

Table 22. Rate Constants Used in Discussion

Reaction	Rate Constant cm <sup>3</sup> molecule <sup>-1</sup> sec <sup>-1</sup> x 10 <sup>12</sup>	Ref.
SO <sub>2</sub> + OH	1.1	a
2,3-dimethylbutane + OH	5.1	b
C <sub>2</sub> H <sub>4</sub> + O <sub>3</sub>	1.87 x 10 <sup>-6</sup>	c
C <sub>3</sub> H <sub>6</sub> + O <sub>3</sub>	1.13 x 10 <sup>-5</sup>	c
t-2-butene + O <sub>3</sub>	1.8 x 10 <sup>-4</sup>	c
c-2-butene + O <sub>3</sub>	1.31 x 10 <sup>-4</sup>	c

<sup>a</sup>J. G. Calvert, F. Su, J. W. Bottenheim and O. P. Strausz, Atmos. Environ. 12, 197 (1978)

<sup>b</sup>K. R. Darnall, A. M. Winer, A. C. Lloyd, J. N. Pitts, Jr., Chem. Phys. Lett., 44, 415 (1976c)

<sup>c</sup>NBS Circular 513 (1977) with temperature taken as 302 K.

Discussion. Examination of the rates of conversion does not reveal any surprises. The rates are quite consistent with the conclusions of Calvert et al. in their thorough review of tropospheric mechanisms for homogeneous oxidation of sulfur dioxide (Calvert et al., 1978). Figure 12 shows final rates of conversion plotted against rate of disappearance of 2,3-dimethylbutane. Discarding one maverick point for experiment 341 yields a regression slope of 0.15 which is statistically indistinguishable from the ratio of hydroxyl rate constants of 0.22. This suggests large experimental error in the conversion rate for experiment 341 which should be around 0.6% per hour instead of 2% per hour. The average of 0.15% per hour in excess of the rate correlated with hydroxyl radical could be attributed to reaction with other species but this intercept is not distinguishable from zero on the basis of these data. The deviations from the regression suggest some promotion due to secondary products from ozone-olefin reactions but experimental error is large enough to make this speculation.

From a control viewpoint the major conclusion from these results is that homogeneous conversion of sulfur dioxide is affected by the same

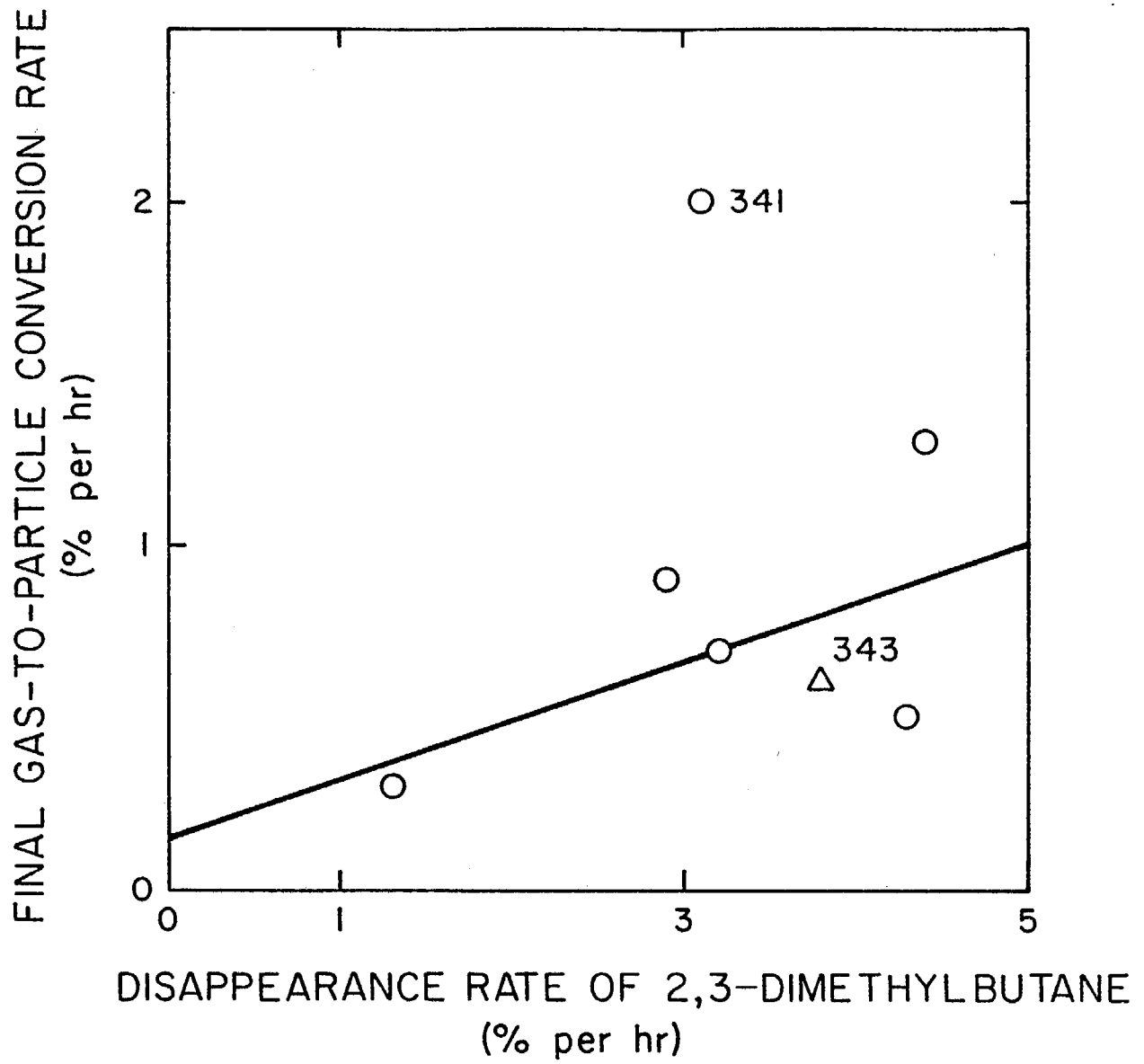


Figure 12. Experimental Data and Regression Calculation for Final Gas-to-Particle Conversion Rates for Sulfur Dioxide vs. Disappearance Rates of 2,3-Dimethylbutane (Regression Calculation Did Not Include #341).

variables that control photochemical reactivity of the hydrocarbon- $\text{NO}_x$  mixture in air. As an example experiment 347 illustrates the suppressant effect of a low hydrocarbon to  $\text{NO}_x$  ratio. The relatively high  $\text{NO}_x$  concentration causes a marked decrease in hydroxyl radical concentration. The same strict emission controls indicated for ozone control will be effective in reducing the homogeneous rate of sulfur dioxide conversion as percent per hour. The only proportionate effect is that of sulfur dioxide concentration because of the relatively large flux of reactive species and the relatively slow rate of the dioxide's reaction with these species.

The enhanced initial rate is due to the higher radical concentration during the  $\text{NO}$  to  $\text{NO}_2$  conversion period when deoxygenation reaction of hydroperoxyl radical with  $\text{NO}$  promotes the rate of appearance of hydroxyl radical. This indicates that the final rates are representative of lower limits for conditions in a polluted atmosphere because continual admixture of nitric oxide from emission sources will tend to promote conversion. However, the estimated initial rates should not be taken quantitatively because of the probable large uncertainties in their estimation. The most that can be said with any confidence is that they are somewhat larger than rates during the final period.

## VII. MONITORING OF NITRATE AEROSOL PRECURSORS

Ammonia, emitted from agricultural and industrial sources in the South Coast Air Basin plays an important role in the stabilization of nitric acid as ammonium nitrate aerosol (National Academy of Sciences, 1977). High levels of particulate nitrates have been measured in the eastern end of the South Coast Air Basin (Grosjean et al., 1976) and characterization of ambient concentrations of both  $\text{NH}_3$  and  $\text{HNO}_3$  are important in understanding mechanisms of gas-to-particle conversion. Only recently has routine monitoring of these nitrogenous compounds in ambient air become possible, using long path Fourier transform infrared absorption spectroscopy (Tuazon et al., 1977; 1978). Using this technique, ambient air monitoring of  $\text{NH}_3$  and  $\text{HNO}_3$  has been carried out on a continuing basis.

Experimental. The experimental techniques used have been described in detail previously (Tuazon et al., 1977; 1978). Four rectangular mirrors, cut from a single 41 cm diameter Pyrex blank, comprise the in-focus end of the cell. The out-of-focus optical assembly consists of four 30 cm diameter mirrors and is 22.5 meters (the average radius of curvature of the eight mirrors) from the nesting mirror assembly. All mirrors are optically polished and gold-coated for maximum reflectivity in the infrared.

The cell housing consists of a rectangular aluminum frame (0.81 x 0.84 x 23 m) enclosed at the bottom and one side with Plexiglas and with 50-micron FEP Teflon on the other two faces.

Coupled with the cell is a Digilab interferometer system housed in an air-conditioned building. The collimated infrared beam from a Nernst glower is modulated by a Digilab Model 296 Michelson IR interferometer capable of spectral resolutions as high as  $0.5 \text{ cm}^{-1}$  and is imaged at the entrance aperture of the cell. The beam exiting from the cell is sent to either of two liquid- $\text{N}_2$  cooled detectors: a photovoltaic InSb detector for the 2000 to  $3900 \text{ cm}^{-1}$  region or a photoconductive HgCdTe detector for the 600 to  $2000 \text{ cm}^{-1}$  region. Data collection and processing are performed with a Data General Nova 1200 computer with 4096 16-bit words of core. A disk unit (128 K words) is used for software storage and partial storage of data. Archival data storage of both raw interferograms and computed spectra is provided by a Kennedy Model 9700 magnetic

tape unit. The Digilab system is also equipped with a Houston Instruments pen plotter, an oscilloscope and a teletype.

The instrumentation on loan to SAPRC from the Environmental Protection Agency was initially set up on the roof of the Webber Hall East building on the UC Riverside campus and became fully operational during August, 1976. This location is 24 m above the ground and provides unobstructed exposure to prevailing winds from the west, north or south. Since July, 1977, the system has been moved alongside the ARB trailer near SAPRC. During ambient monitoring, atmospheric sample is drawn continuously through the cell at a rate of 330 liters  $\text{sec}^{-1}$  (one cell volume every 50 seconds) by a 1/4 hp blower at one end. Air enters the other end of the cell through a 36 cm diameter pipe with an intake two meters above the roof.

Routine data collection was carried out at pathlengths of 1.08 or 0.72 km. Forty interferograms were usually co-added to enhance the signal-to-noise ratio in the interferogram, and thus in the computed spectrum. The spectral resolution routinely employed was  $0.5 \text{ cm}^{-1}$ . At this resolution the vibration-rotation structure of most light molecules present in the atmospheric sample can be resolved and used for positive identification. Data collection with 40 scans, transform computation, routine plotting of a portion of the spectrum and magnetic tape storage could be accomplished within 10 minutes for each detector. Hence, a time resolution of three complete spectra ( $600\text{--}4000 \text{ cm}^{-1}$ ) per hour is available to characterize moving smog fronts.

Strong absorptions due to the  $\text{H}_2\text{O}$  and  $\text{CO}_2$  content of the atmosphere render certain regions of the infrared unsuitable for detection of pollutant molecules. At pathlengths of 1 km and longer, the spectral windows for infrared detection are generally limited to the  $760\text{--}1300 \text{ cm}^{-1}$ ,  $2000\text{--}2230 \text{ cm}^{-1}$  regions. For data analysis spectra are retrieved from storage and ratioed against clean background spectra with the same water content in order to eliminate the majority of interfering water absorptions and to facilitate the measurement of band intensities.

Results and Discussion. The  $\text{NH}_3$  and  $\text{HNO}_3$  concentrations observed are given in Table 23 for three days during a stagnant air episode in October, 1976, and for eight selected days during July, September and October, 1977.

Table 23. Pollutant Concentration (ppb) in Riverside Air<sup>a</sup>

Date	Time <sup>b</sup>	NH <sub>3</sub>	HNO <sub>3</sub>	Date	Time <sup>b</sup>	NH <sub>3</sub>	HNO <sub>3</sub>	
<u>1976</u>				<u>1977</u>				
Oct. 4	1033	6	-	Sept. 2	1435	41	-	
	1208	5	-		1505	52	-	
	1252	3	-		1530	53	-	
	1511	31	-		1600	30	-	
	1603	24	-		1622	27	-	
	1700	18	-		1640	27	-	
	1730	4	-		1700	21	-	
	1759	-	-		1720	21	-	
	1827	-	-		1740	18	-	
	1903	-	-		1800	18	-	
	1913	-	-					
Oct. 5	1522	36	-	Sept. 9	1120	-	11	
	1634	21	-		1213	17	9	
	1705	15	-		1232	13	8	
	1736	20	-		1300	16	8	
	1805	14	-		1335	47	6	
	1833	-	4		1403	41	-	
	1922	-	6		1430	51	-	
	1947	-	4		1450	45	-	
Oct. 6	1142	4	6	Sept. 21	1517	40	-	
	1155	4	4		1545	31	-	
	1258	14	5		1445	23	8	
	1320	23	4		1508	23	-	
	1429	43	4		1525	12	-	
	1514	31	-		1558	8	-	
	1556	22	-		1623	4	-	
	1630	21	-		1645	-	-	
	1658	30	-		1709	-	8	
	1725	25	-		1730	-	8	
	1753	26	-		Sept. 22	1310	21	-
1833	12	-	1335	24		-		
1853	3	-	1403	21		-		
			1430	14		-		
<u>1977</u>								
July 14	1403	31	c	Oct. 5	1500	26	-	
	1432	27	c		1530	20	-	
	1458	17	c		1600	22	-	
	1517	14	c		1630	15	-	
	1537	15	c					
	1557	16	c		1140	-	10	
	1619	13	c,d		1202	-	7	
	1637	4	c,d		1239	-	9	
	1712	-	c		1301	-	10	
	1729	-	c		1330	-	10	
	1749	-	c		1400	-	-	
	1813	-	c		1431	55	-	
	1832	7	c		1500	36	-	
	1852	7	c		1527	26	-	

(continued)

Table 23. (continued)

Date	Time <sup>b</sup>	NH <sub>3</sub>	HNO <sub>3</sub>	Date	Time <sup>b</sup>	NH <sub>3</sub>	HNO <sub>3</sub>
<u>1977</u>				<u>1977</u>			
Oct. 18	1400	-	13	Oct. 26	1230	5	10
	1427	-	8		1302	6	8
	1447	-	8		1331	9	8
	1511	16	6		1400	24	8
	1533	28	-		1430	85	-
	1600	39	-		1500	61	-
	1620	23	-		1530	73	-
	1650	8	-		1600	59	-
	1710	9	-		1630	55	-
	1741	-	-		1700	35	-
	1802	-	8		1730	35	-
	1830	-	6				

<sup>a</sup>Dashes indicate below detection limit [ $\sim 2$  ppb for NH<sub>3</sub> and  $\sim 4$  ppb for HNO<sub>3</sub> (Tuazon, Winer, Graham and Pitts, Proc. 4th Joint Conf. on Sensing of Environmental Pollutants, ACS, 1978, pp 798-802)].

<sup>b</sup>All times Pacific Daylight Time.

<sup>c</sup>No suitable reference spectrum.

<sup>d</sup>Maximum HNO<sub>3</sub> levels  $\sim 15$  ppb.

It can readily be seen that NH<sub>3</sub> levels of  $\sim 20$ - $40$  ppb are common; Riverside is typically downwind of agricultural sources of ammonia, while HNO<sub>3</sub> levels are generally below  $10$  ppb. It can also be seen that on several occasions (October 6, 1976; September 9, 1977; and October 26, 1977) NH<sub>3</sub> and HNO<sub>3</sub> co-exist at appreciable levels, though at other times there appears to be an anticorrelation. Obviously further prolonged monitoring is necessary.

VIII. ASSESSMENT OF OXIDANT-PRECURSOR RELATIONSHIPS UTILIZING  
A COMPUTER KINETIC MODEL

A quantitative understanding of how ozone formation in photochemical air pollution is affected by changes in emissions of its hydrocarbon and nitrogen oxides precursors is necessary for the formulation of cost-effective oxidant control strategies. One technique which is available for the determination of ozone-precursor relationships is the combined smog chamber-modeling approach described by Dimitriades (1977) and Dodge (1977a). This technique, called the "empirical kinetic modeling approach" (EKMA) involves validating a computer kinetic model against smog chamber data, and then removing the portions of the model which are attributed to chamber effects and incorporating into the model the appropriate diurnal light intensities. This model is then used to calculate ozone yields as a function of initial nonmethane hydrocarbon (NMHC) and  $\text{NO} + \text{NO}_2$  ( $\text{NO}_x$ ) concentrations. Although this approach that is currently under active investigation by the EPA [Dimitriades, 1977; Dodge, 1977a; Dodge, 1977b; Environmental Protection Agency, 1978], an independent study of this method, making different assumptions concerning poorly understood chamber effects and utilizing a different data base for model validation, is necessary to test the consistency and reliability of the general method before it is seriously applied in formulating control strategies. We describe our progress in such an independent investigation of the EKMA method.

Smog Chamber Data Base. The smog chamber data used for model validation were the results of selected experiments in the extensive surrogate hydrocarbon-glass chamber program performed at SAPRC under previous contracts for the ARB. The experimental procedures and conditions are described in previous reports (Pitts, 1975b; 1976b) and briefly summarized here.

Irradiations of  $\text{NO}_x$ -hydrocarbon mixtures were carried out in the ~6400 liter all-glass chamber. Oxides of nitrogen and the surrogate hydrocarbon mixture were injected into the chamber, mixed and sampled prior to the initiation of the photolysis. Ozone and  $\text{NO}-\text{NO}_2-\text{NO}_x$  were monitored continuously by ultraviolet absorption and chemiluminescence, respectively. CO, hydrocarbons and PAN were monitored by gas chromatography, and formal-

dehyde was monitored by the chromotropic acid technique. Most of the irradiations were carried out for six hours, though a number of irradiations were of nine hours duration.

The light intensity was measured by periodic determination of  $k_1$ , the  $\text{NO}_2$  photolysis rate, using the method of Holmes et al. (1973). The determinations have some uncertainty because it is difficult to completely remove  $\text{O}_2$  from the chamber, which cannot be evacuated. The value of  $k_1$  believed appropriate for these experiments is  $0.25 \text{ min}^{-1}$ . The relative spectral distribution of the photolyzing radiation was determined in a separate experiment by employing a monochromator-photomultiplier system located facing the lights.

All experiments employed initial  $\text{NO}_x$  consisting of approximately 10%  $\text{NO}_2$  and 90%  $\text{NO}$ . The composition of the surrogate hydrocarbon mixture was chosen to represent the ambient air pollutant burden from all sources in the South Coast Air Basin (Pitts et al., 1975b; 1976b), and is given in Table 24. The results of chromatographic sampling of the hydrocarbons prior to the smog chamber photolyses confirmed that, with the exception of formaldehyde (which appears to be a contaminant in this system), the initial relative hydrocarbon composition observed prior to the photolysis agreed reasonably well with values given on Table 24. Results of over 50 irradiations were used in this study. The experiments used fell into four groups corresponding to initial NMHC levels of:  $0.44 \pm 0.09 \text{ ppmC}$ ;  $0.69 \pm 0.07 \text{ ppmC}$ ;  $1.39 \pm 0.13 \text{ ppmC}$ ; and  $2.23 \pm 0.16 \text{ ppmC}$ . Initial  $\text{NO}_x$  ranged from 0.005 to 0.5 ppm.

Computer Kinetic Models. The two kinetic models employed are based on a detailed propene + n-butane- $\text{NO}_x$ -air photooxidation mechanism which has been developed (Carter et al., 1979) to be consistent with current basic kinetic and mechanistic chemical data and with the well characterized smog chamber experiments carried out at SAPRC using the evacuable chamber facility (Pitts et al., 1977a; Winer et al., 1979). The complete description of this model, its major uncertainties, and detailed comparisons of model predictions with chamber experiments are given elsewhere (Carter et al., 1979), and are not reproduced here.

The two models actually employed in this study differed in some respects from that described by Carter et al. (1979); these differences are

Table 24. Composition of Surrogate Mixture for Simulation of Hydrocarbon Emissions in Los Angeles

Pollutant		Concentration (ppb) when NMHC = 1000 ppC
<u>Reactive, Non-Oxygenated</u>	n-Butane	79.9
	2,3-Dimethylbutane	41.8
	Ethene	17.1
	Propene	4.8
	Cis-2-butene	6.1
	2-Methyl-2-butene	5.7
	Toluene	6.7
	m-Xylene	16.5
<u>Oxygenates</u>	Formaldehyde	22.0
	Acetaldehyde	1.0
	Acetone	0.8
<u>Unreactive</u>	Methane	1140
	Ethane	32.6
	Propane	5.4
	Acetylene	20.6

noted below. Complete computer listings of each of the models are available from the authors.

(a) The propene + n-butane model is a slightly simplified version of the detailed propene + n-butane model. The simplifications concern only predictions of minor organic products, and do not significantly affect the predicted inorganic profiles. The specific differences are:

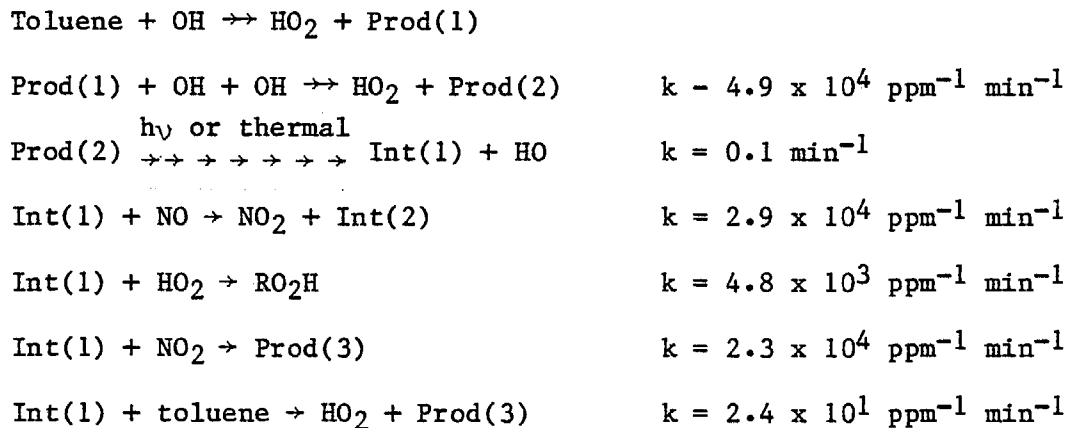
- OH radicals were assumed to react with n-butane only by abstraction of a secondary hydrogen.
- OH was assumed to react with propylene only by internal addition to the double bond.
- $\alpha$ -hydroxy alkoxy radicals formed in the propene system were assumed to decompose much more rapidly than competing processes.
- Secondary reactions of minor organic products, formed less than 10% of the time, were ignored.

In this propene + n-butane model, all the reactive hydrocarbons in the surrogate mixture were represented by propene, n-butane and formaldehyde. Formaldehyde represented all oxygenated hydrocarbons initially present (primarily formaldehyde, see Table 24), and its initial concentration (in ppm) used in the calculations was  $0.026 \times$  initial NMHC (ppmC). n-Butane, 2,3-dimethylbutane, ethene, propene, cis-2-butene, 2-methyl-2-butene, toluene and m-xylene in the surrogate (see Table 24) were represented by propene and n-butane, whose initial concentrations were  $0.060 \times$  NMHC (ppmC) and  $0.172 \times$  NMHC (ppmC), respectively. Those concentrations were chosen so the propene + n-butane mixture had the same ppmC and the same OH reactivity (the sum of the initial hydrocarbon concentrations  $\times$  the OH + hydrocarbon rate constants [Atkinson et al., 1979]) as the hydrocarbon mixture they represented. Relatively unreactive methane, ethane, propane and acetylene were ignored and not represented in the models.

(b) The semi-detailed model had exactly the same inorganic and chamber-dependent mechanisms as the propene + n-butane model, but differed in its treatment of the eight non-oxygenated reactive hydrocarbons. Instead of representing them all by propene + n-butane, they were (with the exception of cis-2-butene and 2-methyl-2-butene) treated separately. Individual reactions for the consumption of all hydrocarbons by OH and for the consumption of all alkenes by OH,  $O_3$ ,  $O(^3P)$  and  $NO_3$  were included

in the model along with the appropriate rate constants for the individual hydrocarbons. Only cis-2-butene and 2-methyl-2-butene were lumped together as a single species reacting with averaged rate constants. (This is a reasonable approximation because they are both almost completely reacted within the first few hours.) However, this is obviously still not a true detailed hydrocarbon photooxidation model because it was assumed that the products of the initial attack (by OH, O<sub>3</sub>, etc.) were the same for all hydrocarbons of the same class. All alkenes gave the same products and reacted with the same mechanism as propene, all alkanes reacted as n-butane, and all aromatics reacted as toluene (see below). This "semi-detailed" model is still highly approximate, but the approximations employed are of a different nature than those in the propene + n-butane model, so comparisons of their predictions should be useful in assessing some of the effects of lumping together the initial consumption reactions of the reactive hydrocarbons.

At present, the mechanism for the photooxidation of aromatic hydrocarbons in NO<sub>x</sub> air mixture is unknown. We found that the following mechanism gave fair fits to at least some toluene-NO<sub>x</sub>-air experiments performed at SAPRC (Atkinson et al., 1979b).



No claim is made for the validity of this mechanism, and it is almost certain that there are significant omissions if not errors. Its most important characteristic is rapid radical production from reactions of some unknown photooxidation product; no toluene smog chamber experiments can be reasonably fit by models which do not have this feature (Atkinson et al.,

1979b; Pitts et al., 1975a). However, even if this mechanism is completely invalid, it should be useful for assessing the effect of treating the aromatic hydrocarbon photooxidation mechanisms differently from those of propene + n-butane.

Model Calculations Simulating Chamber Experiments. In order to simulate the smog chamber results, the model must include provisions for chamber effects. The major chamber-dependent portions of our model concern:

- (a) The photolysis rate constants.
- (b) Radical input from unknown chamber sources.
- (c) The  $\text{N}_2\text{O}_5 + \text{H}_2\text{O} \rightarrow 2\text{HNO}_3$  reaction.
- (d) Ozone destruction on the walls.

The photolysis rate constants can be calculated using published or estimated absorption coefficients and quantum yields, and the measured intensities and spectral characteristics of the photolyzing radiation in the glass chamber. The rate of ozone destruction by the walls is determined by ozone dark decay experiments. The other two chamber-dependent portions of our model are more uncertain, and had to be represented by adjustable parameters in our chamber simulation calculations.

The important uncertain chamber effects concern the radical input rate from unknown sources and the  $\text{N}_2\text{O}_5 + \text{H}_2\text{O}$  rate constants. It is necessary to assume a significant radical input from unknown sources in order to account for radical initiation in smog chamber runs (Carter et al., 1979; Bufalini et al., 1972; Wu et al., 1976; Bufalini et al., 1977). We found that the most satisfactory fits to the data are obtained by assuming an input of hydroxyl radicals at a constant rate throughout the run, where the rate was adjustable for each run. A hydroxyl input rate of  $0.15 \text{ ppb min}^{-1}$  is generally the minimum value required for model calculations to fit chamber experiments, while a rate of  $0.3 \text{ ppb min}^{-1}$  is more typical of experiments with the initial  $\text{NO}_x$  in the 0.2 - 0.5 ppm range. The maximum  $\text{N}_2\text{O}_5 + \text{H}_2\text{O}$  rate constant appears to be around  $2 \times 10^{-5} \text{ ppm}^{-1} \text{ min}^{-1}$  (Carter et al., 1979; Morris and Niki, 1973), but significantly lower values are often required to fit  $\text{NO}_2$  consumption rates in some smog chamber experiments (Demerjian et al., 1974; Carter et al., 1979). The effect of varying these parameters within these ranges was tested in our chamber simulation calculations.

Four sets of chamber simulation calculations, designated A<sub>1</sub>, B<sub>1</sub> and B<sub>2</sub> and C<sub>1</sub> were performed. Calculations A<sub>1</sub>, B<sub>1</sub> and B<sub>2</sub> employed the propene + n-butane model, and show the effect of varying the most uncertain important chamber effect parameters. Calculation A<sub>1</sub> used an OH radical input rate of 0.15 ppb min<sup>-1</sup>, while calculations B<sub>1</sub> and B<sub>2</sub> used 0.30 ppb min<sup>-1</sup>. Calculations A<sub>1</sub> and B<sub>1</sub> assumed the N<sub>2</sub>O<sub>5</sub> + H<sub>2</sub>O reaction was negligible, while calculation B<sub>2</sub> used the maximum rate constant of Morris and Niki (1973). Calculation C<sub>1</sub> employed the semi-detailed model, but otherwise used the same conditions as calculation B<sub>1</sub>. The conditions employed and O<sub>3</sub> yields predicted by these calculations are summarized in Table 25.

Figures 13 and 14 compare six- and nine-hour O<sub>3</sub> yields observed in the surrogate hydrocarbon-glass chamber experiments with those predicted by the four model calculations. For the higher NO<sub>x</sub> experiments, it can be seen that calculations B<sub>1</sub> and C<sub>1</sub> give the best fits to the ozone yields, while for lower NO<sub>x</sub> runs, calculation A<sub>1</sub> appears to be better. This is consistent with the observation that for lower NO<sub>x</sub> runs, lower hydroxyl input rates are required to fit the data. The relatively poor fits to the observed low NO<sub>x</sub> nine-hour O<sub>3</sub> by calculations B<sub>1</sub> and C<sub>1</sub> could also be due in part to the effect of input of NO<sub>x</sub> from the laboratory make-up air. It can also be seen that calculations assuming the rate constant for N<sub>2</sub>O<sub>5</sub> + H<sub>2</sub>O is negligible give better fits to the data and that the predictions of the semi-detailed model (C<sub>1</sub>) closely follows those of the corresponding propene + n-butane calculation (B<sub>1</sub>), except that O<sub>3</sub> predictions of the semi-detailed model are consistently ~10% lower.

It is concluded that the ozone predictions of both the propene + n-butane model and the semi-detailed model can be made consistent with most of the surrogate-glass chamber data if suitably adjusted values of the uncertain chamber effect parameters are used. However, the possibility that significant errors in the chamber-independent portions of the models can be hidden by this adjustment of parameters attributed to chamber effects cannot be discounted. This means that until the important smog chamber effects are more fully understood, the models cannot be completely validated. The best we can hope for at this time is that the models not be inconsistent with the chamber data, and we believe that this more

Table 25. Experimental and Calculated O<sub>3</sub> for Various Initial Surrogate Hydrocarbons and NO<sub>x</sub> Levels for Photolysis<sub>3</sub> in the SAPRC Glass Chamber

INITIAL NMHC (ppbC)	NO <sub>x</sub> (a) (ppm)	APPROXIMATE EXPERIMENTAL O <sub>3</sub> (b) (ppm)		CALCULATED O <sub>3</sub> (ppb)											
		6 Hr.	9 Hr.	CALC. A <sub>1</sub>			CALC. B <sub>1</sub>			CALC. B <sub>2</sub>			CALC. C <sub>1</sub>		
				6 Hr	9 Hr	Max (c)	6 hr	9 Hr	Max	6 Hr	9 Hr	Max	6 Hr	9 Hr	Max
450	10	75	50	63	59	69(3)	(d)	(d)	58(2)	(d)	(d)	58(2)	51	51	54(2)
	50	175	200	167	167	170(7)	1401	144	152(4)	145	141	152(4)	139	133	144(4)
	100	175	250	113	113	203(11)	198	189	198(7)	192	182	190(7)	177	169	177(6)
	150	75	225	58	108	≥107(≥12)	144	213	213(9)	145	202	202(9)	121	185	185(9)
	200	-	-	29	58	≥ 97(≥12)	82	175	214(11)	82	176	203(11)	61	146	183(11)
700	10	-	-	70	63	78(3)	(d)	(d)	68(2)	(d)	(d)	68(2)	54	52	61(2)
	50	200	200	197	191	189(5)	173	162	183(4)	167	156	177(4)	164	154	172(4)
	100	250	275	169	244	253(11)	245	232	245(6)	232	216	232(6)	225	211	225(6)
	200	175	275	158	111	≥172(≥12)	142	259	287(11)	141	253	262(10)	117	228	251(11)
	300	50	150	20	40	≥ 70(≥12)	55	124	≥216(≥12)	55	123	≥221(≥12)	38	93	≥178(≥12)
1500	10	75	100	74	63	90(3)	(d)	(d)	84(2)	(d)	(d)	81(2)	57	51	67(2)
	50	225	250	240	217	243(5)	211	189	232(3)	195	175	220(3)	199	180	217(3)
	100	300	350	295	329	329(9)	322	292	322(6)	283	254	291(5)	303	273	304(5)
	200	375	350	169	274	≥368(≥12)	298	410	413(10)	295	341	346(8)	281	380	380(9)
	300	175	300	75	152	≥231(≥12)	175	310	≥431(≥12)	172	312	362(11)	148	275	≥390(≥12)
	400	50	-	31	72	≥127(≥12)	90	191	≥303(≥12)	89	187	≥311(≥12)	67	151	≥255 ≥12)
2200	10	-	-	(d)	(d)	93(2)	(d)	(d)	88(2)	(d)	(d)	83(2)	55	(d)	66(2)
	50	225	300	248	219	262(4)	223	197	257(3)	199	174	235(3)	211	187	287(3)
	100	350	400	356	349	363(7)	350	311	360(5)	295	262	317(4)	330	294	341(5)
	200	350	425	268	398	≥461(≥12)	404	469	469(9)	374	357	380(7)	392	441	444(8)
	300	250	400	149	266	≥374(≥12)	280	445	≥527(≥12)	274	402	402(9)	255	419	≥487(≥12)
	400	>250	300	70	156	≥247(≥12)	172	317	≥459(≥12)	167	313	≥409(≥12)	144	276	≥416(≥12)
	500	>150	200	33	30	≥147(≥12)	94	207	≥329(≥12)	92	200	≥334(≥12)	72	164	≥275(≥12)

CALCULATION CONDITIONS

OH Input Rate (ppb-min <sup>-1</sup> )	0.15	0.3	0.3	0.15
k(N <sub>2</sub> O <sub>5</sub> +H <sub>2</sub> O+2HNO <sub>3</sub> ) (ppm <sup>-1</sup> min <sup>-1</sup> )	0	0	2 x 10 <sup>-5</sup>	0
Surrogate Model	Propene + n-butane	Propene + n-butane	Propene + n-butane	Detailed

(a) NO<sub>x</sub> = 10% NO<sub>2</sub>, 90% NO

(b) Experimental data is scattered. Values given are obtained from hand-drawn curves through the experimental points, and rounded to the nearest 25 ppb.

(c) Number of parentheses is time (in hours) of O<sub>3</sub> max.

(d) Integration algorithm failed following NO<sub>x</sub> consumption and O<sub>3</sub> maximum.

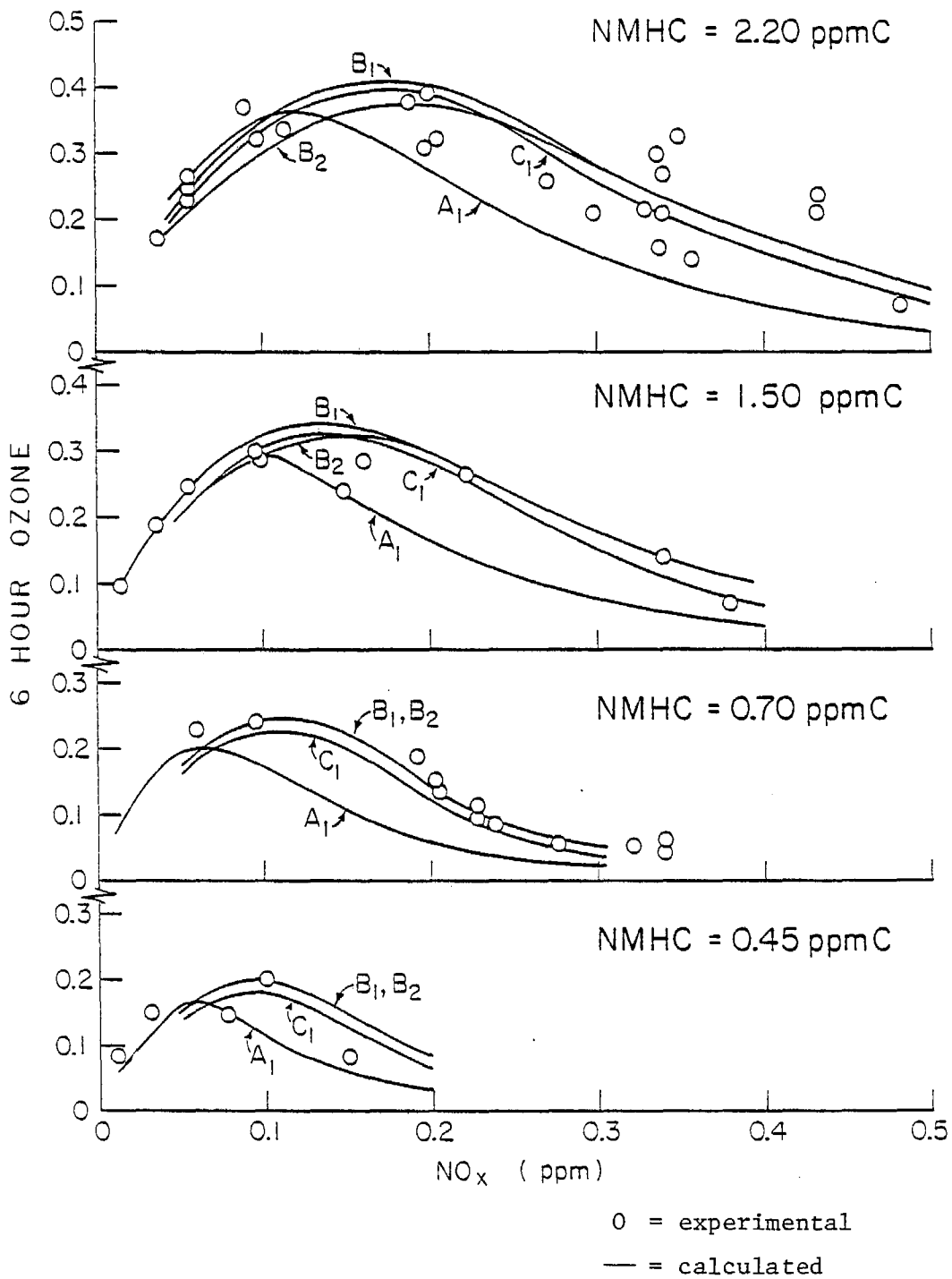


Figure 13. Six-Hour Ozone (ppm) versus NO<sub>x</sub>.

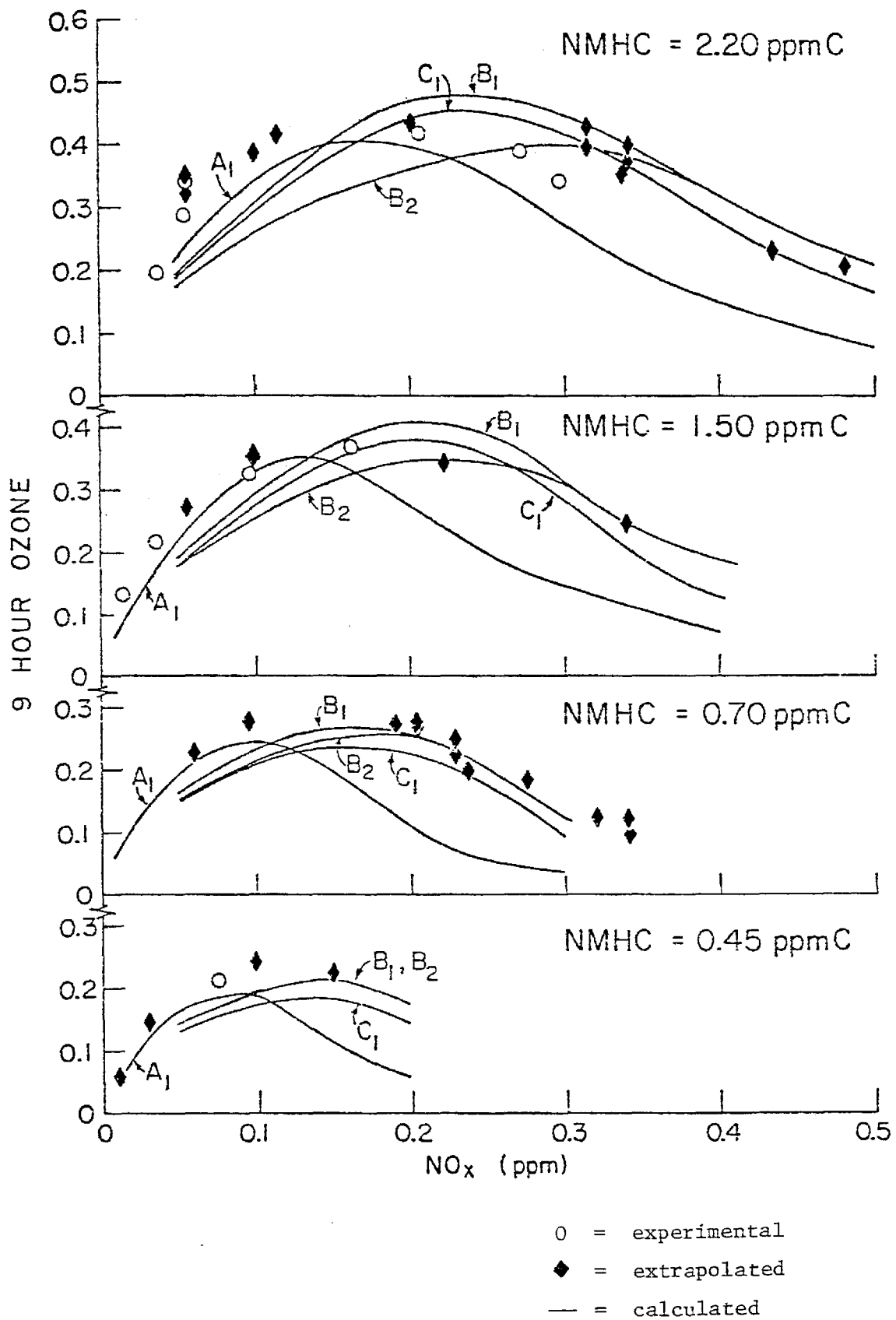


Figure 14. Nine-Hour Ozone (ppm) versus NO<sub>x</sub>.

modest goal has been achieved.

Ambient Air Simulations. Calculations were performed using diurnally varying photolysis rates with the chamber effects removed. The calculation conditions are given in Table 26 along with their designation symbols. The effects on model calculations of altering light intensity and duration due to seasonal changes, of enriching the UV radiation by reducing stratospheric ozone, of altering the emissions or dilution model, and of using the semi-detailed model instead of the propene + butane model have been examined. In addition, calculations were done duplicating the conditions employed by Dodge (1977a) to generate the published calculated ozone isopleths for the ambient air (Dodge, 1977a; Dimitriades, 1977).

The maximum ozone levels attained during the one-day ambient air simulations are summarized for all calculations in Table 27. Figures 15 and 16 plot this maximum ozone against initial  $\text{NO}_x$  (or  $\text{NO}_x$  equivalent to injection rate for calculations "E") for the highest and lowest NMHC levels for the different sets of calculations. (The shapes of the curves for the intermediate NMHC levels are similar.) Figures 15 and 16 can be considered to be cross sections of three-dimensional  $\text{O}_3$ -NMHC- $\text{NO}_x$  surfaces. Figures 17 and 18 compare these calculated  $\text{O}_3$ -NMHC- $\text{NO}_x$  relationships in a more compact manner. Figure 17 plots the maximum  $\text{O}_3$  level attainable for a given NMHC (regardless of  $\text{NO}_x$ ) against NMHC, and Figure 18 plots the  $\text{NO}_x$  level at which this maximum  $\text{O}_3$  is formed for a given initial NMHC (hereafter referred to as the "optimum"  $\text{NO}_x$ ) against NMHC.

The following specific results of the calculations are noted:

- The nature of the  $\text{O}_3$ -NMHC- $\text{NO}_x$  relationships calculated for the ambient air is significantly different from those calculated for smog chamber conditions (compare the dashed curves [chamber simulations] with the solid curves [solar irradiation, no chamber effects] on Figures 17 and 18). Although the curve giving the maximum  $\text{O}_3$  attainable for given NMHC levels (shown on Figure 17) in the chamber simulations is within the range of curves from the ambient air calculations, the dependence of  $\text{O}_3$  on NMHC appears to be somewhat less in smog chamber conditions than in the ambient air. The difference for the curves giving the "optimum"  $\text{NO}_x$  for given NMHC levels are more dramatic (see Figure 18). It can be seen that

Table 26. Conditions Employed in Ambient Air Simulation Calculations

Label	Period	Degrees Latitude	Season <sup>a</sup>	Strat. O <sub>3</sub> (Atm cm)	Dilution (% hr <sup>-1</sup> )	Emissions Model <sup>b</sup>	Hydrocarbon Model <sup>c</sup>
A	9am-6pm	32 N	Equinox	0.295	0	Static <sup>d</sup>	P+B
A <sub>D</sub>	9am-6pm	32 N	Equinox	0.295	0	Static <sup>d</sup>	SD
S	9am-6pm	32 N	Summer	0.295	0	Static <sup>d</sup>	P+B
W	9am-6pm	32 N	Winter	0.295	0	Static <sup>d</sup>	P+B
R	9am-6pm	32 N	Equinox	0.197	0	Static <sup>d</sup>	P+B
D	9am-6pm	32 N	Equinox	0.295	10	Static <sup>d</sup>	P+B
E	6am-6pm	32 N	Equinox	0.295	0	Continuous <sup>d</sup>	P+B
DS	7am-4pm	34 N	Summer	0.295	3	Static <sup>e</sup>	P+B

<sup>a</sup>Equinox: Solar delineation = 0°. Winter: Delineation = -23.5°. Summer: Solar delineation = +23.5°.

<sup>b</sup>Static: Full loading of pollutant at start of simulation. Continuous: No initial loading; continuous pollutant input at rates such that the total dose of NMHC or NO<sub>x</sub> if they did not react would be the same as in the corresponding static simulation.

<sup>c</sup>P+B = propene + butane model used; SD = semi-detailed model used.

<sup>d</sup>NO<sub>2</sub> input = 10% NO<sub>x</sub> input.

<sup>e</sup>NO<sub>2</sub> input = 25% NO<sub>x</sub> input.

Table 27. Calculated 1-Day Ozone Maxima for Various Initial Surrogate Hydrocarbon and NO<sub>x</sub> Levels Assuming Diurnal Solar Irradiation and an Absence of Chamber Effects

NMHC (PPBC)	NO <sub>x</sub> (PPB)	O <sub>3</sub> Maximum (ppb)							
		CALC A <sub>D</sub>	CALC A	CALC S	CALC W	CALC R	CALC D	CALC E	CALC DS
450	5	90	57	86	80	70	56	80	71
	10	134	106	132	108	111	81	143	104
	25	198	177	210	89	182	113	202	166
	50	148	123	243	34	231	83	111	205
	100	41	31	83	7	77	28	24	86
700	10	140	100	134	125	114	89	150	112
	25	225	196	225	155	192	136	238	178
	50	271	245	308	96	273	152	248	245
	75	-	-	323	-	306	-	-	274
	100	133	102	240	24	233	76	80	225
200	24	19	47	6	40	21	15	59	
1500	10	136	96	134	137	124	104	148	124
	25	241	194	231	228	211	171	260	209
	50	352	310	343	278	302	228	372	294
	100	449	411	487	189	436	258	416	396
	150	356	301	527	95	498	197	263	454
	200	239	181	409	38	386	133	132	386
	300	80	53	184	13	158	57	34	190
400	29	23	61	8	50	27	17	84	
2700	10	138	95	135	133	127	108	135	127
	25	235	194	239	237	222	188	251	219
	50	360	311	349	337	329	258	381	320
	75	-	-	-	270	-	-	-	-
	100	519	475	509	350	463	330	528	437
	150	597	529	625	255	567	335	526	-
	200	505	435	677	161	635	282	394	572
	300	291	210	494	40	461	164	142	474
	400	125	78	280	16	244	86	45	286
500	48	34	123	10	98	43	23	155	

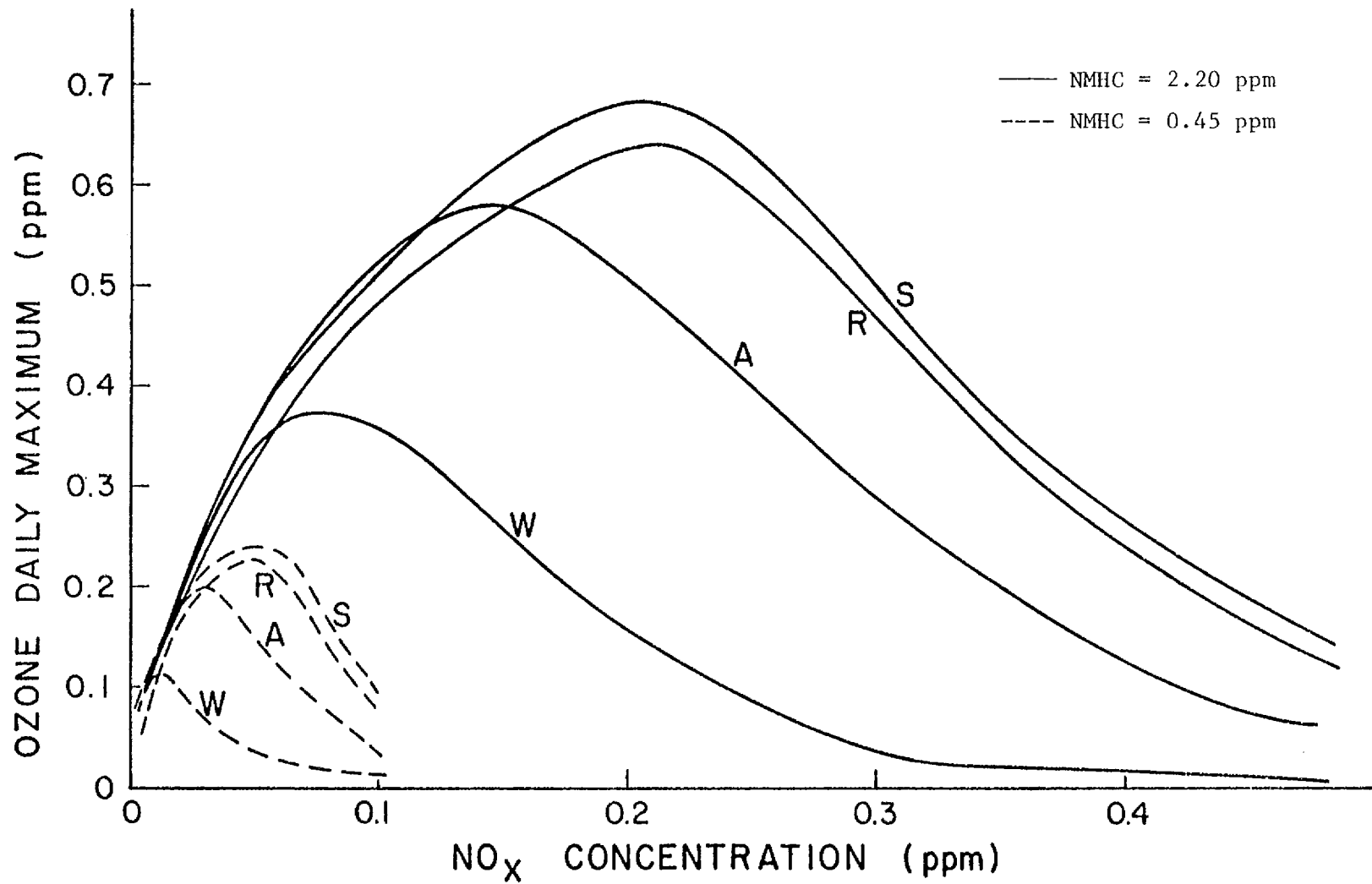


Figure 15. Effect of Season and Stratospheric Ozone Level on Ambient Air Simulations: Calculated Daily Maximum Ozone vs. NO<sub>x</sub> Level for Highest and Lowest NMHC Level.

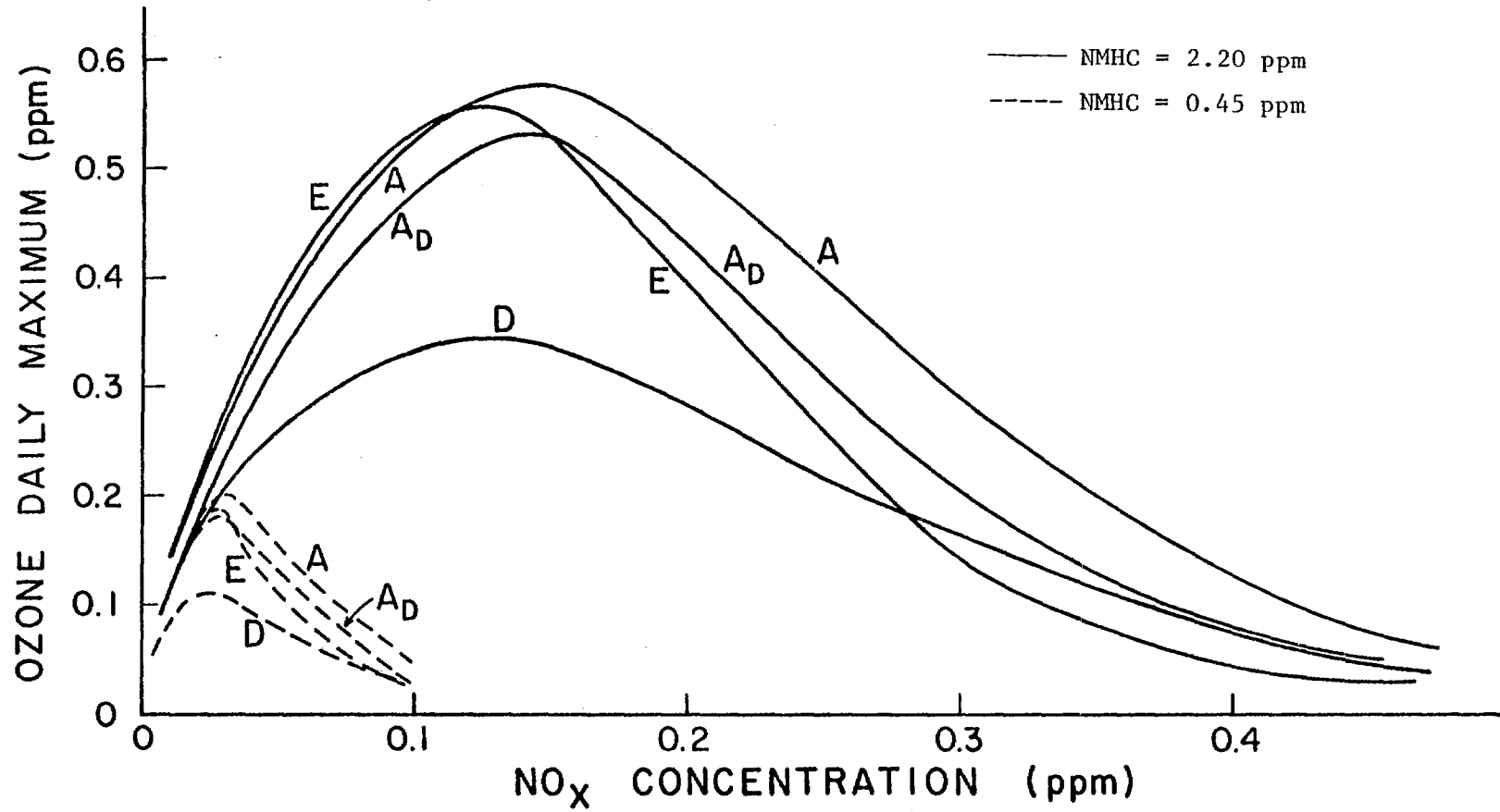


Figure 16. Effect of Model on Ambient Air Simulations: Calculated Daily Maximum Ozone vs. NO<sub>x</sub> Level for Highest and Lowest NMHC Level.

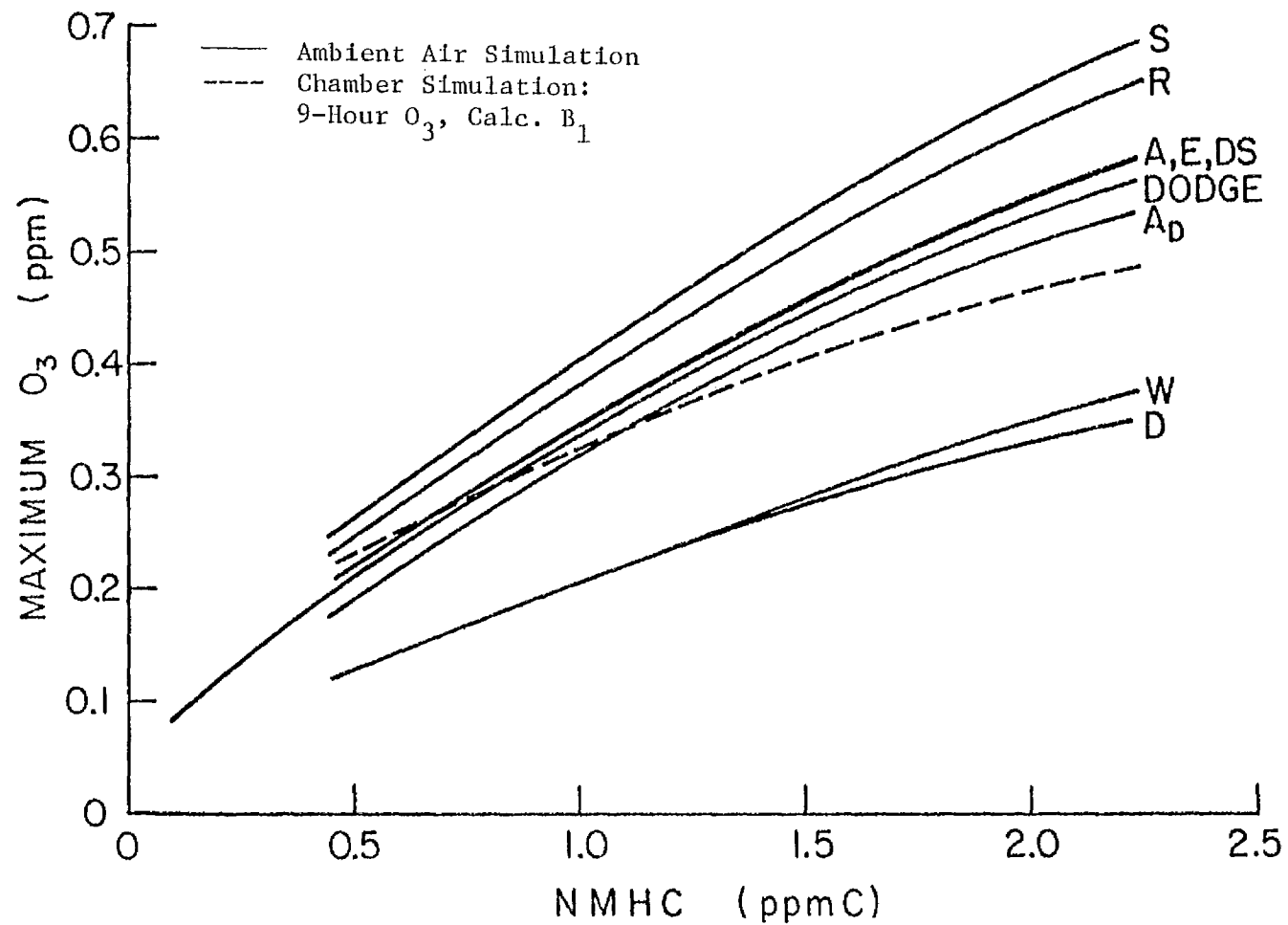


Figure 17. Calculated Maximum Ozone Attainable for Given NMHC Levels.

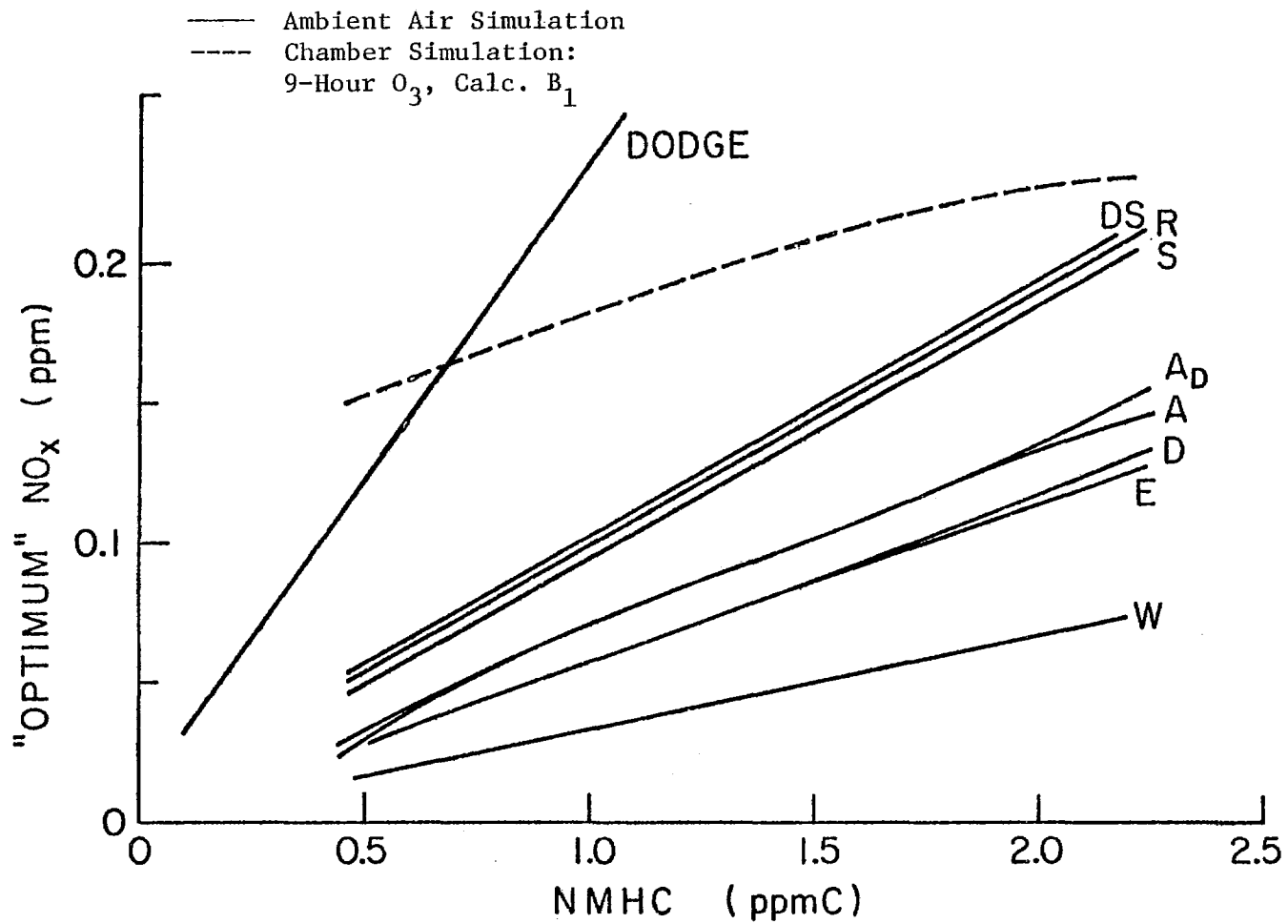


Figure 18. Calculated NO<sub>x</sub> at which Maximum Ozone Attained for Given NMHC Levels. <sup>x</sup>

under smog chamber conditions, the "optimum"  $\text{NO}_x$  is much less strongly affected by the NMHC level than is predicted to be the case with solar irradiation in the absence of chamber effects. Thus it is clear that it is inappropriate to apply  $\text{O}_3$ -NMHC- $\text{NO}_x$  relationships derived directly from smog chamber results to ambient air situations. It is particularly inappropriate to use them for formulating control strategies for  $\text{NO}_x$ .

- As had been observed in the smog chamber simulations, the predictions of the "semi-detailed" model paralleled those of the more approximate "propene + butane" model, except that lower  $\text{O}_3$  yields were formed under all conditions (compare curves "A" and "A<sub>D</sub>" on Figures 16 to 18 for ambient air simulations, and curves "B<sub>1</sub>" and "C<sub>1</sub>" on Figures 13 and 14 for smog chamber simulations). However, the discrepancy between the models was somewhat greater in the ambient air simulations, where the semi-detailed model predicted ~20% less  $\text{O}_3$  than the propene + n-butane model, as opposed to only ~10% difference between these models in the chamber simulations. However considering the differences between these models, it is surprising that the  $\text{O}_3$  discrepancy is only ~20%, and that they both predict essentially the same "optimum"  $\text{NO}_x$  profiles. This suggests that formulation of  $\text{O}_3$  control strategies may not be as sensitive to details of the hydrocarbon photooxidation mechanism as one might have expected. This conclusion requires further investigation, however.

- The greatest differences between the results of our ambient air simulations were due to the effect of season. [Compare curves "W" (Winter), "A" (Spring/Fall), and "S" (Summer) on Figures 15, 17 and 18.] It affects not only the magnitude of the  $\text{O}_3$  yields, but also the  $\text{NO}_x$  levels at which greatest  $\text{O}_3$  is formed. This level increases greatly from winter to summer. The effect of season is greatest at high  $\text{NO}_x$  levels, and is relatively small in conditions of high NMHC/ $\text{NO}_x$  ratios. The change of seasons significantly changes other important aspects of the  $\text{O}_3$ -NMHC- $\text{NO}_x$  relationships. The amount that  $\text{O}_3$  formation increases in the summer or decreases in the winter is strongly affected by the initial NMHC and  $\text{NO}_x$  levels used in the calculations. Therefore, it is probably not correct to say that one need not consider the effect of season if one is interested only in the relative effects on  $\text{O}_3$  of changing NMHC or  $\text{NO}_x$  emissions. This means it is inappropriate to apply a single set of  $\text{O}_3$ -NMHC- $\text{NO}_x$  relations

(or isopleth plot) for making predictions relating to O<sub>3</sub> control independent of season.

- The enriched UV resulting in a large reduction in stratospheric O<sub>3</sub> (33%) has almost the same effect on the O<sub>3</sub>-NMHC-NO<sub>x</sub> relationships as does going from spring to summer [compare curves "A" (spring/fall), "R" (spring/fall, reduced stratospheric O<sub>3</sub>) and "S" (summer, normal stratospheric O<sub>3</sub>) on Figures 15 - 18. The maximum O<sub>3</sub> yields are increased and the NO<sub>x</sub> levels at which these maxima occur are also increased when stratospheric O<sub>3</sub> is reduced. Thus a large reduction in stratospheric O<sub>3</sub> (far greater than currently predicted to result from anthropogenic causes) can have a significant impact on not only the amount of O<sub>3</sub> formed in the polluted troposphere, but also on how it depends on emitted NMHC and NO<sub>x</sub>.

- Unlike changes in season or stratospheric O<sub>3</sub>, increasing the dilution rate results in reducing O<sub>3</sub> yields by similar magnitude at most initial NMHC and NO<sub>x</sub> levels, without otherwise significantly affecting the nature of the O<sub>3</sub>-NMHC-NO<sub>x</sub> relationships. Increasing the dilution rate from 0 to 10% per hour results in approximately a 20-45% reduction in calculated O<sub>3</sub> at most of the NMHC and NO<sub>x</sub> levels examined. (Compare curves "D" and "A" on Figures 16 - 18). Although the greatest reduction in O<sub>3</sub> due to dilution occurs near the "optimum" NMHC/NO<sub>x</sub> ratios, it does not appear to be a poor approximation to conclude that dilution reduces O<sub>3</sub> by similar factors at all initial NMHC and NO<sub>x</sub> levels. These results suggest that uncertainties related to dilution of pollutants may not be significant if one is concerned with only the relative effect of changes in O<sub>3</sub> caused by changing NMHC or NO<sub>x</sub> emissions.

- The differences between the predictions of the models assuming full loading of pollutant at the start of the simulation and the model assuming constant pollutant injection is surprisingly small, considering that the calculations assumed two opposite extremes of emission models. (Compare curves "A" and "E" on Figures 16 to 18. Continuous emissions result in a significant reduction in predicted O<sub>3</sub> at the higher NO<sub>x</sub> levels (presumably due to the reaction of O<sub>3</sub> with emitted NO), but this effect is much smaller than the effect of season. For NO<sub>x</sub> ≤ "optimum," the differences in the models predictions are not particularly great.

This suggests that if one measures primary pollutant emissions by total daily dose (concentration x time, assuming no reactions), one need not be too concerned with the extent to which the primary pollutant is initially present or continuously emitted, for the purpose of making predictions concerning O<sub>3</sub> formation, except when considering high NO<sub>x</sub>/NMHC conditions.

Comparison of Our Model with the Dodge Model. Figures 17 and 18 give, respectively, plots of maximum O<sub>3</sub> and "optimum" NO<sub>x</sub> against NMHC derived from the published O<sub>3</sub> isopleth plots calculated by Dodge (1977a). (These curves are labeled "DODGE" on the figures.) Also shown on Figures 17 and 18 given in Table 27 are results of calculations employing the conditions used in the Dodge calculations, but using our model (labeled "DS"). It can be seen that while our models agree closely on the calculated maximum O<sub>3</sub> obtainable at given NMHC levels (see Figure 17) they disagree very significantly on the calculated NO<sub>x</sub> at which this maximum is attained (see Figure 18). The Dodge model predicts that the greatest O<sub>3</sub> formation occurs at over twice the NO<sub>x</sub> levels than those predicted by our model. Thus, the predictions of our models concerning the effect on O<sub>3</sub> of changes of NO<sub>x</sub> emissions, or of NMHC emissions at specified NO<sub>x</sub> levels, are significantly different.

Although both our calculations and those of Dodge employed the technique of modifying chamber-tested models to be suitable to ambient air simulations, there are a number of significant differences between our studies which could be the cause of the discrepancies between our predictions. The Dodge model was adjusted to fit a different smog chamber data base than was ours. The detailed kinetic mechanism upon which the Dodge calculations were based was the propene + n-butane model of Durbin, Hecht and Whitten (1975). Although this model is similar to ours (Carter et al., 1979) in that the reactive hydrocarbons are represented by propene + n-butane, there are several potentially important differences in the homogeneous chemical mechanisms, and, perhaps most importantly, the two models treat chamber effects differently.

At the current state of our knowledge, it appears that the model predictions of the maximum O<sub>3</sub> formation potential at a given NMHC level are much more reliable than their predictions of the dependence of O<sub>3</sub> on initial NO<sub>x</sub>. In order to improve this situation, more modeling studies

are required to more clearly identify which of the many uncertain aspects of chamber consistent models most strongly affect ambient air simulations, and more experimental studies are required to elucidate these critical areas. At the present time, the most important uncertainties probably concern chamber effects. The discrepancies between the existing models indicate that there are still too many uncertainties for this combined smog chamber-modeling technique to be used with any confidence in developing control strategies for ozone formation.



## IX. LONG-TERM AND MULTIPLE DAY SMOG CHAMBER IRRADIATIONS

A large number (~130) of surrogate hydrocarbon-NO<sub>x</sub>-air irradiations have been carried out at the Statewide Air Pollution Research Center under California Air Resources Board funding under controlled conditions and at constant light intensities (Pitts, 1975b; 1976b). These irradiations, most of which were carried out for six hours, constitute a data base which is a necessary prerequisite to the development of a validated chemical computer model of photochemical smog formation, as well as for the formulation of NO<sub>x</sub>-NMHC-O<sub>3</sub> relationships. The previous SAPRC surrogate data base consists of six-hour irradiations of NO<sub>x</sub>-hydrocarbon-air mixtures at several discrete NMHC levels (0.4, 0.7, 1.4 and 2.2 ppmC). In order to extend this data base, and any resulting computer model which is based on six-hour irradiations at constant light intensity to ambient conditions, it is necessary to adapt the model to the actual conditions encountered in polluted urban atmospheres, for example, diurnally varying radiation for periods up to 12 hours or more.

Our approach has been to carry out 12-hour irradiations at four selected NMHC/NO<sub>x</sub> ratios (using two of the NMHC levels employed in the previous studies) at both constant light intensity (typically 70%) and with a quasi-diurnal light intensity. Duplicate irradiations were carried out for many of these systems to check reproducibility. In addition the effects on O<sub>3</sub> production of changing light intensity (70% to 100%), of chamber temperature (~303 K to ~308 K) and of relative humidity (2% to 50%) were investigated.

Experimental. This work was carried out in the all-glass chamber using the general experimental system and techniques described in Section II. The following experimental details are unique to this study.

The diurnal variation of light intensity was based on the profile of volumetric UV light intensity as a function of solar time as calculated previously in these laboratories (Nieboer et al., 1976). Figure 19 shows the summer solstice profile for the latitude of Los Angeles which was used to estimate step functions for the relative light intensities within the chamber for a twelve hour irradiation. The automated light system consists of a SeaLectro Corporation 14 contact, 60 position programmable cam switch driven by a 12 hour timing motor. The timer is activated by a start

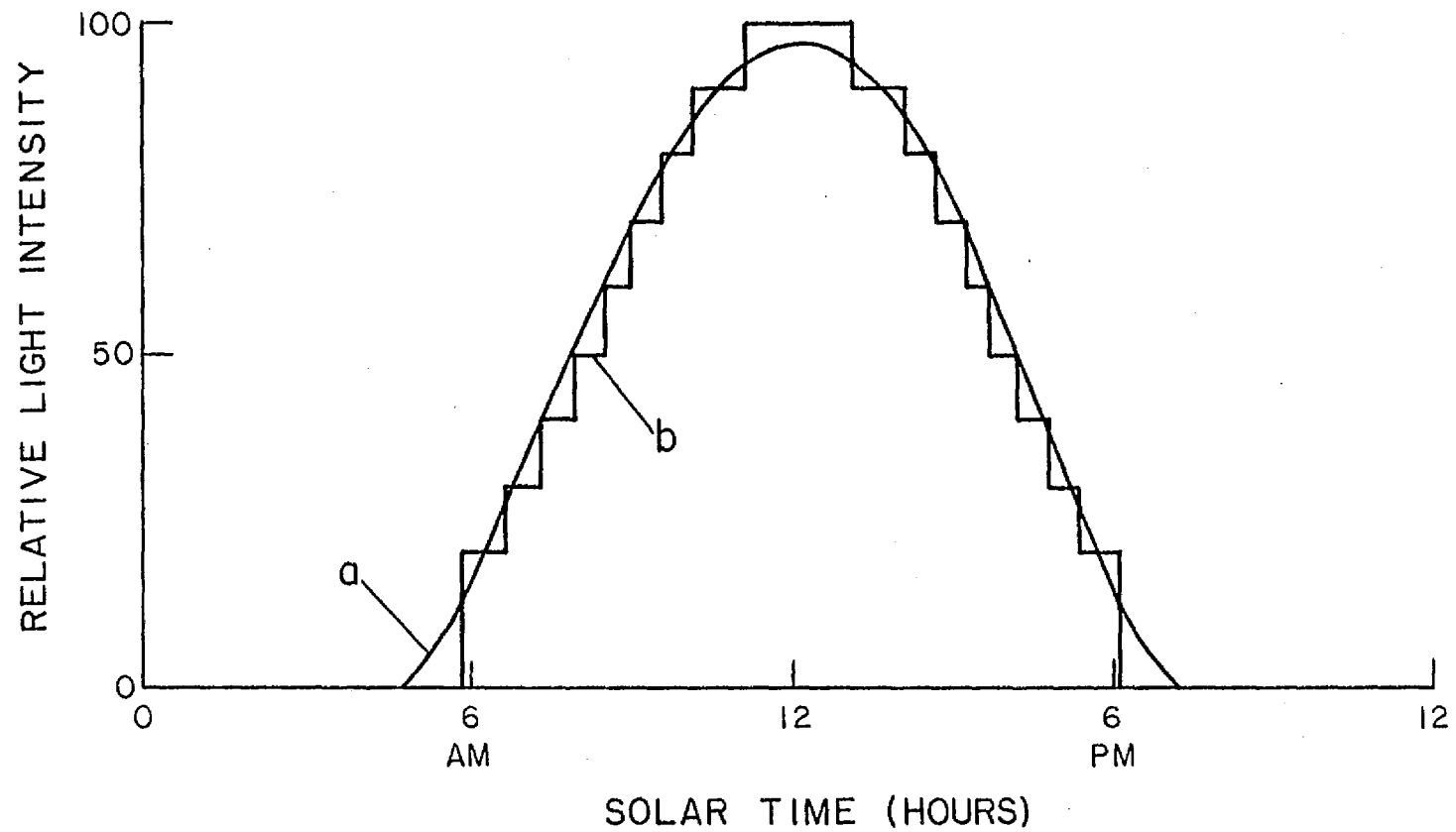


Figure 19. Diurnal Variation of Light Intensity Profiles: (a) Volumetric UV Light Intensity as a Function of Solar time; (b) Relative Intensities Used in AGC 12-Hour Irradiations.

button, and automatically stops at the end of the 12 hour cycle.

The light system also has two sets of manual override switches to facilitate manual operation of the lights. One set controls each individual lamp ballast; each switch in the other set controls 10% of the lights.

In the automatic mode, when a contact is activated, it supplies 5 volts DC from a separate power supply to the solid state relays. Each relay applies power to a single lamp ballast. Each contact accuates 4 lamp ballasts, which corresponds to 10% of the total light, and is programmable in 12 minute increments over a 12 hour period with small plastic tabs. The lamp turn-on and turn-off sequence is arranged so that all lamps will have approximately the same on time to ensure uniform lamp aging.

The light intensity within the chamber was determined frequently (at least three times) during the course of each experiment by measuring the rate of the photolysis of  $\text{NO}_2$  in  $\text{N}_2$  within a quartz tube suspended within the all-glass chamber. This technique is based on that developed by Zafonte et al. (1977) at the ARB laboratories. The effect on  $k_1$  values of  $\text{NO}_2$  flow rate through the quartz tube, of the choice of  $\text{NO}_x$  monitoring instrument, of data recording procedures and of position of the quartz tube within the chamber were studied.

The all-glass chamber was used in the same manner as in the previous surrogate experiments (AGC 10-156), i.e., without the Teflon film liner used in other programs to prevent the replacement of chamber air with the room air, which normally occurs at a total (exchange and sampling) rate of  $\sim 2\% \text{ hr}^{-1}$ . At longer irradiation times and/or at low initial  $\text{NO}_x$  and HC levels, the concentrations of  $\text{NO}_x$  and organic compounds in the room air can begin to alter significantly the relative concentrations within the chamber, especially on heavy smog days, some of which occurred during the course of this program. In order to obtain some information concerning the input flux of  $\text{NO}_2$  and hydrocarbons, measurements of the room air concentrations of these species were taken occasionally during the course of many of these experiments.

Results and Discussion. The experimental conditions and the actinometry data for each experiment are given in Tables 28 and 29, respectively. Reactivity data for oxidant formation are summarized in Table 30 as the 6-

Table 28. Initial Conditions for Long-Term Irradiations

Run No.	Experimental Conditions			Initial Concentrations (ppm)				
	Lights <sup>a</sup>	Avg. Temp. (K)	Avg. RH (%)	Surr. NMHC <sup>b</sup> (ppmC)	NO <sub>x</sub> <sup>c</sup>	NMHC/NO <sub>x</sub>	NO <sub>2</sub> /NO <sub>x</sub>	HCHO
228	100	309	45	2.23	0.228	9.8	0.39	0.016
229	Di <sup>d</sup>	308	46	2.43	0.203	12.0		0.000
230	100	308	48	2.52	0.205	12.3	0.39	0.028
231	100	308	3	2.42	0.221	11.0	0.33	0.010
232	100	307	22	2.44	0.217	11.2	0.39	0.020
310	70	302	65	2.30 <sup>e</sup>	0.192	12.0	0.37	0.025
311	Di	303	46	2.33	0.190	12.3	0.37	0.006
312	70	302	40	2.36	0.199	11.9	0.37	0.036
313	70	303	43	0.77	0.189	4.1	0.38	0.027
314	Di	303	47	0.79	0.189	4.2	0.37	0.022
315	85	303	48	2.28	0.187	12.2	0.35	0.016
316	70	303	47	2.31	0.190	12.2	0.37	0.027
317	100	305	44	2.33	0.192	12.1	0.36	0.021
318	70	309	44	2.35	0.194	12.1	0.36	0.015
320	70	303	35	2.20	0.110	20.0	0.40	0.013
321	Di	303	37	2.31	0.108	21.4	0.38	0.021
322	Di	303	42	2.41	0.207	11.6	0.39	0.014
323	70	303	49	2.38	0.203	11.7	0.36	0.015
324	70	303	15	2.39 <sup>e</sup>	0.215	11.1	0.38	0.020
325	70	303	46	0.85	0.106	8.0	0.39	0.029
326	Di	303	49	0.88	0.100	8.8	0.35	0.026
327	Di	303	42	0.92 <sup>e</sup>	0.192	4.8	0.35	0.006
328	70	303	45	2.47	0.103	24.0	0.35	0.013

<sup>a</sup>Given as percent of maximum or Di = diurnal variation; see Table 29 for actinometry data.

<sup>b</sup>The twelve hydrocarbons in the surrogate mixture as monitored at the beginning of the run; does not include methane, trace aldehydes, ketones or nonsurrogate HC; neopentane in runs #321 and 323 also not in total.

<sup>c</sup>NO + NO<sub>2</sub>, Teco 14B data.

<sup>d</sup>Diurnal variation done manually; percent of total lights on (time at that percent) are: 40 (1 hr), 50 (2 hr), 90 (2 hr), 100 (2 hr), 90 (2 hr), 50 (2 hr), 40 (1 hr).

<sup>e</sup>Pre-T = 0 or extrapolated values used for one or more hydrocarbons.

Table 29. Actinometry Data for Long-Term Irradiations

Run No.	% Lights	Time	NO <sub>2</sub> flow (lpm)	k <sub>1</sub> (min <sup>-1</sup> )		Instrument		
				DACS	Strip Chart			
310	70	~0900	2	.225		TECO		
			1	.240				
			.626	.234				
				~1300	2		.239	
					2		.244	
				~1700	1		.236	
					.626		.234	
				2	.248			
				1	.237			
				.626	.233			
311	40 50 70 100 100 100	0940	2	.125		TECO		
		~1000	1	.168				
			1	.218				
		~1300	2	.375				
		1345	1	.372				
		1400	.8	.390				
312	70	~1000	2	.226		TECO		
			1023	1	.252			
			1047	.77	.252			
			1254	1	.246			
			1447	1	.243			
313	70		0921	1	.238	TECO		
			1335	1	.226			
			1700	1	.238			
314	40 70 100 70 40	0922 1108 1342 1700 1526	1	.165		TECO		
			1	.243				
			1	.346				
			1	.240				
			1	.159				
315	85	1020	1	.313		TECO		
		1028	1	.380	.397	Bendix		
		1225	1	.360	.384	Bendix		
		1245	1	.302		TECO		
		1255	1	.406	.380	Bendix		
		1430	1	.356	.378	Bendix		
		1448	1	.303		TECO		
		1454	1	.328	.378	Bendix		

Table 29. (Continued)

Run No.	% Lights	Time	NO <sub>2</sub> flow (lpm)	k <sub>1</sub> (min <sup>-1</sup> )		Instrument
				DACS	Strip Chart	
316	70	0937	1	.297	.326	Bendix
		0957	1	.248		TECO
		1004	1	.332	.316	Bendix
		1212	1	.282	.302	Bendix
		1230	1	.252		TECO
		1243	1	.359	.302	Bendix
		1330	1	.302	.302	Bendix
		1349	1	.240		TECO
		1359	1	.327	.300	Bendix
317	100	0939	1	.482	.470	Bendix
		1207	1	.414	.456	Bendix
		1238	1	.354		TECO
		1245	1	.447	.456	Bendix
		1344	1	.434	.458	Bendix
318	70	0924	1	.303	.287	Bendix
		1225	1	.286	.312	Bendix
		1434	1	.329	.306	Bendix
320	70	0937	1	.363	.348	Bendix
		1236		.336	.337	Bendix
		1350		.339	.337	Bendix
321	0	0714	(NO) (NO <sub>2</sub> )	.034 2.22	.043 2.24	
	40	0926	1	.225	.209	Bendix
	80	1125	1		.353	Bendix
	100	1303	1	.426	.435	Bendix
322	30	0910	1	.185	.166	Bendix
	70	1100	1	.303	.324	Bendix
	100	1307	1	.421	.455	Bendix
323	70	0935	1	.306	.314	Bendix
	70	1217	1	.281	.310	Bendix
	70	1355	1	.281	.308	Bendix
324	70	0920	1	.281	.314	Bendix
	70	1255	1	.292	.305	Bendix
	70	1352	1	.332	.313	Bendix

Table 29. (Continued)

Run No.	% Lights	Time	NO <sub>2</sub> flow (lpm)	k <sub>1</sub> (min <sup>-1</sup> )		Instrument
				DACS	Strip Chart	
325	70	0945	1	.323	.318	Bendix
	70	1248	1	.335	.311	Bendix
	70	1350	1	.301	.320	Bendix
326	30	0904	1	.134	.150	Bendix
	100	1400	1	.461	.430	Bendix
327	30	0853	1	.156	.157	Bendix
	70	1100	1	.335	.314	Bendix
	100	1318	1	.425	.433	Bendix
328	70	0938	1	.324	.314	Bendix
	70	1207	1	.297	.317	Bendix
	70	1418	1	.331	.320	Bendix

Table 30. Reactivity Data (Ozone, PAN and Nitrogen Dioxide) for Long-Term Irradiations

Run No.	O <sub>3</sub> (ppm)			PAN (ppm)			NO <sub>2</sub> (ppm)		
	6 hr	9 hr	12 hr	6 hr	9 hr	12 hr	6 hr	9 hr	12 hr
228	0.447	0.547	0.564	0.029	0.033	0.030	0.069	0.030	0.023
229	0.318	0.476	0.459	0.022	0.031	0.029	0.089	0.037	0.023
230	0.459	0.557	0.567	0.033	0.036	0.031	0.055	0.038	0.034
231	0.383	0.523	0.562	0.025	0.030	0.028	0.092	0.066	0.057
232	0.420	0.550	0.572	0.030	0.035	0.032	0.092	0.061	0.053
310	0.261	0.333	0.357	0.027	0.031	0.034	0.071	0.048	0.036
311	0.303	0.391	0.347	0.030	0.038	0.035	0.068	0.040	0.032
312	0.286	0.362	0.386	0.027	0.034	0.035	0.080	0.051	0.043
313	0.077	0.130	0.182	0.005	0.007	0.010	0.107	0.089	0.074
314	0.093	0.149	0.154	0.005	0.007	0.010	0.107	0.091	0.072
315	0.283	0.379	0.403	0.028	0.034	0.035	0.063	0.037	0.029
316	0.269	0.337	0.362	0.031	0.037	0.038	0.062	0.035	0.029
317	0.376	0.457	0.462	0.033	0.035	0.034	0.057	0.039	---
318	0.325	0.408	0.420	0.027	0.031	0.028	0.067	0.036	0.029
320	0.286	0.315	0.322	0.029	0.029	0.026	0.034	0.031	0.031
321	0.300	0.349	0.322	0.030	0.029	0.026	0.030	0.028	0.025
322	0.320	0.415	0.374	0.023	0.030	0.028	0.078	0.047	0.039
323	0.249	0.322	0.352	0.023	0.029	0.031	0.076	0.044	0.033
324	0.247	0.342	0.401	0.020	0.027 <sup>a</sup>	0.031	0.115	0.088	0.060
325	0.122	0.176	0.213	0.009	0.011 <sup>a</sup>	0.013	0.049	0.043	0.032
326	0.144	0.198	0.188	0.008	0.011	0.013	0.045	0.034	0.025
327	0.061	0.100	0.105	0.004	0.005	0.006	0.104	0.097	0.085
328	0.291	0.308	0.310	0.029	0.028	0.026	0.025	0.024	0.024

<sup>a</sup>interpolated

9- and 12-hour concentrations of O<sub>3</sub>, PAN and NO<sub>2</sub>. To facilitate discussion of the results, the experimental conditions are summarized in Table 31 according to initial NMHC and NO<sub>x</sub> levels.

a) Effect of Relative Humidity

Preliminary experiments (AGC 228-232) were conducted to test the feasibility of the diurnal light intensity study and to test the effect of relative humidity on oxidant production (See Table 31).

Concentration-time profiles for these five runs are given in Figure 20. The excellent agreement for the replicate runs (228, 230) indicates that the small decrease in the initial rate of ozone production as the RH is lowered (231, 232) is probably larger than the experimental uncertainty of this series. However, while a later sequential pair of experiments (323, 324) conducted at lower light intensity and temperature (70%, 303 K) shows a similar humidity effect (see Figure 21) in the first six hours of irradiation, differences in ozone production are not greater than the experimental uncertainty of the four replicate standard runs (see following section).

b) Reproducibility

The standard run is defined as the NMHC ~2.2 ppmC, NO<sub>x</sub> ~0.19 ppm experiment conducted at 303 K and 50% RH. This run was carried out with constant light intensity at four random times during the course of this study (310, 312, 316, 323). The ozone concentration-time profiles are shown in Figure 22. The 12-hour ozone concentrations range from 0.351 to 0.386 ppm giving a mean value of  $0.37 \pm 0.02$ . Similar reproducibility was obtained for a pair of standard runs carried out with diurnal variation of light intensity (311, 322). This pair and the two extreme results for the constant intensity runs are shown in Figure 23. Excellent reproducibility was obtained for a pair of runs (320, 328) at NMHC ~2.2 ppmC, NO<sub>x</sub> ~0.11 ppm with constant light intensity (see Figure 24) and very poor results for a pair (314, 327) at NMHC ~0.8 ppmC, NO<sub>x</sub> ~0.19 ppm with diurnal light intensity (see Figure 25).

c) Constant vs. Diurnal Light Intensity

The ozone concentration-time profiles illustrating the effect of diurnal variation of light intensity relative to that for constant intensity (70%) are given in Figures 23 through 26. As expected these

Table 31. Experimental Conditions for Long-Term Irradiations Summarized According to Initial NMHC and NO<sub>x</sub> Levels

Initial Concentration			Light Intensity <sup>b</sup> (% max)	Temp. <sup>c</sup> (K)	RH <sup>c</sup> (%)	Run No.	O <sub>3</sub> at 12 hr (ppm)
Surrogate NMHC <sup>a</sup> (ppmC)	NO <sub>x</sub> (ppm)	NMHC/NO <sub>x</sub>					
2.4 <sup>d</sup>	0.22	11	100	307	50	228,230	.564, .561
			100	307	22	232	.572
			100	307	2	231	.562
			di	307	50	229	.459
2.2	0.19	12	70	303	50	310,312, 316,323	.351, .386, .361, .352
			70	303	15	324	.403
			70	308	50	318	.42
			di	303	50	311,322	.347, .386
			85	303	50	315	.400
			100	303	50	317	.465
2.2	0.11	20	70	303	50	320,328	.322, .310
			di	303	50	321	.325
0.8	0.19	4	70	303	50	313	.182
			di	303	50	314,327	.154, .102
0.8	0.11	7	70	303	50	325	.215
			di	303	50	326	.188

<sup>a</sup>Surrogate NMHC are the hydrocarbons in the surrogate mixture as monitored in the chamber at the beginning of the run and do not include trace aldehydes, ketones, and nonsurrogate HC.

<sup>b</sup>di = pseudo-diurnal variation over 12 hrs.; timer controlled.

<sup>c</sup>Approximate values; precise data are given on data sheets in the archives.

<sup>d</sup>Preliminary runs (228-232); diurnal variation was done manually and is not the same intensity profile as that of remaining runs.

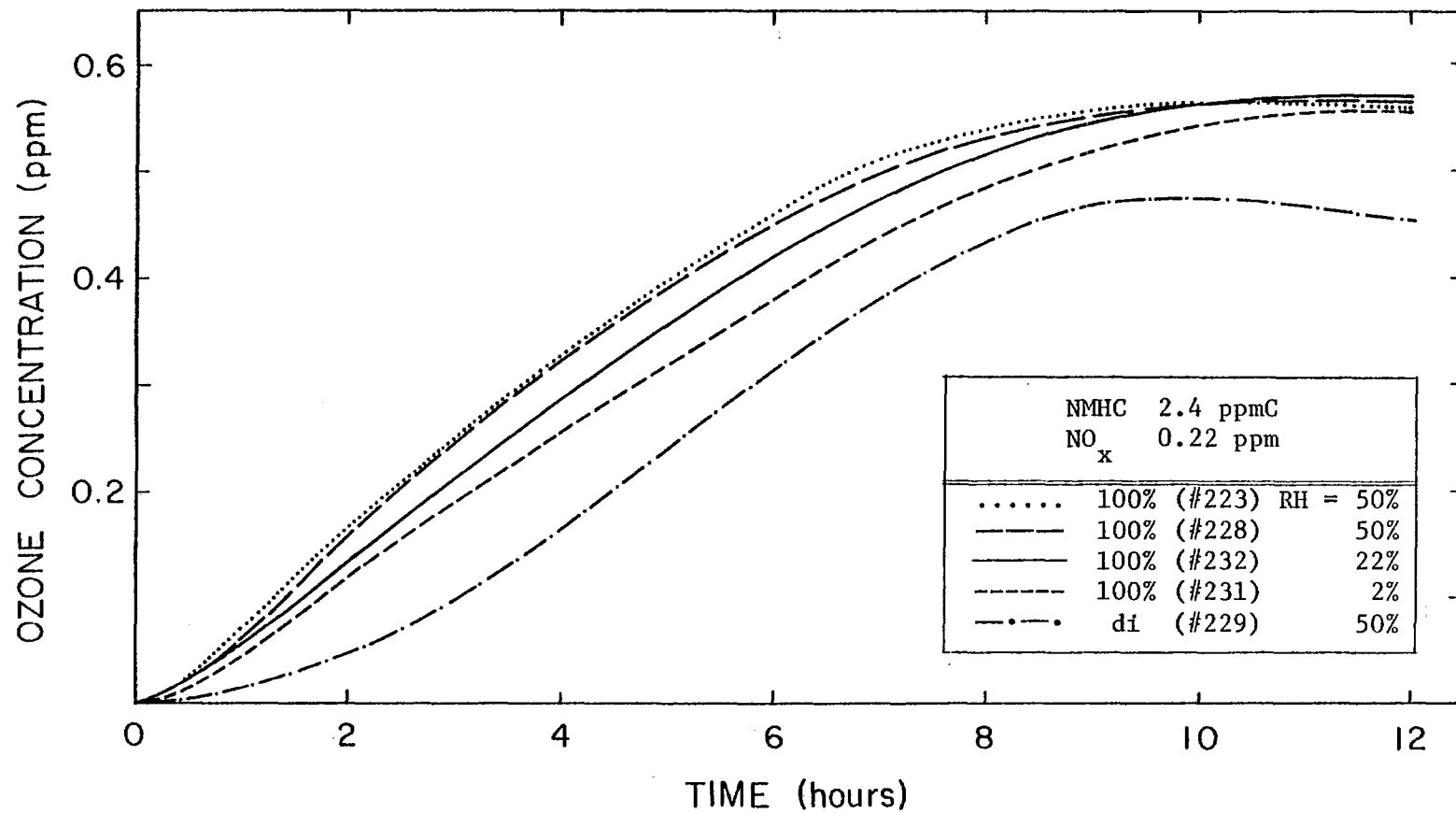


Figure 20. Effect of Relative Humidity on Ozone Production for 100% Constant Light Intensity, 307 K.

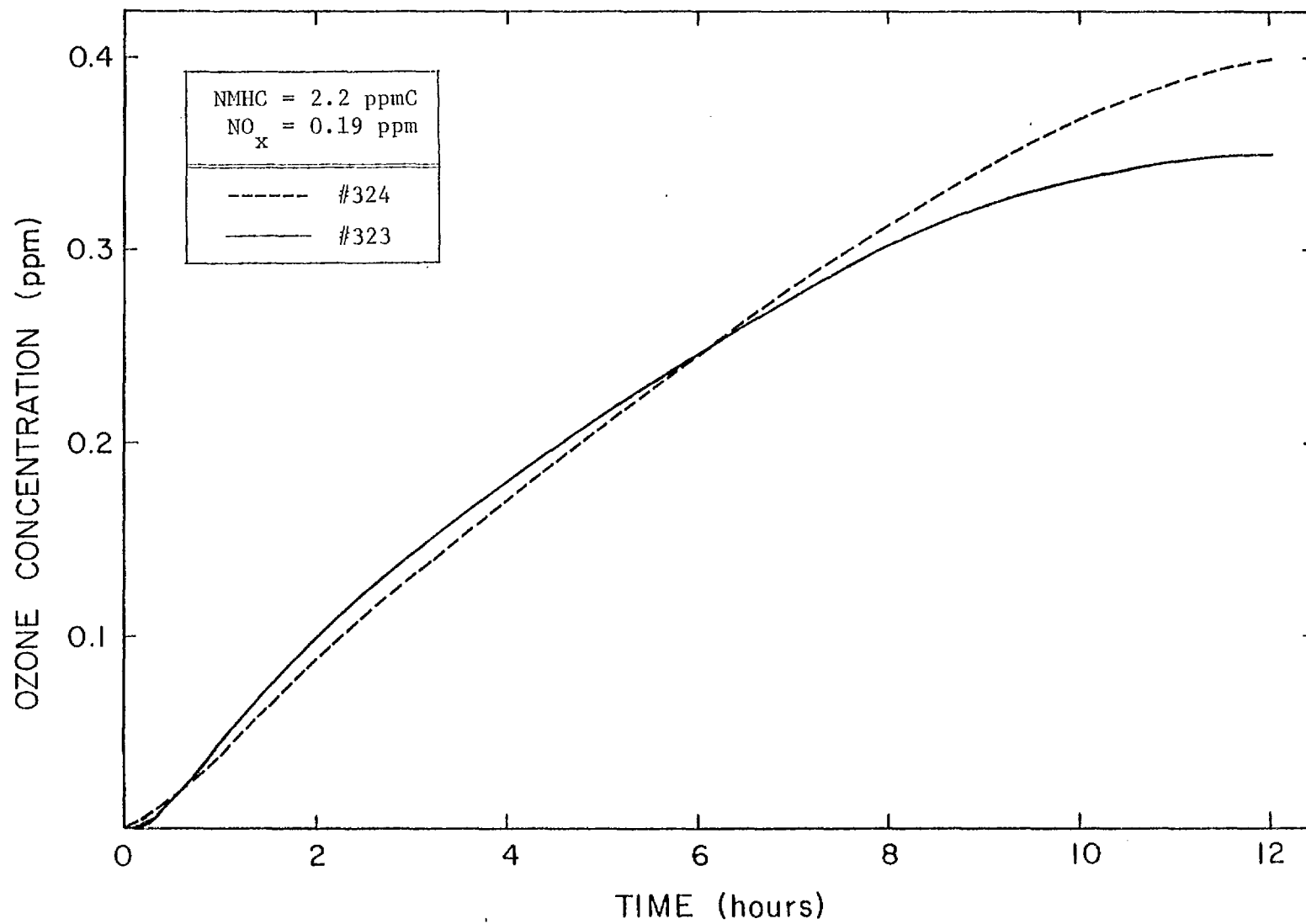


Figure 21. Effect of Relative Humidity on Ozone Production for 70% Constant Light Intensity, 303 K.

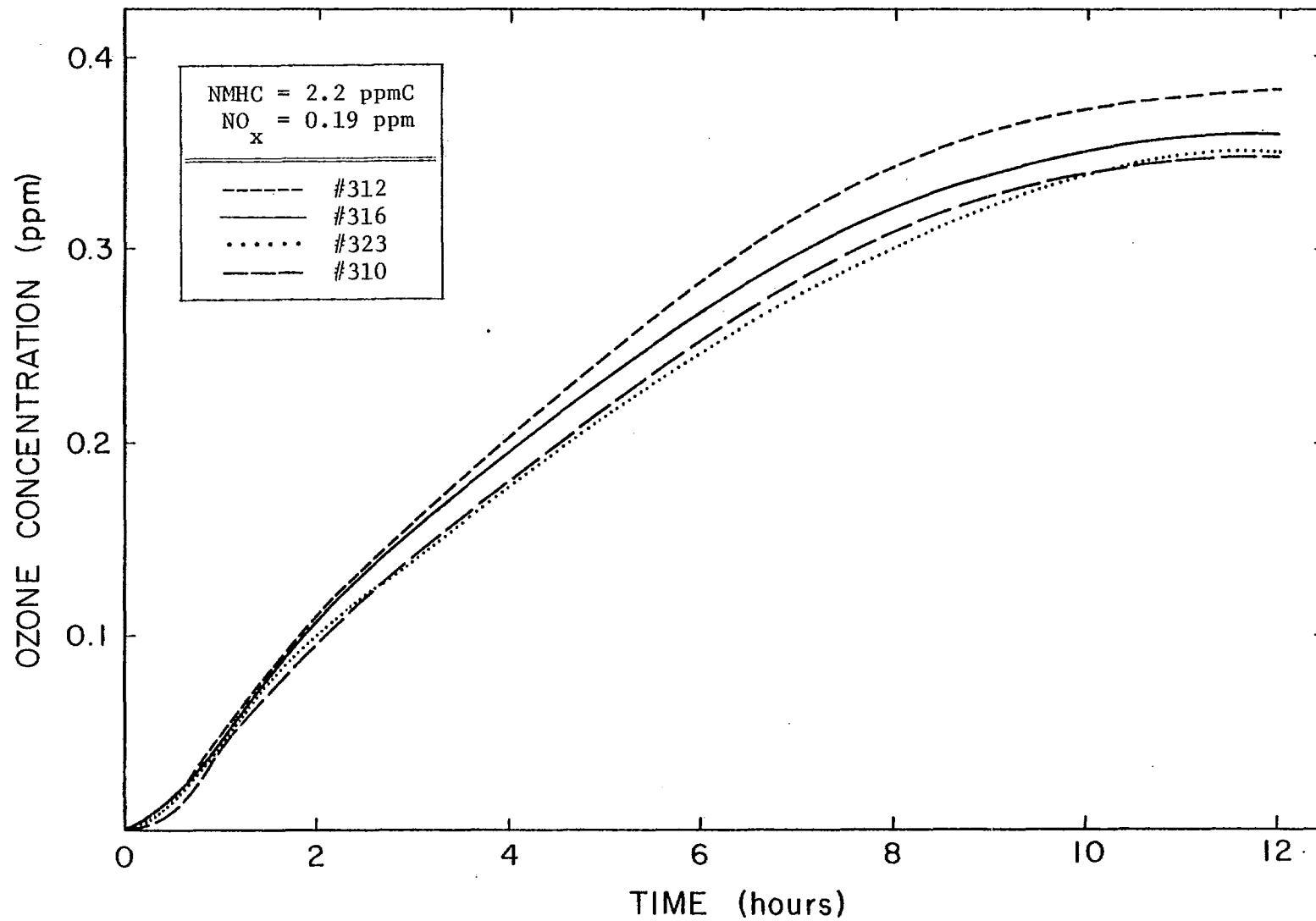


Figure 22. Ozone Profiles for Replicate Standard 12-Hour Experiments at Constant Light Intensity (70%).

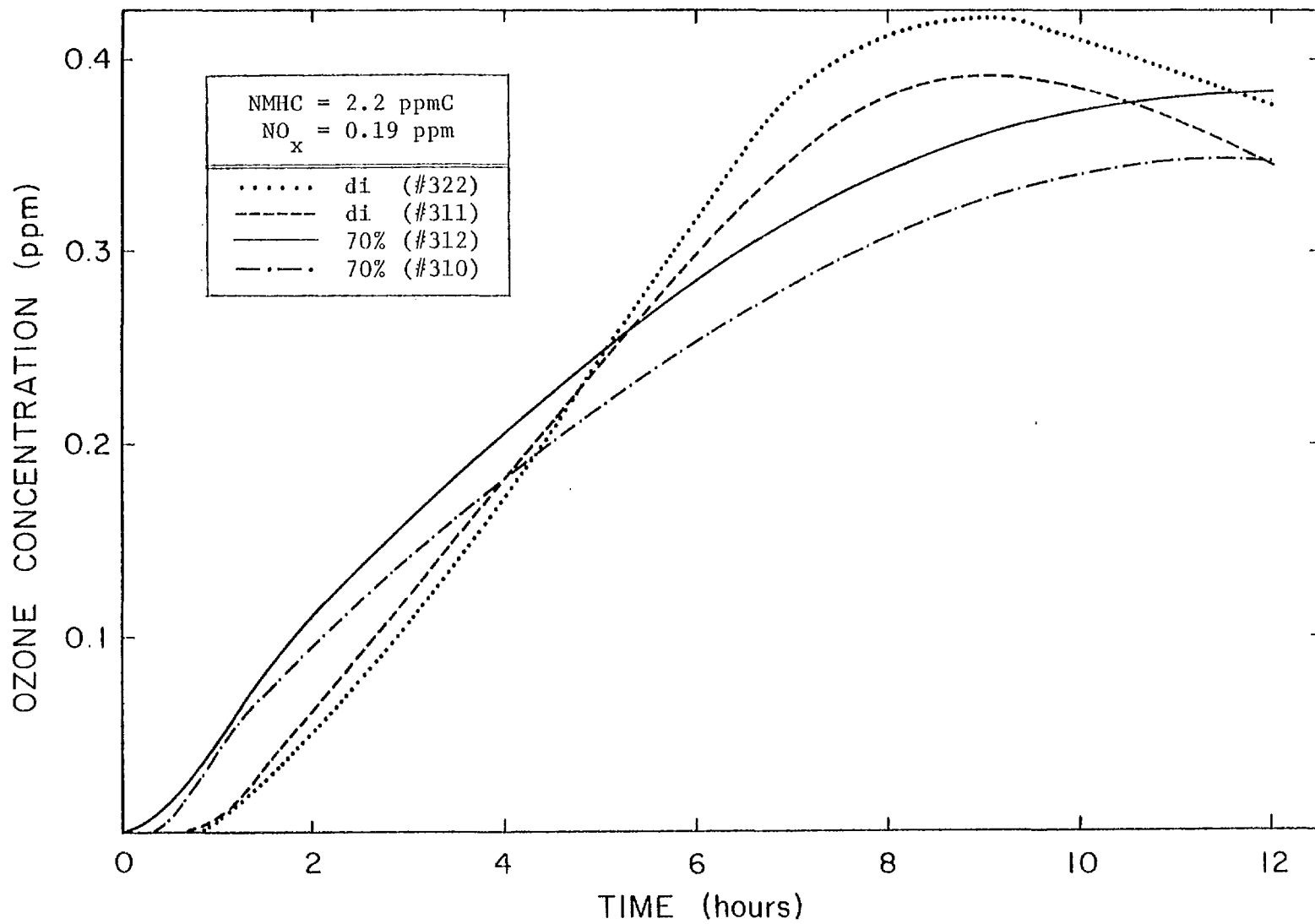


Figure 23. Ozone Profiles for Replicate Standard 12-Hour Experiments at Constant and Diurnal Light Intensities.

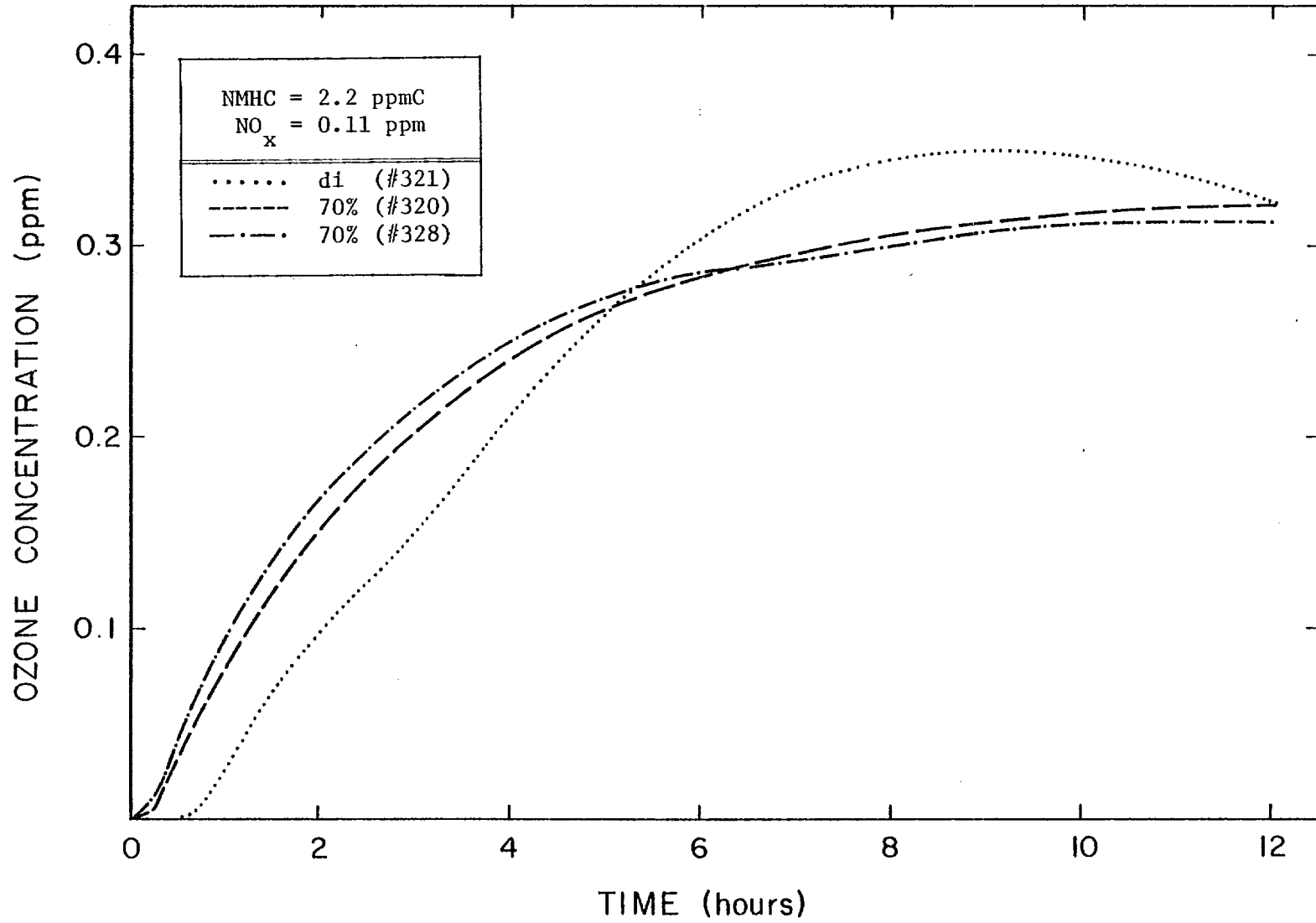


Figure 24. Ozone Profiles for Runs with High Initial NMHC/NO<sub>x</sub> Ratio (20).

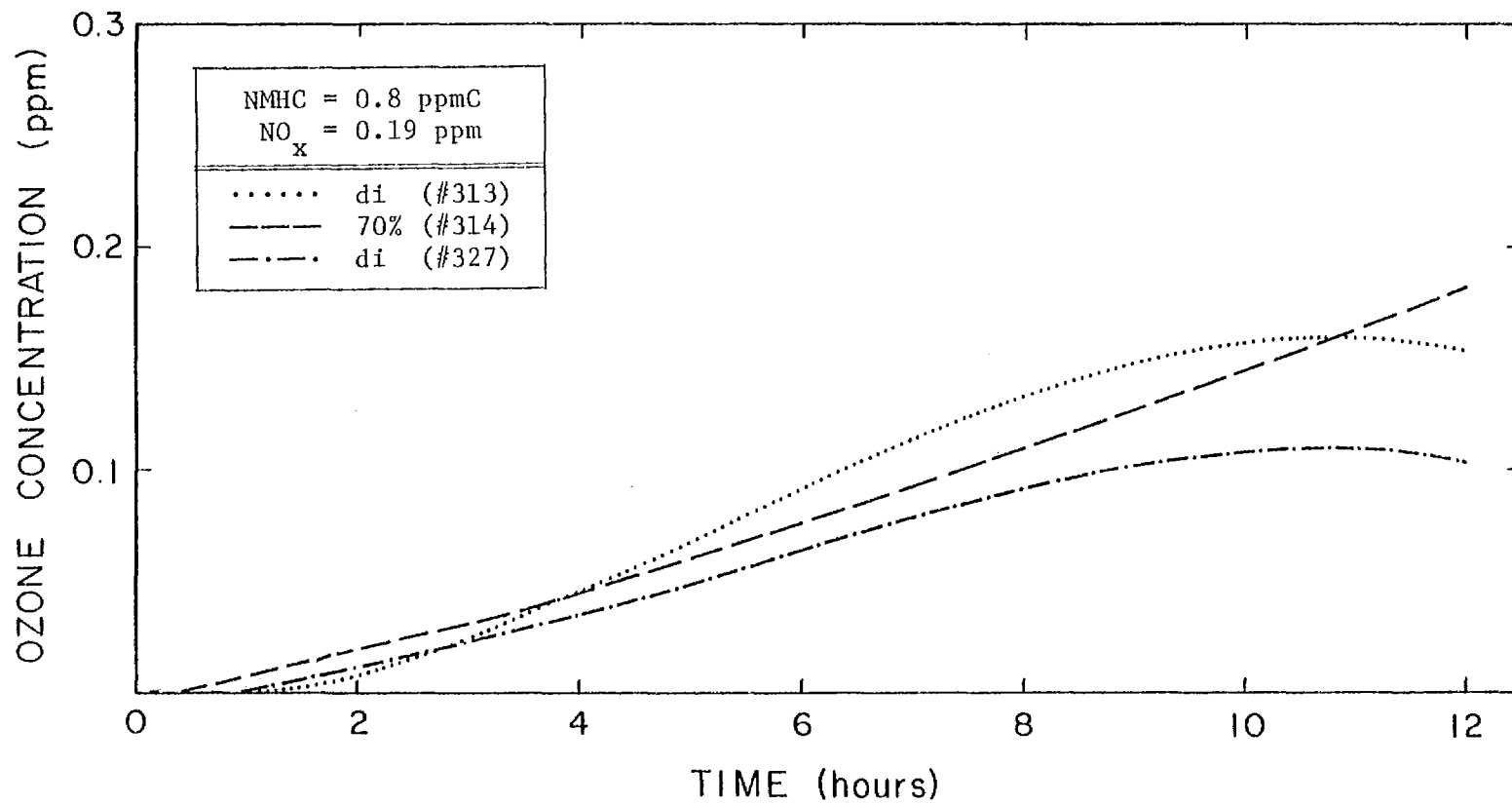


Figure 25. Ozone Profiles for Runs with Low Initial NMHC/NO<sub>x</sub> Ratio (4).

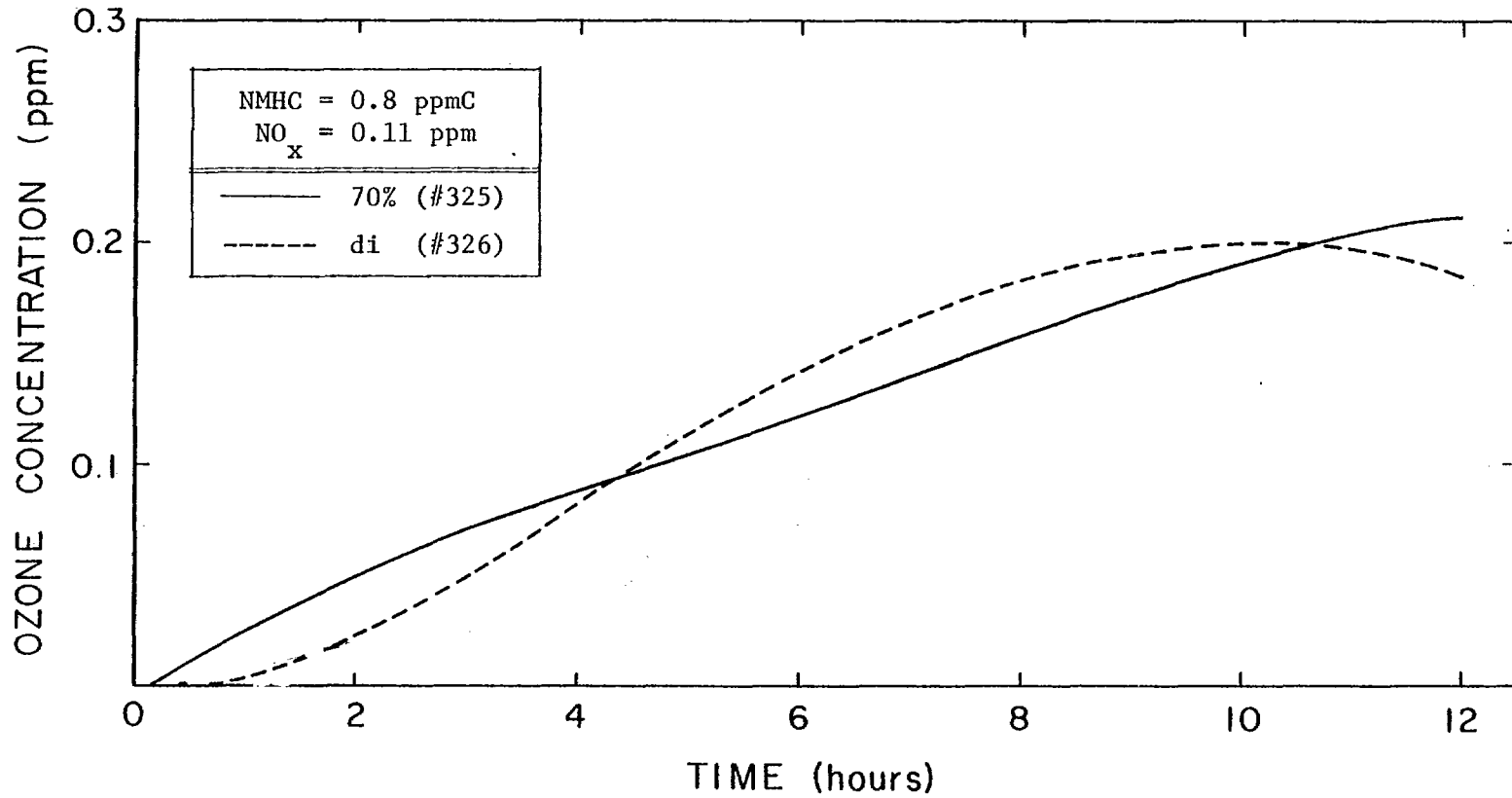


Figure 26. Ozone Profiles for Runs with Intermediate Initial NMHC/NO<sub>x</sub> Ratio (7).

curves are of significantly different shapes. However, at any given time after 6 hours of irradiation the ozone concentrations differ by no more than ~0.05 ppm at the higher NMHC level and ~0.025 ppm at the lower NMHC level. Thus, in the latter half of a 12-hour smog chamber day, the ozone produced by a pseudo-diurnal variation of light intensity is within 20% (30% if variation observed from duplicate experiments is included) of that produced for constant light intensity at 70% of maximum. This gives an indication of the uncertainty associated with using the previously obtained, constant-light intensity data base for application to ambient conditions. In addition, these experiments provide a data base for model validation using diurnal variation of light intensity.

d) Effects of Temperature and Light Intensity

The significant effects which both temperature and increased constant light intensity have on the rate of ozone production is shown in Figure 27. Approximately a 20% increase in final ozone concentration occurs for a 5°K increase in temperature and a ~30% increase occurs for an increase in light intensity from 70% to 100% of maximum. The reference standard run used here (316) is near the mean of the replicate standard runs (See Figure 22) and, except for Run 317 at 303 K and 85% intensity, the enhanced rate of ozone production is clearly greater than the experimental uncertainty. Based on the above enhancements, the calculated 12-hour ozone for 308 K and 100% intensity would be approximately 0.58 ppm which compares favorably with the ~0.57 ppm observed in the preliminary runs at 100% intensity and 307 K.

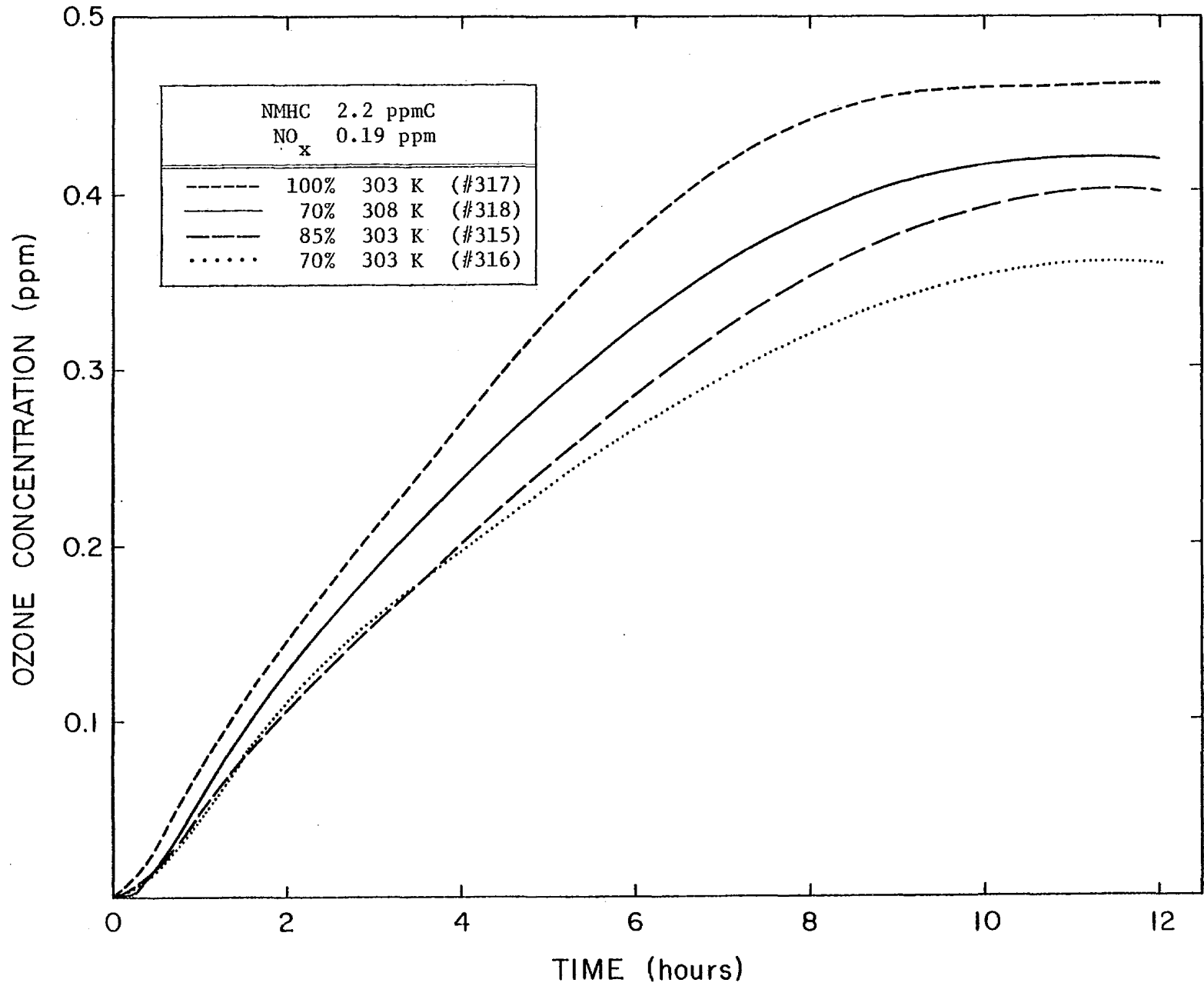


Figure 27. Effects of Temperature and Light Intensity on Ozone Production.



## X. ASSESSMENT OF OXIDANT-PRECURSOR RELATIONSHIPS UTILIZING AN EMPIRICAL MATHEMATICAL APPROACH

Previous surrogate ozone data have been condensed into the form of an empirical relationship relating all ozone levels  $\geq 0.05$  ppm for an irradiation period of up to 10 hours of irradiation time and for various initial precursor concentrations. The estimates of the parameters have been verified against the entire file of surrogate data using a non-linear parameter estimation procedure. This procedure for reducing the data in terms of orthonormal polynomials has been briefly described in a previous report (Pitts et al., 1976b) and has now been carried to a useful conclusion. The results and conclusions derived from this procedure are summarized below and the procedure is then discussed in detail.

Resolution of the experimental data with respect to an orthonormal set yields three numbers,  $A_0$ ,  $A_1$  and  $A_2$ , for each ozone profile which accurately represent the experimental ozone profiles after the  $\text{NO}$  to  $\text{NO}_2$  conversion period. The trends of these numbers with precursor concentrations have been investigated and empirical representations found which allow estimation of the ozone concentrations from the precursor concentrations with a standard error of  $\pm 0.06$  ppm. The quantity  $[A_0^2 + A_1^2 + A_2^2]^{1/2}$  measures overall trends in ozone concentration over a period of around ten hours, a consequence of profile representations in terms of orthonormal polynomials (see below). This quantity is best regarded as a root mean square (rms) estimate of the average ozone concentrations for a ten hour period. Its dependence on precursor concentration is shown in Figure 28. The salient features are: (1) At high precursor ratios [ $\geq 16$  ppmC (ppm  $\text{NO}_x$ ) $^{-1}$ ] rms ozone increases monotonically with increasing primary pollutant concentrations, implying decreasing ozone on dilution. (2) At lower ratios ozone first increases then decreases with increasing primary pollutant concentrations and each ratio has a corresponding NMHC concentration producing the maximum rms ozone for the ratio. For example from Figure 28 we have the optimum ratio, NMHC concentration pairs (16,  $>4$  ppmC) (8, 1.9 ppmC), (4, 0.75 ppmC), (2,  $<0.4$  ppmC) with rms ozone maxima increasing with the ratio.

When considering the implications of Figure 28 it must be remembered that it refers to root mean square ozone concentrations, an average

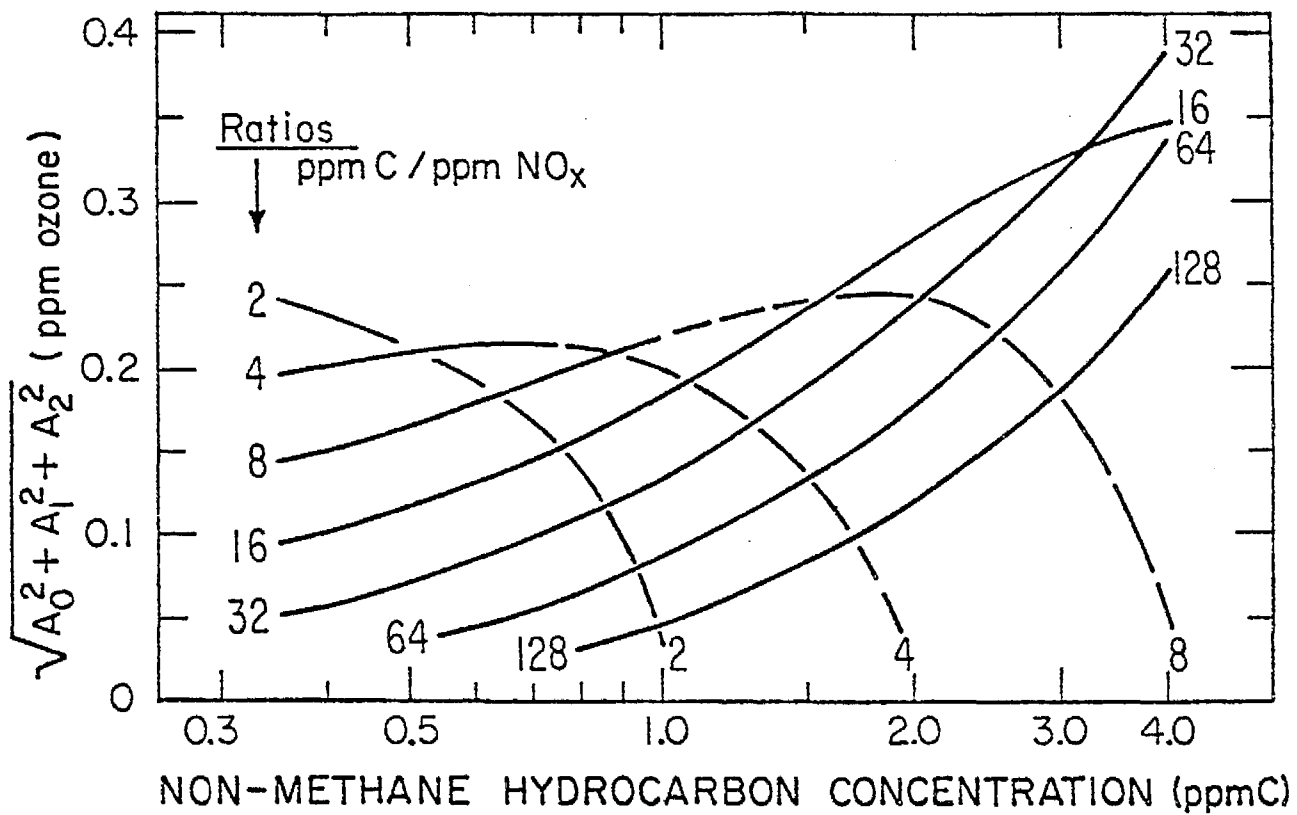


Figure 28. Root Mean Square Ozone Concentrations at Various Precursor Ratios as Functions of Initial NMHC Concentrations.

depending heavily on the higher concentration portions of the profiles. Profile shape is determined by the three relative quantities  $A_0/[A_0^2 + A_1^2 + A_2^2]^{1/2}$ ,  $A_1/[A_0^2 + A_1^2 + A_2^2]^{1/2}$  and  $A_2/[A_0^2 + A_1^2 + A_2^2]^{1/2}$ . One of these quantities is dependent on the other two since their squares add up to one. As  $A_0$  is found to be always positive for the surrogate data, the quantity  $A_0/[A_0^2 + A_1^2 + A_2^2]^{1/2}$  seems the best choice as the dependent shape-determining quantity. The behavior of the remaining two quantities with varying precursor concentrations is illustrated in Figures 29 and 30. Typical plots of the profile shapes, as ozone concentration referred to rms ozone versus time, are shown in Figures 31 and 32. Figures 29 and 30 indicate that the profile shapes are essentially independent of precursor concentrations and depend mainly on the ratio if this is larger than 16. Figure 31 indicates that these high ratio profiles are concave downward with some indications that ozone production is decreasing to give a broad maximum at about ten hours. Profiles at very high ratios (e.g., 64) and long times reflect the onset of a chamber artifact manifested by the final upward trend of ozone concentration. This is caused by the slow replacement of the chamber atmosphere by outside ambient air to replace analytical sampling streams, an appreciable perturbation at low  $\text{NO}_x$  concentrations. (This particular artifact can be avoided in future experiments by use of a Teflon bag inside the chamber.)

According to Figures 29 and 30, the profile shapes become more dependent on absolute pollutant levels at lower ratios. Figures 31 and 32 show that in fact the ratio is still very important in determining shape. The joint dependence of shape parameters on pollutant levels in Figures 29 and 30 cause minor variations in curvature. As the ratio decreases, the profiles become concave upward and most of them are still rapidly increasing at ten hours; the rms ozone in these cases reflects a large contribution from the extreme of the irradiation period. The salient feature of the dependence on absolute levels at low ratios is a tendency towards peaking out at quite low precursor concentrations. For example, this occurs at between eight and nine hours in Figure 32 for 0.35 ppmC and 0.09 ppm  $\text{NO}_x$  giving a predicted maximum ozone concentration of  $0.27 \pm 0.06$  ppm from reference to Figure 28.

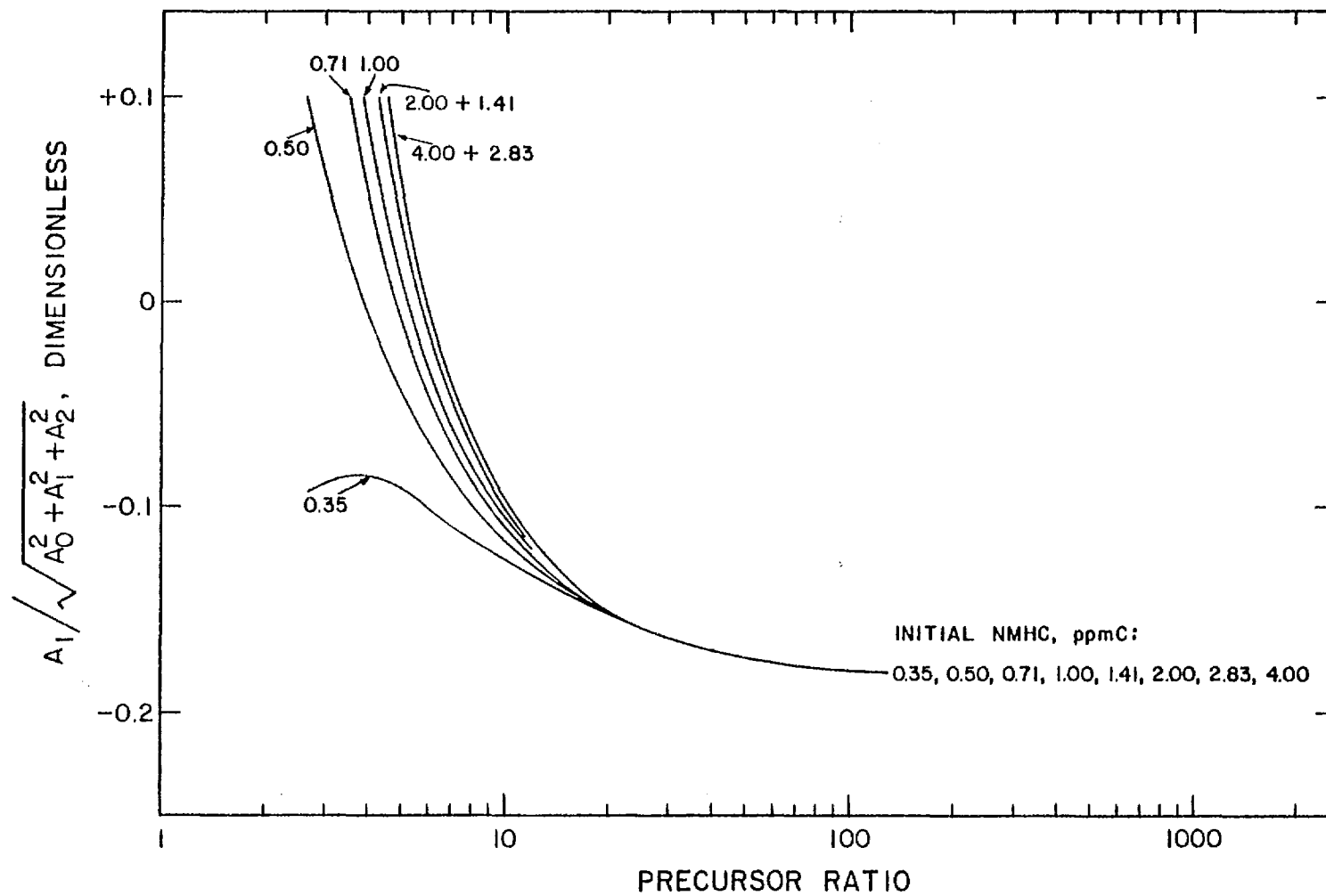


Figure 29. Relative Contribution of Second Jacobi Polynomial to Ozone Profiles as a Function of Precursor Ratio for Various Initial NMHC Concentrations.

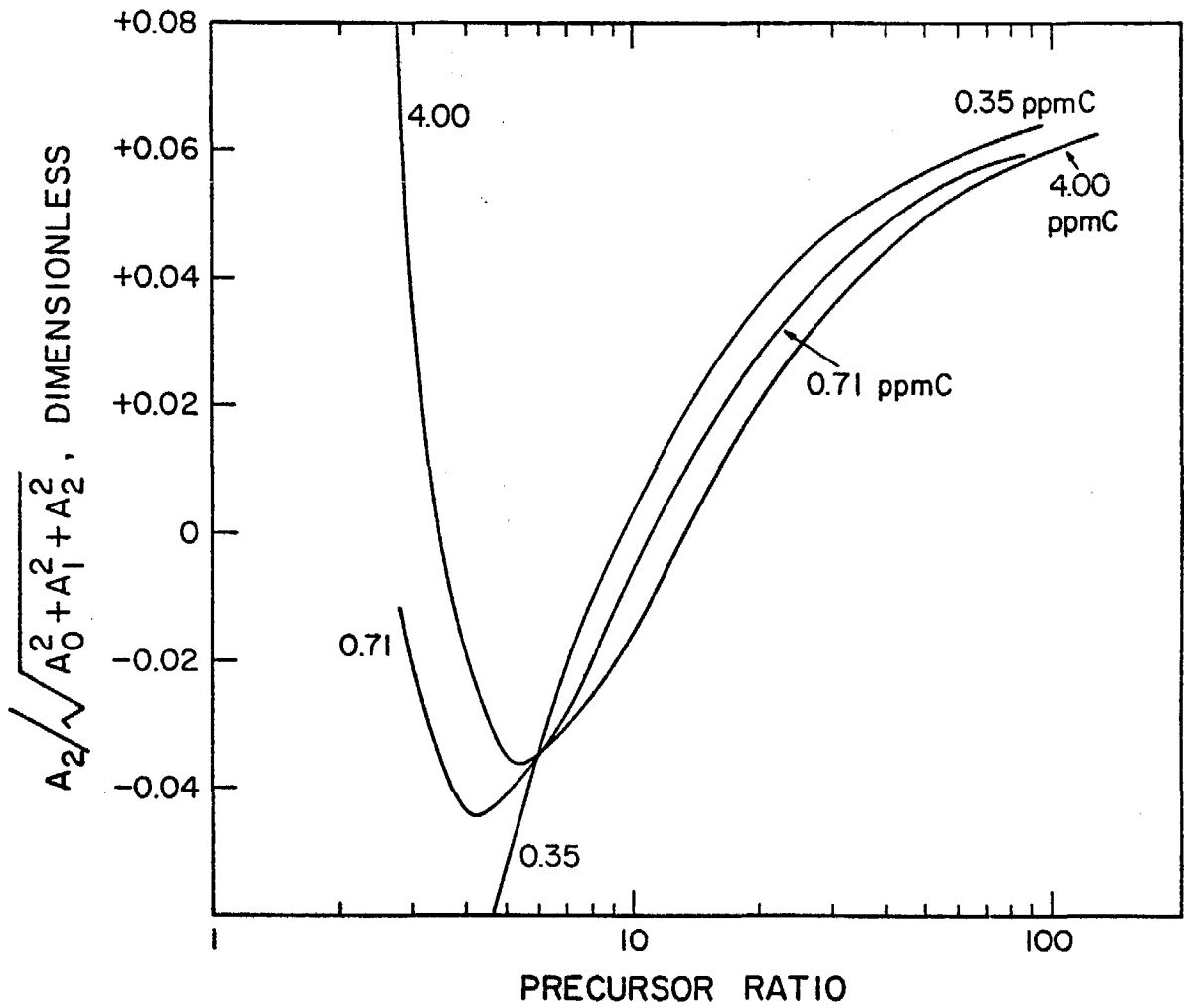


Figure 30. Relative Contribution of the Third Jacobi Polynomial to Ozone Profiles as a Function of Precursor Ratio for Various Initial NMHC Concentrations.

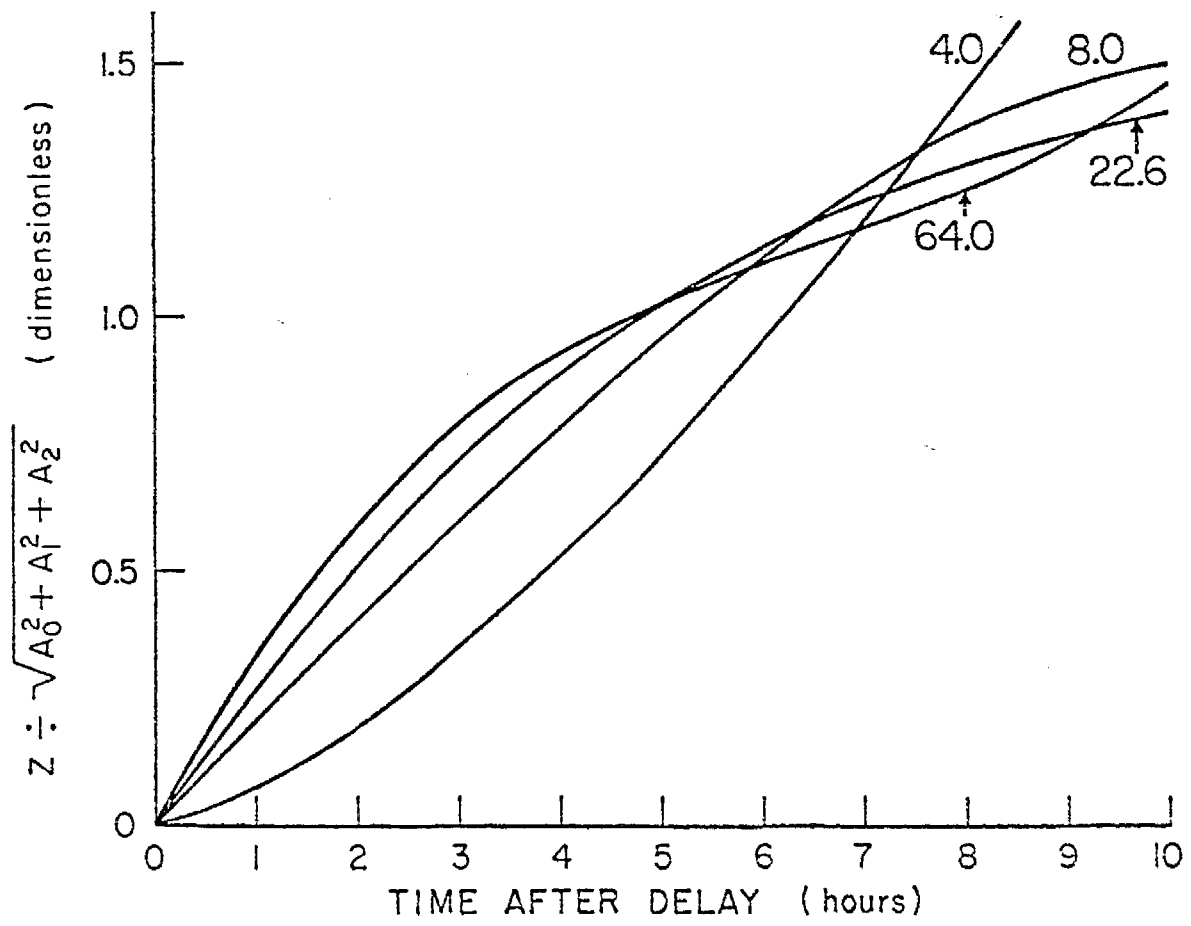


Figure 31. Representative Dimensionless Ozone Profiles.

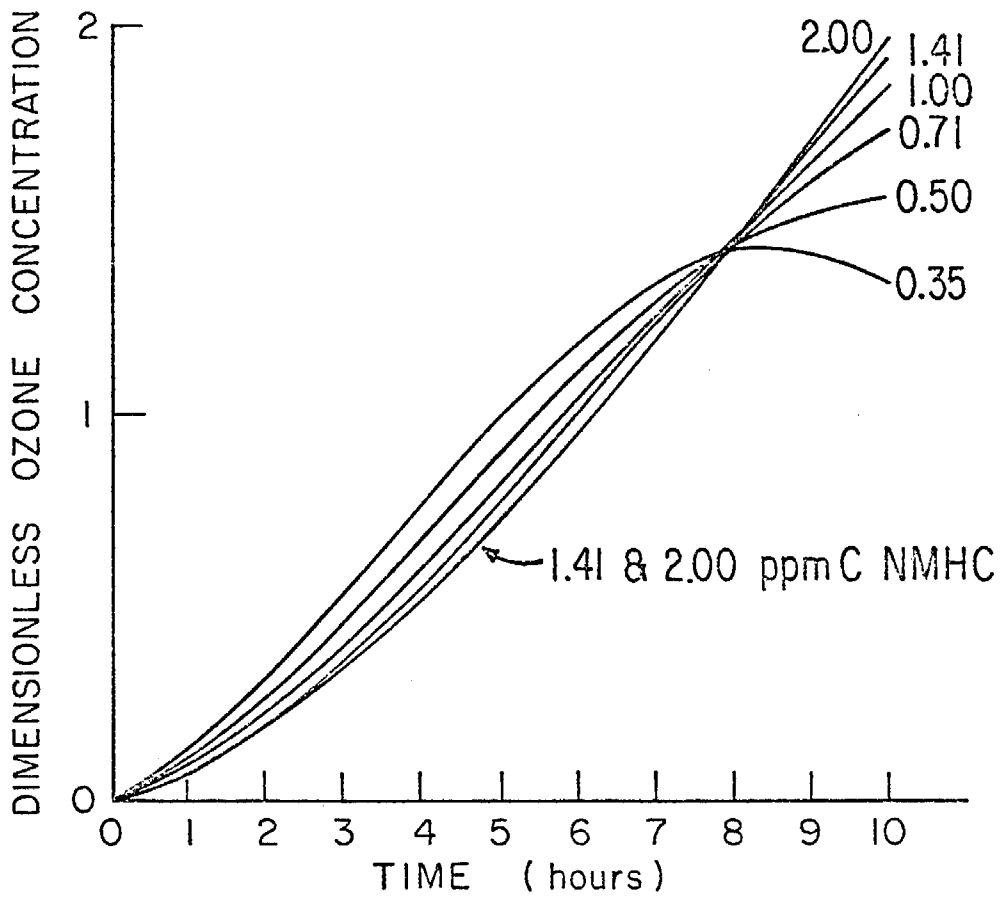


Figure 32. Profile Shapes at Precursor Ratio of 4 for Various NMHC Concentrations.

This view of the surrogate data forcefully brings out the intimate relationship between hydrocarbon and nitrogen oxides control. The most important implications of the analysis are illustrated by Figure 28. The behavior at lower ratios and higher precursor concentrations has important implications for downwind oxidant control around urban areas and the effects of NO<sub>x</sub> reductions for this situation. Dilution of these pollutant mixtures can lead to increased rms ozone levels with the major contributions to the mean at long irradiation times (see discussion of profile shapes above). Reduction of nitrogen oxides to increase the ratio is always helpful for these cases although it can concurrently increase ozone levels at moderate dilutions.

Details of Analysis Procedure. To facilitate the data analysis each surrogate ozone profile was broken into two time segments. The rising profile after the NO to NO<sub>2</sub> conversion period was linearly back-extrapolated to cut the time axis at a time t<sub>d</sub>, the "delay time." The length of the delay and the following profile were separately related to precursor concentrations.

The delay time t<sub>d</sub> can be suitably represented by:

$$t_d = \frac{N}{(p_1 + p_3 N^2) + r (p_2 + p_4 N^2)} \quad (1)$$

Here t<sub>d</sub> = delay time in hrs; N = initial NO<sub>x</sub> concentration in ppm; C = initial NMHC concentration in ppmC; r = precursor ratio C/N, and the p's are parameters. The values of p<sub>1</sub> to p<sub>4</sub> as estimated by least squares analysis of the data are:

$$\begin{aligned} p_1 &= 0.19973 \text{ ppm hr}^{-1} \\ p_2 &= -0.00084 \text{ ppm}^2 \text{ ppmC}^{-1} \text{ hr}^{-1} \\ p_3 &= -1.06170 \text{ ppm}^{-1} \text{ hr}^{-1} \\ p_4 &= 0.29840 \text{ ppmC}^{-1} \text{ hr}^{-1} \end{aligned}$$

in "units" to give delay times in hours when nitrogen oxides are expressed in ppm and the ratio is expressed in terms of ppmC ppm<sup>-1</sup>. Figure 33 shows delay time contours calculated from equation 1 using these parameter estimates. Also shown are lines of constant ratio which illustrate that the delay time decreases on dilution of the precursor mix before irradiation. At low precursor concentrations the delay is determined primarily by

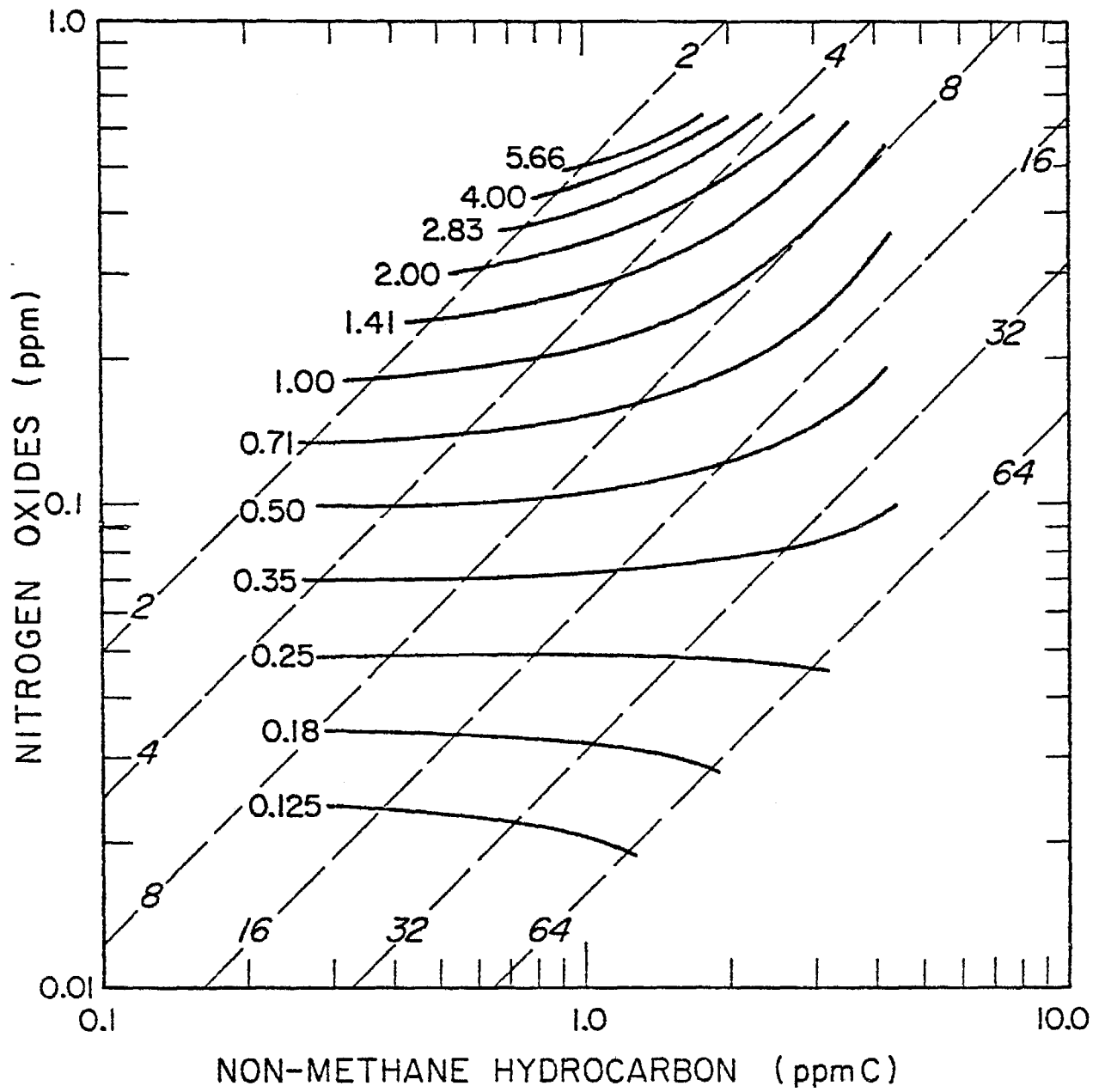


Figure 33. Delay Time Contours on the Logarithmic NMHC-NO<sub>x</sub> Plane for Surrogate (Delay in Hours).

the NO<sub>x</sub> concentration (90% NO, 10% NO<sub>2</sub>).

The curves of Figure 28 are drawn only for experimentally studied precursor concentrations. Caution is advised when applying equation 1 outside of this region. Equation 1 has singularity loci which can be expressed by

$$N = \sqrt{-\frac{p_1 + p_2 r}{p_3 + p_4 r}}$$

$$= 0.0530 \sqrt{\frac{237.8 - r}{3.558 - r}}$$

This equation is satisfied by imaginary roots for all of the ratios shown in Figure 33 except  $N = 0.652$  ppmC = 1.304 ppmC ( $r = 2$ ) indicating that the close neighborhood of this point should be avoided in using equation 1. The influence of the imaginary roots is manifested by the differing sense of curvature of the contours below and above 0.053 ppm NO<sub>x</sub>, a concentration also found to be significant for chamber ozone yields (Pitts et al., 1975b; 1976b).

Ozone profiles after the delay time were fitted with a truncated expansion in terms of orthonormal polynomials. Most surrogate profiles can be regarded as modulated straight lines. The system of orthonormal polynomials chosen to represent the profiles embodies this observation by choosing a squared linear function of time as the weighting function and incorporating the square root of the weighting function as a common factor for the profile expansion. A finite time interval after the delay was mapped onto the 0-1 interval by the transformation

$$x = 0.1 (t-t_d) \quad (2)$$

Here  $x$  is the aforementioned linear time function,  $t$  = time in hours and  $t_d$  = delay time in hours. This arbitrary choice restricts the mathematical validity of the orthonormal expansion to a period of ten hours after the delay time. The expansion is supported by experimental data over somewhat shorter periods, ranging from about 5 to 9 hours; use of the expansion near the upper time limit is somewhat of an extrapolation of the data.

The above choices (weighting function, interval of representation) uniquely determine the orthonormal polynomials to be used for a continuous representation of the profiles (Hochstrasser, 1965). These are a set of Jacobi polynomials. It turns out the first three of this infinite set are adequate for representation of all of the experimentally encountered profiles and these are given below, multiplied by the common factor, the square root of the weighting function.

$$x G_0(x) = x \sqrt{3} \quad (3)$$

$$x G_1(x) = x \sqrt{5} (4x-3) \quad (4)$$

$$x G_2(x) = x \sqrt{7} (15 x^2 - 20x + 6) \quad (5)$$

Graphs of the three functions are given in Figure 34.

The profiles are represented as

$$z = A_0 x G_0(x) + A_1 x G_1(x) + A_2 x G_2(x) \quad (6)$$

where  $z$  = ozone concentration at time  $t$  and the  $A$ 's are to be determined from the experimental data. This was done by the least squares procedure using the discrete ozone data given in the computer printouts for each experiment. Resynthesizing the profiles from the  $A$  estimates resulted in calculated ozone concentrations which agreed with the experimental data within the estimated analytical precision for concentrations of 0.05 ppm or greater. Consequently, each of the profiles after the delay are adequately represented by a set of three numbers.

The  $A$ 's were then related to precursor concentrations by empirical regressions. Preliminary attempts revealed that this process could be expedited if  $A_1$  and  $A_2$  were rendered dimensionless by division by  $A_0$ , a step transferring some of the difficulties with  $A_1$  and  $A_2$  to regressing  $A_0$  onto precursor concentrations. The final results of this procedure are truncated expansions in negative powers of the precursor ratio:

$$A_0 = p_5 + \frac{1}{\sqrt{r}} [p_6 + p_7 C] + \frac{1}{r} [p_8 C + p_9 C^{3/2}] \quad (7)$$

$$\frac{A_1}{A_0} = p_{10} + \frac{1}{r} [p_{11} + \frac{p_{12}}{C}] + \frac{1}{r^2} [p_{13} + \frac{p_{14}}{C}] \quad (8)$$

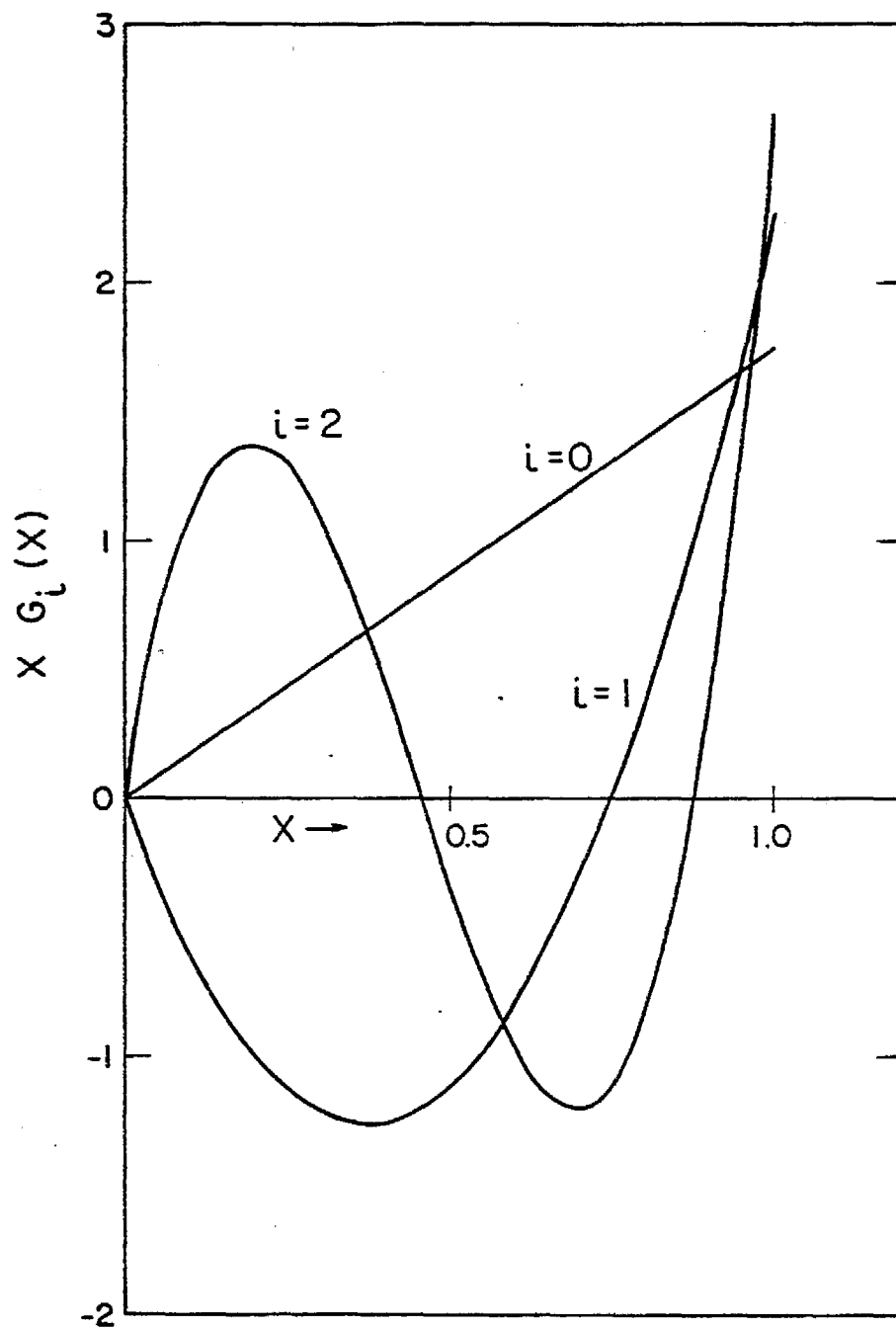


Figure 34. Graphs of First Three Orthonormal Polynomials.

$$\frac{A}{A_0} = p_{15} + \frac{1}{r} \left[ p_{16} + \frac{p_{17}}{C} \right] + \frac{1}{r^2} \left[ p_{18} + \frac{p_{19}}{C} \right] \quad (9)$$

where C is initial NMHC concentration as ppmC. Table 34 shows estimates of the parameters  $p_5$  to  $p_{19}$  along with the "units" required to rationalize the dimensions of the A's.

Table 32. Parameter Estimates

Parameter	Estimate	Parameter	Estimate
5	-0.07330 ppm	12	+0.06460 ppmC <sup>2</sup> ppm <sup>-1</sup>
6	+0.39970 ppm <sup>1/2</sup> ppmC <sup>1/2</sup>	13	+3.69020 ppmC <sup>2</sup> ppm <sup>-2</sup>
7	+1.10180 ppm <sup>1/2</sup> ppmC <sup>-1/2</sup>	14	-1.76140 ppmC <sup>3</sup> ppm <sup>-2</sup>
8	-0.68760	15	+0.07330
9	-1.22600 ppmC <sup>-1/2</sup>	16	-1.27478 ppmC ppm <sup>-1</sup>
10	-0.18800	17	+0.18066 ppmC <sup>2</sup> ppm <sup>-1</sup>
11	+0.56240 ppmC <sup>-1</sup> ppm <sup>-1</sup>	18	+3.71376 ppmC <sup>2</sup> ppm <sup>-2</sup>
		19	-1.07172 ppmC <sup>3</sup> ppm <sup>-2</sup>

These parameter estimates along with the estimates of  $p_1$  to  $p_4$  were checked against the complete data file of ozone profiles for the surrogate as minimum rms percent error estimators using a nonlinear parameter estimation procedure (Bard, 1974). The result was no readjustment of parameter values and a minimum error of estimate of 37%. The absolute error of estimate is  $\pm 0.06$  ppm indicating that most of the contributions to the percent error arises in estimating low ozone concentrations between 0.05 and 0.20 ppm. Errors at these concentrations are strongly affected by imprecise delay time estimates from the use of equation 1.

Nineteen parameters are required to represent the surrogate ozone profiles. This mode of condensing the data is not frugal with parameters. Parsimony is desirable for an empirical data reduction to ease data interpretation and to increase the precision of estimation. This

analysis could be regarded as an intermediate step towards a more parsimonious representation which is certainly possible, as indicated by graphical presentation of the results in the summary above. This additional computing effort cannot be justified before completion of the proposed series of long irradiation experiments which may yield different results because of extensive precautions against chamber artifacts. The large number of parameters in the present representation of the data indicates that only overall predicted trends should be taken seriously; small details are likely to be due to overrepresentation in terms of parameters.

Mathematically the quantities  $A_0$ ,  $A_1$ ,  $A_2$  represent components relative to a Jacobi polynomial space and can be treated like vector components. Figure 28 shows the length of this vector in ppm ozone as a function of NMHC concentration for various precursor ratios. This quantity scales the various ozone profiles yielding dimensionless ozone versus the time-proportional quantity,  $x$ . The shape of these profiles depend on two quantities,  $A_1/\sqrt{A_0^2 + A_1^2 + A_2^2}$  and  $A_2/\sqrt{A_0^2 + A_1^2 + A_2^2}$ . A third positive quantity  $A_0/\sqrt{A_0^2 + A_1^2 + A_2^2}$  also contributes to the shape but is not independent of the first two since the squares must sum to one. Figures 29 and 30 show the shape-determining quantities as a function of precursor ratio for various NMHC concentrations. The ratio of precursor concentrations is the factor having the greatest influence on profile shape. Absolute precursor concentrations have a relatively small influence on shape for ratios greater than 4 but a strong influence on the rms ozone concentrations.

XI. COMPUTER ARCHIVING OF SAPRC/ARB SURROGATE  
HYDROCARBON-NO<sub>x</sub>-AIR DATA BASE

Under previous contracts with the ARB we provided detailed chemical and physical data for more than 150 surrogate hydrocarbon-NO<sub>x</sub>-air smog chamber irradiations, amounting to a data base of over 50,000 individual values. Although these data are available in the previous progress reports in printed form, such a large data base can only be efficiently and effectively utilized with the aid of a computer. For this reason these data are being archived in computer-readable formats so that they can be disseminated on computer tapes and can be employed to their maximum potential by any workers with access to appropriate computing facilities.

This project has been divided into four major tasks: (1) Definition of the organization of the data as it will be used on the computer; (2) Processing and storing of all the data under that organization; (3) The writing and debugging of programs for retrieving the data from the direct access data set; and (4) Definition of the organization of the data as it is to be stored on tape for dissemination, and writing and debugging the programs required to move the data to the tape from the direct access data set, and vice-versa.

At the present time, tasks (1) and (3) are largely complete, task (2), converting the data into the archive disc data set (ADDS) format is currently in progress, and task (4), converting the data to computer tape format is still in the planning stages.

In the following sections, the details of the organization of the archive disc data set as currently envisioned and the problems involved in converting data from past runs are described. Also given is a brief summary of the computer programs which have been developed in this project, and an anticipated time scale for its completion.

Organization of the Disc Data Set. In order to maximize speed and to minimize input/output operations, the experimental data are stored on disc or a direct access data set. The data set is maintained by FORTRAN programs on an IBM 370 system, but the programs should be useable, with minimum modification, on any computer system with a FORTRAN compiler which supports direct access I/O. The data sets consist of several thousand 180 byte (180 x 8 bit) records, with the exact number of records to be deter-

mined once all the data is read in. For each record on the data set, there is associated record number, which must be specified when reading data from or writing data onto the data set. In the subsequent discussion, the "location" of data on this data set will refer to the record number for the record where the data is stored; or in the case of data requiring several records, the record number of the first of the several contiguous records containing that data.

The first record on the data set gives (1) the record number above which new data can be written without destroying the old; (2) the location of the pointer used to locate the glass chamber (AGC) data; (3) the location of the pointer locating evacuable chamber (EC) data (not used for ARB-surrogate runs) and (4) the location of the array of the 16 character code names for the measured species and physical parameters. (At the present time, the latter is stored on separate data sets. This will be changed before dissemination of the data.)

The records containing the pointers to the glass chamber (or evacuable chamber) data consist of up to 315 pairs of 2-byte integers. The first number in each pair is the AGC (or EC) run number, the second is the location of the directory record for that run.

The directory record for a given run contains the following information: (1) the run title, briefly describing the experiment; (2) the date and time the irradiation began; (3) the  $\text{NO}_2$  photolysis rate constant association with the run; (4) the location of spectral distribution data for the photolyzing light for this run, and the number of wavelengths in the spectral distribution; (5) the total rate of sample withdrawal due to monitoring; (6) the total number of GC samples taken; (7) the location of the initial condition data (useful for initiating model calculations simulating the run); (8) the location of the calibration data used for some of the measurements; (9) the number of comments used to describe special conditions or miscellaneous results for the run, and the location of the comments; (10) the number of different time sets for which data monitored in the run are reported; and (11) the number of species or physical parameters monitored in this run (data channels), and the location of the pointer locating the data for those measurements.

The records containing the pointer locating the data for the run

contain the following information for each data channel: (1) the code number for the species or the physical parameters measured. This number can range from 0-255, and is associated with a 16 character name in an array stored elsewhere on the data set (located as indicated on record #1); (2) the time set number, and the location of the times for which data points for this data channel are stored; (3) the number of data points and the location of the data; (4) the instrument numbers. (This allows for giving data separately for the same compound or physical parameter obtained by more than one technique); (5) a code number giving the unit (i.e., ppm, %, liters, ppmC, etc.) in which the data is given; and (6) an indication as to whether the data has flagged points.

For each data channel, the data and the times at which data are taken can be read from the records indicated in the pointer record. If the data is flagged, the flags are entered with the data. The flag consists of one character with a standard meaning or with a meaning defined by the comments stored with the run. (For example "?" means uncertain data.) A data value of 1,000,000 means no data was taken at the associated time point.

The following example illustrates how a program could use this data set. Suppose one wishes to retrieve the acetaldehyde data for run AGC-113. By convention, the code number for acetaldehyde used by our data processing programs is 99, and the 16 character name is "CCHO" (padded to the right with blanks). If the 16 character name is input, the program could determine the code number by finding which element of the array of names read from the data set matches the input name; alternately, the code number could be input directly. To obtain data for run AGC-113, the program reads the pointer records for the glass chamber runs, searches through the first of the pair of integers on this record for the number 113, and then reads the run directory record from the location given by the corresponding second number of the pair. From the run directory, the program determines the location of the data pointer records, which is then read. (If more than one data channel is to be read in for a given run, these steps need not be repeated.) To read, for example, acetaldehyde data, the program then searches through the data from the data pointer record to determine the location of data associated with code number 99 (99 = acetaldehyde), and then the data associated flags (if any) are read from that location.

This organization may seem to be more complicated than necessary for archiving purposes, but the data set is also being used for storing, processing and editing data created in our ongoing chamber programs. This organization appears to serve reasonably well the often conflicting requirements for flexibility necessary to allow for new types of data as our chamber programs evolve, for ease of editing new data, for efficiency of disc storage space, and for efficiency of memory and processing time for computer programs which process and/or retrieve the data.

Archiving Data from Past Runs. The data for runs previously done in the SAPRC-ARB (and other chamber programs) exist in a variety of forms. For runs done before AGC 351, all data exist on computer cards created as input to the program which printed the data for the reports. Unfortunately, as time went on, there were modifications in our data processing procedure, so the card data exist in several formats. For some runs, the chromatography data are in a different format than the other data, while for more recent runs they are not. In addition, for most runs done after AGC 133-150, data from automatic monitoring instruments were stored on computer tapes, which were subsequently archived on a special disc data set created for that purpose. Thus, in order to archive these data, computer programs which can read these data in a variety of formats had to be written.

Unfortunately, archiving the data from the past runs cannot be handled entirely by computer programs alone. The organization of some of the previous data is inconsistent with the organization being used on our current disc data set. The most serious problem arises from measurements of the same compounds made simultaneously using different instruments or techniques. The current organization has, for each data channel one ID number identifying the type of compound or physical parameter measured, and another identifying the measurement technique (if more than one used). Previously, data channels had only one identifying number; if a compound was measured in more than one way, some of the data were treated as a "special channel", which was handled differently, or in some cases the data were merged into the same channel, requiring at some time points more than one data point or requiring the entry of two identical time points into the format to handle both measurements. An additional complication is that it must be decided which channel is to be used in computing totals such as

required to obtain total carbon, total nitrogen, or to correct nitrate interferences in NO<sub>2</sub> measurements (Winer et al., 1974). Because of the variety of ways this was treated, these data can only be made consistent with the present organization on a case-by-case basis.

Additional problems include measurements which were unknown at the time they were made but which are now known; compounds which were previously treated as special channel which have since been given regular ID numbers; the need to assign calibration numbers for runs done before different calibrations were used; the necessity to input data which was previously given only in comments, if at all (such as k values, number of GC samples, total sampling rates, etc.); and the need to make sure the data being archived are not based on assumptions which have since been re-evaluated. Because of the large number of runs to be archived and the variety of ways in which data have been collected and treated, case-by-case examination is necessary before archiving; this process is quite time-consuming.

The current status of the archiving effort is that the necessary computer programs have been written and are running, the cards for most of the old runs have been modified so they can be read by these programs, and the processing of those runs has begun. Because of the quantity of the data and the variety of matters which must be handled, the probability for human error -- both in writing the programs and modifying the cards -- is high; we are now correcting the problems one-by-one as they become apparent. Because of this, the rate of processing the old runs is now rather slow, but it is expected to accelerate as the problems become resolved.

Computer Programs. As discussed above, a number of computer programs are required for preparing the archive disc data set. The programs which have been written and are in current use for this purpose are listed below:

A. A program to read new raw data from input magnetic tapes and write corrected values onto the disc data set.

B. A program to read new raw data from cards and store corrected values on the disc data set.

C. A program to convert all old data formats (inorganic species and measured parameters on cards or on tape, and organic species on cards) into the new format on the disc data set.

D. A program to write calculated species such as total hydrocarbon, total nitrogen, total nitrate, water, etc. onto the disc data set. This program also prints all data or select data for any run number.

E. A program to edit the disc data set.

The following has been written, but is undergoing slight modifications:

F. A program to produce final printouts and/or plot for report.

The following further programs will be supplied on tape along with the attached data:

1. A program to obtain printouts of the data for selected individual chamber runs directly from the data archive tape.

2. A program to initialize the disc data set.

3. A program to copy data for selected individual chamber runs from the archive tape to the disc data set.

4. A program to read the disk data set and obtain printouts for selected runs.

These programs are not in their final form at this time, but will be completed prior to submission of the data. In addition, a users manual will be supplied which gives a sufficiently detailed description of the organization of the data so that other programs for specific applications desired can be written by the user.

Anticipated Schedule for Completion. The rate of completion of this project should be determined by the rate of archiving the data from the past runs. The necessary procedures for this task have been worked out, and data from representative runs have been successfully converted to the archive format. This project is now ongoing and is expected to be completed by December 1979. Developing and testing the programs required for converting the ADDS data set to tape format and visa versa will occur simultaneously with the completion of the archiving task, and these steps are not expected to significantly affect the time of completion of this project.

## XII. REFERENCES

- AIHL (1969): Analysis of total oxidant content of the atmosphere (2% potassium iodide method). Recommended method No. 2, California State Department of Public Health, Air and Industrial Hygiene Laboratory, January, 1969, Berkeley, California.
- Air Resources Board (1975): Comparison of oxidant calibration procedures. Final Report of the Ad Hoc Committee to the California Air Resources Board, Sacramento, California, February 3, 1975.
- Atkinson, R. (1977): Private communication.
- Atkinson, R. and Pitts, J. N., Jr. (1975): Rate constants for the reaction of OH radicals with propylene and the butenes over the temperature range 297-425 K. *J. Chem. Phys.*, 63, 3591-3595.
- Atkinson, R. and Pitts, J. N., Jr. (1978): Kinetics of the reaction of  $O(^3P)$  atoms and OH radicals with 2-methyl-2-butene. *J. Chem. Phys.*, 68, 2992-2994.
- Atkinson, R., Darnall, K. R., Winer, A. M., and Pitts, J. N., Jr. (1976a): Tropospheric reactivity of halocarbons. Final Report to E. I. duPont de Nemours and Co., Inc., February 1, 1976.
- Atkinson, R., Perry, R. A., and Pitts, J. N., Jr. (1976b): Rate constants for the reaction of OH radicals with 2-methyl-2-butene over the temperature range 297-425 K. *Chem. Phys. Lett.*, 38, 607-610.
- Atkinson, R., Perry, R. A. and Pitts, J. N., Jr. (1977): Absolute rate constants for the reaction of  $O(^3P)$  atoms with n-butane and  $NO(M=Ar)$  over the temperature range 298-439 K. *Chem. Phys. Lett.*, 47, 197-202.
- Atkinson, R., Darnall, K. R., Lloyd, A. C., Winer, A. M. and Pitts, J. N., Jr. (1979a): Kinetics and mechanisms of the reactions of the hydroxyl radical with organic compounds in the gas phase. *Adv. Photochem.*, 11, 375-488.
- Atkinson, R., Carter, W. P. L., Darnall, K. R., Winer, A. M. and Pitts, J. N., Jr. (1979b): A smog chamber and modeling study of the gas phase  $NO_x$ /air photooxidation of toluene and the cresols. In preparation.
- Bard, Y. (1974): Non-linear parameter estimation. Academic Press, New York.
- Bradley, J. N., Hack, W., Hoyermann, K. and Wagner, H. G. (1973): Kinetics of the reaction of hydroxyl radicals with ethylene and with  $C_3$  hydrocarbons. *J. Chem. Soc., Faraday Trans. I*, 69, 1889-1898.
- Bufalini, J. J., Kopczynski, S. L., and Dodge, M. C. (1972): Contaminated smog chambers in air pollution research. *Environ. Lett.*, 3, 100-109.

- Bufalini, J. J., Walter, T. A., and Bufalini, M. M. (1977): Contamination effects on ozone formation in smog chambers. *Environ. Sci. Technol.*, 11, 1181-1185.
- Butler, R., Solomon, I. J. and Snelson, A. (1978): Pressure-dependence of CO + OH rate constant in O<sub>2</sub> and N<sub>2</sub> mixtures. *Chem. Phys. Lett.*, 54, 19-24.
- Calvert, J. G., Su, F., Bottenheim, J. W. and Strausz, O. P. (1978): Mechanism of the homogeneous oxidation of sulfur dioxide in the troposphere. *Atmos. Environ.*, 12, 197-226.
- Campbell, I. M. and Goodman, K. (1975): Reaction of O(<sup>3</sup>P) atoms with nitromethane vapour at 295 K. *Chem. Phys. Lett.*, 34, 105-108.
- Campbell, I. M., Handy, B. J. and Kirby, R. M. (1975): Gas phase chain-reaction of H<sub>2</sub>O<sub>2</sub> + NO<sub>2</sub> + CO. *J. Chem. Soc., Faraday Trans. 1*, 71, 867-874.
- Campbell, I. M., McLaughlin, D. F. and Handy, B. J. (1976): Rate constants for reactions of hydroxyl radicals with alcohol vapors at 292 K. *Chem. Phys. Lett.*, 38, 362-364.
- Carter, W. P. L., Lloyd, A. C., Sprung, J. L. and Pitts, J. N., Jr. (1979): Computer modeling of smog chamber data: Progress in validation of a detailed mechanism for the photooxidation of propene and n-butane in photochemical smog. *Int. J. Chem. Kinet.*, 11, 45-101.
- Cercignani, C. and Pagani, C. D. (1966): Variational approach to boundary-value problems in kinetic theory. *Phys. Fluids*, 9, 1167-1173.
- Coutant, R. W. (1977): Effect of environmental variables on collection of atmospheric sulfate. *Environ. Sci. Technol.*, 11, 873-878.
- Darley, E. F., Kettner, K. A. and Stephens, E. R. (1963): Analysis of peroxyacyl nitrates by gas chromatography with electron capture detection. *Anal. Chem.*, 35, 589-591.
- Darnall, K. R., Carter, W. P. L., Winer, A. M., Lloyd, A. C., and Pitts, J. N., Jr. (1976a): Importance of RO<sub>2</sub> + NO in alkyl nitrate formation from C<sub>4</sub>-C<sub>6</sub> alkane photooxidations under simulated atmospheric conditions. *J. Phys. Chem.*, 80, 1948-1950.
- Darnall, K. R., Lloyd, A. C., Winer, A. M., and Pitts, J. N., Jr. (1976b): Reactivity scale for atmospheric hydrocarbons based on reaction with hydroxyl radical. *Environ. Sci. Technol.*, 10, 692-696.
- Darnall, K. R., Winer, A. M., Lloyd, A. C., and Pitts, J. N., Jr. (1976c): Relative rate constants for reaction of OH radicals with selected C<sub>6</sub> and C<sub>7</sub> alkanes and alkenes at 305 ± 2 K. *Chem. Phys. Lett.*, 44, 415-418.

- Darnall, K. R., Atkinson, R. and Pitts, J. N., Jr. (1978): Rate constants for the reaction of the OH radical with selected alkanes at 300 K. *J. Phys. Chem.*, 82, 1581-1584.
- Darnall, K. R., Atkinson, R., and Pitts, J. N., Jr. (1979): Observations of biacetyl from the reaction of OH radicals with o-xylene: evidence for ring cleavage. *J. Phys. Chem.*, 83, 1943-1946.
- Davidson, J. A. and Thrush, B. A. (1975): Reaction of oxygen atoms with methyl and ethyl nitrates. *J. Chem. Soc., Faraday Trans. I*, 71, 2413-2420.
- Demerjian, K. L., Kerr, J. A., and Calvert, J. G. (1974): The mechanism of photochemical smog formation. *Adv. Environ. Sci. Technol.*, 4, 1-262.
- Dimitriadis, B. (1977): An alternative to the Appendix-J method for calculating oxidant- and NO<sub>2</sub>-related control requirements. *In: Proceedings of the International Conference on Photochemical Oxidant Pollution and Its Control*, Vol. II, EPA 600/3-77-001b, pp. 871-879.
- Dimitriadis, B. and Joshi, S. B. (1977): Applicability of reactivity criteria in oxidant related emission control in the U.S.A. *In: Proceedings of the International Conference on Photochemical Oxidant Pollution and its Control*, Vol. II, EPA 600/3-77-001b, pp. 705-711.
- Dodge, M. C. (1977a): Combined use of modeling techniques and smog chamber data to derive ozone-precursor relationships. *In: Proceedings of the International Conference on Photochemical Oxidant Pollution and Its Control*, Sept. 12-17, 1976, Vol. II, EPA 600/3-77-001b, p. 881-889.
- Dodge, M. C. (1977b): Effect of selected parameters on predictions of a photochemical model. June, 1977, EPA 600/3-77-048.
- Doyle, G. J., Lloyd, A. C., Darnall, K. R., Winer, A. M. and Pitts, J. N., Jr. (1975): Gas phase kinetic study of relative rates of reaction of selected aromatic compounds with hydroxyl radicals in an environmental chamber. *Environ. Sci. Technol.*, 9, 237-241.
- Doyle, G. J., Bekowies, P. J., Winer, A. M., and Pitts, J. N., Jr. (1977): A charcoal adsorption air purification system for chamber studies investigating atmospheric photochemistry. *Environ. Sci. Technol.*, 11, 45-51.
- Durbin, P. A., Hecht, T. A., and Whitten, G. Z. (1975): Mathematical modeling of simulated smog. *Systems Applications, Inc.*, EPA 650/4-75-026.
- Environmental Protection Agency (1978): Air quality criteria for ozone and other photochemical oxidants. Volume I (Preprint), April, 1978, EPA 600/8-78-004.

- Fowkes, F. M. (1965): Attractive forces at interfaces. Chapter 2, Proc. Symp. on Chemistry and Physics of Interferences, Washington, DC, 1964, ACS, Washington, DC, pp. 1-12.
- Fuchs, N. A. and Sutugin, A. G. (1971): High-dispersed aerosols. Topics in current aerosol research. In: International Reviews in Aerosol Physics and Chemistry, G. M. Hidy and J. R. Block (eds.), Pergaman Press, New York, Vol. III, pp 1-60.
- Gordon, S. and Mulac, W. A. (1975): Reaction of  $\text{OH}(X^2\Pi)$  radical produced by pulse-radiolysis of water vapor. Int. J. Chem. Kinet., Symp. 1, 289-299.
- Gorse, R. A. and Volman, D. H. (1974): Photochemistry of the gaseous hydrogen peroxide carbon-monoxide system. II: Rate constants for hydroxyl radical reactions with hydrocarbons and for hydrogen atom reactions with hydrogen peroxide. J. Photochem., 3, 115-122.
- Greiner, N. R. (1970): Hydroxyl radical kinetics by kinetic spectroscopy. VI. Reactions with alkanes in the range 300-500 K. J. Chem. Phys., 53, 1070-1076.
- Grosjean, D., Doyle, G. J., Mischke, T. M., Poe, M. M., Fitz, D. R., Smith, J. P., and Pitts, J. N., Jr. (1976): The concentration, size distribution, and modes of formation of particulate, sulfate, and ammonium compounds in the eastern part of the Los Angeles Basin. Presented at the 69th Annual APCA Meeting, Paper 76-20.3, Portland, OR, June 27-July 1.
- Harker, A. B. and Burton, C. S. (1975): A study of the mechanism and kinetics of the reaction of  $\text{O}(^3\text{P})$  atoms with propane. Int. J. Chem. Kinet., 7, 907-917.
- Harper, W. R. (1967): Contact and frictional electrification. Oxford, New York, pp. 91-96.
- Henry, P. S. H. (1953): The role of asymmetric rubbing in the generation of static electricity. Brit. J. Appl. Physics, Supplement, 2, S31-S36.
- Herron, J. T. and Huie, R. E. (1973): Rate constants for the reactions of atomic oxygen [ $\text{O}(^3\text{P})$ ] with organic compounds in the gas phase. J. Phys. Chem. Ref. Data, 2, 467-518.
- Hochstrasser, V. W. (1965): Orthogonal polynomials. In: Handbook of Mathematical Functions, J. Abramowitz and M. Stegun, eds., Dover Press, New York.
- Holmes, J. R., O'Brien, R. J., Crabtree, J. H., Hecht, T. A. and Seinfeld, J. H. (1973): Measurements of ultraviolet radiation intensity in photochemical smog studies. Environ. Sci. Technol., 7, 519-523.

- Huie, R. E. and Herron, J. T. (1975): Temperature dependence of the rate constants for reactions of ozone with some olefins. *Int. J. Chem. Kinet.*, Symposium No. 1, 1, 165-181.
- Husar, J. D., Husar, R. B. and Stubits, P. K. (1975): Determination of submicrogram amounts of atmospheric particulate sulfur. *Analyt. Chem.*, 47, 2062-2065.
- Japar, S. J., Wu, C. H. and Niki, H. (1974): Rate constants for the reaction of ozone with olefins in the gas phase. *J. Phys. Chem.*, 78, 2318-2320.
- Lloyd, A. C., Darnall, K. R., Winer, A. M. and Pitts, J. N., Jr. (1976a): Relative rate constants for reactions of the hydroxyl radical with series of alkanes, alkenes, and aromatic hydrocarbons. *J. Phys. Chem.*, 80, 789-794.
- Lloyd, A. C., Darnall, K. R., Winer, A. M. and Pitts, J. N., Jr. (1976b): Relative rate constants for the reactions of OH radicals with isopropyl alcohol, diethyl and di-n-propyl ether at  $305 \pm 2$  K. *Chem. Phys. Lett.*, 42, 205-209.
- Morris, E. D., Jr. and Niki, H. (1971): Reactivity of hydroxyl radicals with olefins. *J. Phys. Chem.*, 75, 3640-3641.
- Morris, E. D., Jr. and Niki, H. (1973): Reaction of dinitrogen pentoxide with water. *J. Phys. Chem.*, 77, 1929-1932.
- Morris, E. D., Jr., Stedman, D. H. and Niki, H. (1971): Mass spectrometric study of the reactions of the hydroxyl radical with ethylene, propylene and acetaldehyde in a discharge flow system. *J. Amer. Chem. Soc.*, 93, 3570-3572.
- National Academy of Sciences (1977): Ozone and other photochemical oxidants. National Academy of Sciences, Washington, D.C.
- Nieboer, H., Carter, W. P. L., Lloyd, A. C. and Pitts, J. N., Jr. (1976): The effect of latitude on the potential for formation of photochemical smog. *Atmos. Environ.*, 10, 731-734.
- Overend, R. P., Paraskevopoulos, G. and Cvetanovic, R. J. (1975): Rates of OH radical reactions. I. Reactions with H<sub>2</sub>, CH<sub>4</sub>, C<sub>2</sub>H<sub>6</sub>, and C<sub>3</sub>H<sub>8</sub> at 295 K. *Can. J. Chem.*, 53, 3374-3382.
- Owens, C. M. and Roscoe, J. M. (1976): The reactions of atomic oxygen with methanol and ethanol. *Can. J. Chem.*, 54, 984-989.
- Parratt, L. G. (1961): Probability and experimental errors in science. John Wiley and Sons, New York, NY.
- Perry, R. A. (1977): Gas phase kinetics of the hydroxyl radical. Ph.D. Thesis, August, 1977, University of California, Riverside, 275 p.

- Perry, R. A., Atkinson, R. and Pitts, J. N., Jr. (1976): Rate constants for the reaction of OH radicals with n-butane over the temperature range 297-420 K. J. Chem. Phys., 64, 5314-5316.
- Perry, R. A., Atkinson, R. and Pitts, J. N., Jr. (1977a): Kinetics of the reactions of OH radicals with C<sub>2</sub>H<sub>2</sub> and CO. J. Chem. Phys., 67, 5577-5584.
- Perry, R. A., Atkinson, R. and Pitts, J. N., Jr. (1977b): Kinetics and mechanism of the gas phase reaction of OH radicals with aromatic hydrocarbons over the temperature range 296-473 K. J. Phys. Chem., 81, 296-304.
- Pitts, J. N., Jr., Doyle, G. J., Lloyd, A. C., and Winer, A. M. (1975a): Chemical transformations in photochemical smog and their applications to air pollution control strategies. Second Annual Report for National Science Foundation-Research Applied to National Needs Grant No. AEN73-02904-A02.
- Pitts, J. N., Jr., Winer, A. M., Darnall, K. R., Doyle, G. J. and McAfee, J. M. (1975b): Chemical consequences of air quality standards and of control implementation programs: roles of hydrocarbons, oxides of nitrogen, and aged smog in the production of photochemical oxidant. Final Report, California Air Resources Board Contract No. 3-017, July.
- Pitts, J. N., Jr., Bekowies, P. J., Winer, A. M., Doyle, G. J., McAfee, J. M. and Wilson, K. W. (1975c): The design and construction of an environmental chamber facility for the study of photochemical air pollution. Final report, California ARB Grant No. 5-067-1, in preparation.
- Pitts, J. N., Jr., Lloyd, A. C., Winer, A. M., Darnall, K. R. and Doyle, G. J. (1976a): Development and application of a hydrocarbon reactivity scale based on reaction with the hydroxyl radical. 69th Annual Air Pollution Control Association Meeting, Portland, OR, Paper No. 76-31.1, June 27-July 1.
- Pitts, J. N., Jr., Winer, A. M., Darnall, K. R., Doyle, G. J. and McAfee, J. M. (1976b): Chemical consequences of air quality standards and of control implementation programs: roles of hydrocarbons, oxides of nitrogen, and aged smog in the production of photochemical oxidant. Final Report, California Air Resources Board Control No. 4-214, May.
- Pitts, J. N., Jr., McAfee, J. M., Long, W. D. and Winer, A. M. (1976c): Long-path infrared spectroscopic investigation at ambient concentrations of the 2% neutral buffered potassium iodide method for determination of ozone. Environ. Sci. Technol., 10, 787-793.

- Pitts, J. N., Jr., Winer, A. M., Darnall, K. R., Doyle, G. J., McAfee, J. M., Bekowies, P. J. and Long, W. D. (1976d): A smog chamber study of the role of hydrocarbons, oxides of nitrogen and aged smog in the production of photochemical oxidants. I. Facilities methodology, and results for six-hour irradiations. In preparation.
- Pitts, J. N., Jr., Darnall, K. R., Winer, A. M. and McAfee, J. M. (1977a): Mechanisms of photochemical reactions in urban air, Vol. II, Smog Chamber Studies, EPA-600/3-77-014b.
- Pitts, J. N., Jr., Winer, A. M., Darnall, K. R., Lloyd, A. C. and Doyle, G. J. (1977b): Hydrocarbon reactivity and the role of hydrocarbons, oxides of nitrogen, and aged smog in the production of photochemical oxidants. In: Proceedings of the International Conference on Photochemical Oxidant Pollution and Its Control, Vol. II, EPA-600/3-77-001b, pp. 687-704.
- Pitts, J. N., Jr., Winer, A. M., Doyle, G. J. and Darnall, K. R. (1978): Reactivity scale for atmospheric hydrocarbons based on reaction with hydroxyl radical. Environ. Sci. Technol., 12, 100-102.
- Ravishankara, A. R., Wagner, S., Fischer, S., Smith, G., Schiff, R., Watson, R. T., Tesi, G. and Davis, D. D. (1978): Int. J. Chem. Kinet., 10, 783-804.
- Roberts, P. T. and Friedlander, S. K. (1976): Analysis of sulfur in deposited aerosol particles by vaporization and flame photometric detection. Atmos. Environ., 10, 403-408.
- Salter, J. F. and Thrush, B. A. (1977): Reaction of oxygen atoms with methyl and ethyl nitrates. J. Chem. Soc., Faraday Trans. I, 73, 1098-1103.
- Smith, R. G., Bryan, R. J., Feldstein, M., Levadie, B., Miller, F. A., Stephens, E. R. and White, N. G. (1970): Tentative method of analysis for formaldehyde content of the atmosphere (colorimetric method). H. L. S., 7, (1) Supplement, 87-91.
- Spicer, C. W. and Miller, D. F. (1974): Nitrogen balance in smog chamber studies. Presented at the 67th Annual Meeting of the Air Pollution Control Association, June, 1974, Denver, Colorado.
- Stephens, E. R. (1973): Hydrocarbons in polluted air. Summary report, Coordinating Research Council, Project CAPA-5-68, June 1973; NTIS No. PB 230 993/AS.
- Stephens, E. R. and Burlison, F. R. (1969): Distribution of light hydrocarbons in ambient air. J. Air. Pollut. Contr. Assoc., 19, 929-936.
- Stephens, E. R. and Price, M. A. (1973): Analysis of an important pollutant: peroxyacetyl nitrate. J. Chem. Educ., 50, 351-354.

- Stuhl, F. (1973): Rate constant for the reaction of OH with N-C<sub>4</sub>H.  
Z. Naturforsch., 284, 1383-1384.
- Tuazon, E. C., Winer, A. M., Graham, R. A. and Pitts, J. N., Jr. (1977):  
Application of a kilometer pathlength FT-IR spectrometer to analysis  
of trace pollutants in ambient and simulated atmospheres. In: Con-  
ference Proceedings of 4th Joint Conference on Sensing of Environmental  
Pollutants, November 6-11, 1977, New Orleans, LA.
- Tuazon, E. C., Graham, R. A., Winer, A. M., Easton, R. R., Pitts, J.N., Jr.  
and Hanst, P. L. (1978): A kilometer pathlength Fourier-transform  
infrared system for the study of trace pollutants in ambient and synthe-  
tic atmospheres. Atmos. Environ., 12, 865-875.
- Volman, D. H. (1975): Comments made in General Discussion Section III.  
Int. J. Chem. Kinet., Symp 1, 358.
- Winer, A. M., Peters, J. W., Smith, J. P. and Pitts, J. N., Jr. (1974):  
Response of commercial chemiluminescent NO-NO<sub>2</sub> analyzers to other  
nitrogen-containing compounds. Environ. Sci. Technol., 8, 1118-1121.
- Winer, A. M., Lloyd, A. C., Darnall, K. R. and Pitts, J. N., Jr. (1976):  
Relative rate constants for the reaction of the hydroxyl radical with  
selected ketones, chloroethenes and monoterpene hydrocarbons. J.  
Phys. Chem., 80, 1635-1639.
- Winer, A. M., Lloyd, A. C., Darnall, K. R., Atkinson, R. and Pitts, J. N.,  
Jr. (1977): Rate constants for the reaction of OH radicals with  
n-propyl acetate, sec-butyl acetate, tetrahydrofuran and peroxyacetyl  
nitrate. Chem. Phys. Lett., 51, 221-226.
- Winer, A. M., Graham, R. A., Doyle, G. J., Bekowies, P. J., McAfee, J. M.  
and Pitts, J. N., Jr. (1979): An evacuable environmental chamber and  
solar simulator facility for the study of atmospheric photochemistry.  
Adv. Environ. Sci. Technol., 11, in press.
- Wu, C. H., Japar, S. M. and Niki, H. (1976): Relative reactivities of  
HO-hydrocarbon reactions from smog studies. J. Environ. Sci. Health,  
A11, 191-200.
- Zafonte, L., Rieger, P. L. and Holmes, J. R. (1977): Nitrogen dioxide  
photolysis in the Los Angeles atmosphere. Environ. Sci. Technol.,  
11, 483-487.

XIII. LIST OF PUBLICATIONS FROM SAPRC-ARB CHAMBER PROGRAM

- A Novel 20 KW Solar Simulator Designed for Air Pollution Research  
Proceedings of Seventh Conference on Space Simulation (NASA) Special  
Publication 336, Los Angeles, California, November 12-14, 1973, Paper  
No. 66, pp. 811-825  
J. H. Beauchene, P. J. Bekowies, J. M. McAfee, A. M. Winer, L. Zafonte,  
and J. N. Pitts, Jr.
- Response of Commercial Chemiluminescent NO-NO<sub>2</sub> Analyzers to other Nitrogen  
Containing Compounds  
Environ. Sci. Technol., 8, 1118 (1974)  
A. M. Winer, J. W. Peters, J. P. Smith, and J. N. Pitts, Jr.
- Experimentally Validated Mechanisms, Models and Control Strategies for  
Photochemical Air Pollution  
Proceedings of the Second Annual NSF-RANN Trace Contaminants Confer-  
ence, Asilomar, California, August 29-31, 1974, LBL-3217, pp. 50-53  
J. N. Pitts, Jr., W. P. Carter, K. R. Darnall, G. J. Doyle, W. Kuby,  
A. C. Lloyd, J. M. McAfee, C. Pate, J. P. Smith, J. L. Sprung, and  
A. M. Winer
- Gas Phase Kinetic Study of Relative Rates of Reaction of Selected Aromatic  
Compounds with Hydroxyl Radicals in an Environmental Chamber  
Environ. Sci. Technol., 9, 237 (1975)  
G. J. Doyle, A. C. Lloyd, K. R. Darnall, A. M. Winer, and J. N.  
Pitts, Jr.
- Long-Path Infrared Spectroscopic Investigation at Ambient Concentrations  
of the 2% Neutral Buffered Potassium Iodide Method for Determination of  
Ozone  
Environ. Sci. Technol., 10, 787 (1976)  
J. N. Pitts, Jr., J. M. McAfee, W. D. Long, and A. M. Winer
- Infrared Absorptivity of the 9.6  $\mu$ m Ozone Band as a Function of Spectral  
Resolution and Abundance  
J. Quant. Spectrosc. Radiat. Transfer, 16, 829 (1976)  
J. M. McAfee, E. R. Stephens, D. R. Fitz, and J. N. Pitts, Jr.
- Relative Rate Constants for Reaction of the Hydroxyl Radical with a Series  
of Alkanes, Alkenes, and Aromatic Hydrocarbons  
J. Phys. Chem., 80, 789 (1976)  
A. C. Lloyd, K. R. Darnall, A. M. Winer, and J. N. Pitts, Jr.
- Relative Rate Constants for the Reaction of the Hydroxyl Radical with  
Selected Ketones, Chloroethenes, and Monoterpene Hydrocarbons  
J. Phys. Chem., 80, 1635 (1976)  
A. M. Winer, A. C. Lloyd, K. R. Darnall, and J. N. Pitts, Jr.

Reactivity Scale for Atmospheric Hydrocarbons Based on Reaction with Hydroxyl Radical

Environ. Sci. Technol., 10, 692 (1976)

K. R. Darnall, A. C. Lloyd, A. M. Winer, and J. N. Pitts, Jr.

Development and Application of a Hydrocarbon Reactivity Scale Based on Reaction with the Hydroxyl Radical

69th Annual Air Pollution Control Association Meeting, Portland, Oregon, June 27-July 1, 1976, Paper No. 76-31.1

J. N. Pitts, Jr., A. C. Lloyd, A. M. Winer, K. R. Darnall, and G. J. Doyle

Relative Rate Constants for the Reactions of OH Radicals with Isopropyl Alcohol, Diethyl and Di-n-Propyl Ether at  $305 \pm 2$  K

Chem. Phys. Lett., 42, 205 (1976)

A. C. Lloyd, K. R. Darnall, A. M. Winer, and J. N. Pitts, Jr.

Hydrocarbon Reactivity and the Role of Hydrocarbons, Oxides of Nitrogen, and Aged Smog in the Production of Photochemical Oxidants

Proceedings of the International Conference on Photochemical Oxidant Pollution and Its Control, Raleigh, North Carolina, Sept. 13-17, 1976, EPA-600/3-77-0016, January 1977, pp. 687-704

J. N. Pitts, Jr., A. M. Winer, K. R. Darnall, A. C. Lloyd, and G. J. Doyle

Relative Rate Constants for the Reaction of OH Radicals with Selected C<sub>6</sub> and C<sub>7</sub> Alkanes and Alkenes at  $305 \pm 2$  K

Chem. Phys. Lett., 44, 415 (1976)

K. R. Darnall, A. M. Winer, A. C. Lloyd, and J. N. Pitts, Jr.

Charcoal-Adsorption Air Purification System for Chamber Studies Investigating Atmospheric Photochemistry

Environ. Sci. Technol., 11, 45 (1977)

G. J. Doyle, P. J. Bekowies, A. M. Winer, and J. N. Pitts, Jr.

Atmospheric Chemical and Physical Transformations of Oxides of Nitrogen

State of California Air Resources Board Photochemical/Transport Workshop, University of California, Los Angeles, California, January 6-7, 1977

J. N. Pitts, Jr., D. Grosjean, A. M. Winer, K. R. Darnall, and G. J. Doyle

Rate Constants for the Reaction of OH Radicals with n-Propyl Acetate, sec-Butyl Acetate, Tetrahydrofuran and Peroxyacetyl Nitrate

Chem. Phys. Lett., 51, 221 (1977)

A. M. Winer, A. C. Lloyd, K. R. Darnall, R. Atkinson, and J. N. Pitts, Jr.

Rate Constants for the Reaction of the OH Radical with Selected Alkanes at 300 K

J. Phys. Chem., 82, 1581 (1978)

K. R. Darnall, R. Atkinson, and James N. Pitts, Jr.

Ultraviolet and Infrared Absorption Cross Sections of Gas Phase  $\text{HO}_2\text{NO}_2$   
Geophys. Res. Lett., 5, 909 (1978)  
R. A. Graham, A. M. Winer, and J. N. Pitts, Jr.

Kinetics and Mechanisms of the Reactions of the Hydroxyl Radical with  
Organic Compounds in the Gas Phase  
Advan. Photochem., 11, 375 (1978)  
R. Atkinson, K. R. Darnall, A. C. Lloyd, A. M. Winer, and J. N.  
Pitts, Jr.

Smog Chamber Study of the Correlation of Hydroxyl Radical Rate Constants  
with Ozone Formation  
Environ. Sci. Technol., 13, 822 (1979)  
A. M. Winer, K. R. Darnall, R. Atkinson, and J. N. Pitts, Jr.

Atmospheric Measurements of Trace Pollutants by Kilometer Pathlength FT-IR  
Spectroscopy  
Advan. Environ. Sci. Technol., in press (1979)  
E. C. Tuazon, A. M. Winer, R. A. Graham, and J. N. Pitts, Jr.

An Evacuatable Environmental Chamber and Solar Simulator Facility for the  
Study of Atmospheric Photochemistry  
Advan. Environ. Sci. Technol., in press (1979)  
A. M. Winer, R. A. Graham, G. J. Doyle, P. J. Bekowies, J. M. McAfee,  
and J. N. Pitts, Jr.

Simultaneous Concentrations of Ammonia and Nitric Acid in a Polluted  
Atmosphere and Their Equilibrium Relationship to Particulate Ammonium  
Nitrate  
Environ. Sci. Technol., in press (1979)  
G. J. Doyle, E. C. Tuazon, T. M. Mischke, R. A. Graham, A. M. Winer,  
and J. N. Pitts, Jr.

CARB LIBRARY



07289